MODELING OF COMPLEX PHYSICS & COMBUSTION DYNAMICS IN A COMBUSTOR WITH A PARTIALLY PREMIXED TURBULENT FLAME

Mina Shahi

MODELING OF COMPLEX PHYSICS & COMBUSTION DYNAMICS IN A COMBUSTOR WITH A PARTIALLY PREMIXED TURBULENT FLAME

Mina Shahi

This research was financially supported by the European Commission in the Marie Curie Actions Networks for Initial Training, under call FP7-PEOPLE-2007-1-1-ITN, Project LIMOUSINE with project number 214905.

Modeling of Complex Physics & Combustion Dynamics in a Combustor with a Partially Premixed Turbulent Flame

Shahi, Mina

PhD thesis, University of Twente, Enschede, The Netherlands, September 2014

ISBN: 978-90-365-3712-4
DOI: 10.3990/1.9789036537124

MODELING OF COMPLEX PHYSICS & COMBUSTION DYNAMICS IN A COMBUSTOR WITH A PARTIALLY PREMIXED TURBULENT FLAME

DISSERTATION

To obtain

The degree of doctor at the University of Twente,

on the authority of the rector magnificus,

Prof.dr. H. Brinksma,

on account of the decision of the graduation committee,

to be publicly defended

on Wednesday 24th of September 2014 at 12:45

by

Mina Shahi

Born on April 23th, 1984

In Tehran, Iran

The dissertation is approved by:

Prof.dr.ir. T. H. Van der Meer	Promotor
Dr.ir. J.B.W. Kok	Assistant promotor

Composition of the graduation committee:

Chairman and secretary:

Prof.dr. G. P. M. R. Dewulf	University of Twente

Promotor:

Prof.dr.ir. T. H. Van der Meer	University of Twente

Assistant promotor:

Dr.ir. J.B.W. Kok	University of Twente

Members:

Prof.dr.ir. A.de Boer	University of Twente
Prof.dr.ir. B. J. Geurts	University of Twente
Prof.dr.ir. D. M. J. Smeulders	Eindhoven University of Technology
Prof.dr.ir. I. Lopez Arteaga	Eindhoven University of Technology
Dr.ir. R. Hagmeijer	University of Twente

To my parents and my husband Amir

Summary

To avoid the formation of the high temperature stoichiometric regions in flames in a gas turbine combustor, and hence the formation of nitric oxides, an alternative concept of combustion technology was introduced by means of lean premixed combustion. This way the low nitric oxide emission targets of industrial gas turbine engines for power generation can be realized. However, the low emission of nitric oxides and carbon monoxide of the lean premixed combustion of natural gas comes at the cost of increased sensitivity to thermoacoustic instabilities. These are driven by the feedback loop between heat release, pressure and flow/mixture fluctuations. The pressure oscillations induced by thermoacoustic instabilities can reach very high amplitudes, possibly leading to severe damage and a significant reduction of the life time of the gas turbine engine. For this reason, it is important to be able to assess in the design phase already if a gas turbine combustor will have a stable flame at certain given conditions. To this end, tools and models for the accurate prediction of the amplitude and frequency of pressure oscillations is essential.

The work presented in this dissertation focuses on the numerical modeling of the interaction between the coupled fields of flow, pressure and heat to predict the occurrence of self-excited high amplitude pressure oscillations. Calculations are done on a laboratory scale atmospheric combustion test rig, in conditions representative of gas turbine combustion systems.

In the first part of the thesis modeling of the non-reacting and reacting flow over a backward facing step is presented. Different combustion and turbulence models are applied to find the models giving the best predictions. Since in many circumstances the occurrence of instability is related to large scale motion, the generated data in the combustible flow over a backward facing step can be used in the subsequent investigation of flame characteristics in more complex configurations of a gas turbine.

In this thesis, two coupled approaches are considered for the numerical computations. In the first one, phenomena in fluid and structure are computed using a simultaneous solution procedure in one computational domain. Here, the coupled equations for both solid and fluid domain are solved together using the ANSYS-CFX code and using the same time step for both fluid and solid regions.

In this approach, the meshing strategy and size of the grid in the solid part of the domain will play a very important role in determining the magnitude for the pressure fluctuations. The coupling between the structure and the fluid is very strong at the interface. This analysis is referred in the thesis as a Conjugated Heat Transfer (CHT) approach.

In the second coupled approach, the interaction between the fluid and structure is linked to the vibrating walls using the partitioned approach with the strong coupling scheme. Here, two separate solvers (ANSYS-CFX and ANSYS Multiphysics) with appropriate interface boundary conditions for the flow domain and the structural domain operate in a coupled way. Information will be exchanged between two codes dynamically every time step. This analysis is referred in the thesis as the two-way FSI approach.

Prior to the above mentioned investigations (CHT and FSI), in the second and third parts of the paper the analysis and validation of fluid-only calculations are performed. In this method, the so-called zero-way coupling approach, the feedback from the vibrating walls to the acoustic field inside the combustion chamber is neglected. Here the effects of the grid type on the accuracy of the predicted data are examined first, and then the influence of the turbulent combustion modeling on the predicted flame dynamics is evaluated. Since in this approach the damping/amplification effect caused by the liner (caused by for example heat loss or deformation) is not taken into account, it is important to find an accurate boundary condition representing the condition as close as possible to the real physical state. For this reason different thermal boundary conditions are applied and the effects on characterizing of the instabilities are evaluated.

The results of the fluid-only simulation showed the overprediction in the main frequency and magnitude of occurred thermoacoustic instability. Computations using the isothermal liner predicted onset of instabilities well. In this case the predicted frequency deviated 9.5% from the experimental data. However, modeling of the thermal interaction of the liner structure and the reacting flow using the CHT approach can improve the predictions and give access to the heat penetration depth in the liner. In this approach thermo-acoustic instability was predicted with error below 1%. The fluid-structure interaction model (FSI) predicted correctly the frequency of the instability; however the amplitude of the computed pressure signals was overpredicted with respect to the measured data. The main vibrating frequency was also predicted correctly. Obtained calculated and measured data

shows that the feedback from the vibrating liner to the pressure oscillations (i.e. acoustic field) is minor.

Samenvatting

Teneinde de vorming van stoichiometrische gebieden in vlammen in een gasturbineverbrandingskamer te voorkomen, en daarmee ook de vorming van stikstof oxiden, is voor gasturbines een alternatieve verbrandingstechnologie geintroduceerd door middel van mengselarme voorgemengde verbranding. Hiermee kan voldaan worden aan steeds strenger wordende eisen aan de maximale stikstofoxide emissie voor industriele gasturbine motoren voor krachtopwekking. De gerealiseerde lage emissie van stikstofoxiden en koolmonoxide door toepassing van de nieuwe verbrandingstechnologie leidt echter tot een verhoogde gevoeligheid voor thermo-akoestische instabiliteiten. Deze worden gedreven door de terugkoppelingslus tussen vrijkomende warmte, druk- en stromingsfluctuaties. De drukoscillaties die worden veroorzaakt door de thermo-akoestische instabiliteiten kunnen zeer hoge amplituden bereiken, waardoor ernstige schade en een sterk verkorte levensduur van de gasturbine kan ontstaan. Om deze reden is het belangrijk al in de ontwerpfase van een gasturbineverbrandingskamer te kunnen bepalen of onder gegeven omstandigheden een stabiele vlam wordt gerealiseerd. Hiervoor is de beschikbaarheid van nauwkeurige modellen voor de voorspelling van amplitude en frequentie van drukoscillaties noodzakelijk.

Het werk gepresenteerd in deze dissertatie focusseert zich op de numerieke modellering van de interactie tussen de gekoppelde velden van stroming, druk en warmte voor de voorspelling van het optreden van spontane druk oscillaties met hoge amplitude.

In het eerste deel van de thesis wordt de modellering van de stroming, zowel met als zonder chemische reacties, over een backward facing step gepresenteerd. Verschillende verbrandings- en turbulentiemodellen worden toegepast teneinde het meest geschikte model te vinden. Gezien het feit dat het optreden van instabiliteit vaak is gerelateerd aan grootschalige stromingspatronen, kunnen de resultaten ook worden toegepast op de meer gecompliceerde configuraties als aangetroffen in een gas turbine verbrandingskamer.

In dit proefschrift worden twee gekoppelde methoden beschouwd voor de numerieke berekeningen. Bij de eerste methode worden de phenomenen in zowel fluidum als structureel domein in een oplossingsdomein numeriek opgelost. De gekoppelde vergelijkingen voor beide domeinen worden simultaan opgelost met behulp van de ANSYS-CFX code, met dezelfde tijdstap voor zowel fluidum als

structureel domein.in deze aanpak speelt de strategie voor het bepalen van de discrete punten in het rekendomein een belangrijke rol voor de berekening van de amplitude van de druk fluctuaties. De koppeling tussen structuur en fluidum is heel sterk op het grensvlak. In deze thesis wordt aan deze aanpak gerefereerd als de Conjugated Heat Transfer (CHT) aanpak.

In de tweede method wordt de interactie tussen fluidum en structuur gekoppeld aan de wandvibratie met behulp van een gepartioneerde aanpak met een schema voor sterke koppeling. Hier worden twee afzonderlijke oplossingsmethoden en rekendomeinen gebruikt (ANSYS-CFX and ANSYS Multiphysics), die worden gekoppeld door middel van geschikte randvoorwaarden en interpolaties op het grensvlak. De grensvlakinformatie wordt tussen beide codes uitgewisseld op iedere tijdstap. In deze thesis wordt aan deze aanpak gerefereerd als de twee-weg FSI aanpak.

Voorafgaand aan de bovengenoemde onderzoeken (CHT en FSI), in het tweede en derde deel van dit werk, zijn de analyse en validatie berekeningen uitgevoerd van het ‘fluïdum-only’ domein . In deze werkwijze, de zogenaamde ‘zero-way coupling approach’ wordt de terugkoppeling van de vibrerende wanden naar het akoestische veld in de verbrandingskamer verwaarloosd. Hierbij zijn de effecten van het roostertype op de nauwkeurigheid van de voorspelde gegevens eerst onderzocht, en vervolgens de invloed van de turbulente verbranding modellering op de voorspelde vlamdynamiek geëvalueerd. Aangezien bij deze benadering de demping / amplificatie-effecten veroorzaakt door de verbrandingskamerwand (door bijvoorbeeld warmteverlies of vervorming) niet in aanmerking wordt genomen, is het belangrijk om een accurate randvoorwaarde te kiezen die de werkelijke fysische toestand zo dicht mogelijk benadert. Daarom worden verschillende thermische randvoorwaarden toegepast en de effecten op de eigenschappen van de instabiliteiten geëvalueerd.

De resultaten van de fluïdum-only simulatie toonde een voorspelling met overschatting van de frequentie en grootte van de opgetreden thermo instabiliteit. Berekeningen met de isotherme verbrandingskamerwand voorspelde het begin van de instabiliteiten correct. In dit geval week de voorspelde frequentie 9,5% af van de experimentele data. Echter, het modelleren van de thermische interactie van de verbrandingskamer wand en de reagerende stroom met behulp van de CHT aanpak kan de voorspellingen verbeteren en houden rekening met de warmte penetratiediepte in de wand. Bij deze benadering werd thermo-akoestische instabiliteit voorspeld met een afwijking kleiner dan 1%. Het fluidum-structuur

interactie model (FSI) voorspelde correct de frequentie van de instabiliteit, maar de amplitude van de berekende druksignalen werd hoger voorspeld dan gemeten. De belangrijkste vibratiefrequentie werd correct voorspeld. Zowel de gemeten en voorspelde resultaten laten zien dat de terugkoppeling van de vibrerende wand naar het akoestisch veld gering is.

Contents

Contents

1

Introduction

1.1 Motivation

Gas turbines are used in a broad range of applications including military, marine or industrial use where weight is a primary factor, and also in power generation or energy sectors. A gas turbine has the advantage of fuel flexibly as it can accommodate all type of combustible gases and all types of combustible liquids. Gas turbines are essentially composed of three major components: compressor, combustor and power turbine. In the compressor section, ambient air is drawn in and compressed (up to 30 times ambient pressure), and then pressurized air is directed to the combustion section in which fuel (usually natural gas, although other fossil fuels such as synthesis gas[1] are being used) is introduced, ignited and burned. Hot gases from the combustor section are diluted with additional air from the compressor and directed to the power turbine, where hot gases are expanded down to the exhaust pressure, producing a shaft work output. The resulting power output of the turbine is used for driving the compressor and the generator. Different sections of a modern gas turbine engine, the Siemens SGT5-8000H, are shown in Figure 1-1.

The combustion process in a gas turbine can be classified as diffusion combustion or lean premixed stage combustion, based on whether the fuel and air are mixed in the chamber itself, or mixed before entering into the combustion chamber. In the diffusion flame combustion, the mixing of the fuel and air as well as the combustion process takes place in the primary flame zone simultaneously, generating regions of near-stoichiometric mixture where the temperature is quite

1 Syngas, also known as synthesis gas, synthetic gas or producer gas, can be produced from a variety of different materials that contain carbon. These can include biomass (wood gas), plastics, coal, municipal waste or similar materials.

high. The existence of a near-stoichiometric region with very high temperature results in excessive levels of NO_X. There are several technologies such as water or stream injection known as "wet diffusion combustion" that can be applied to reduce the combustion temperature and hence satisfying the severe NO_X regulations. However the traditional methods of reducing NO_X emissions like water and steam injections are limited in their ability to reach the extremely low level emissions as required to meet today's regulations. Table 1-1 presents some of the worldwide requirements which apply for stationary gas turbines.

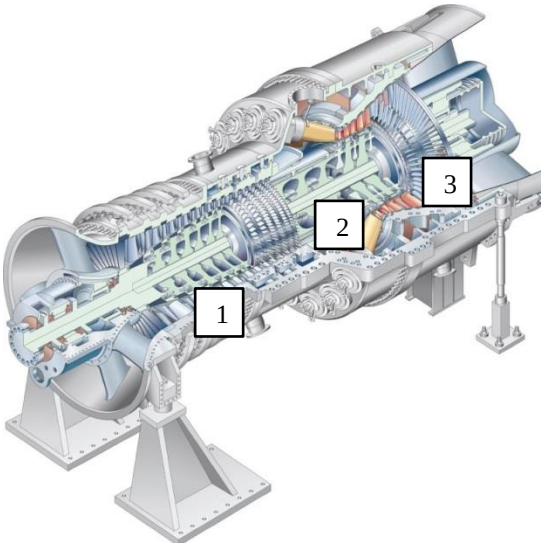

Figure 1-1: The SGT5-8000H developed by Siemens: 1- compressor, 2-combustion chamber, 3- turbine section

Table 1-1: Emission limits for ground based gas turbines [1]

Country	NO_x (@ 15% O_2)	CO (@ 15% O_2)	Rates power
ECC	25 vppm	Not stated	>50MWth
France	40 vppm	80 vppm	>20MWth
Italy	29 vppm	48 vppm	>50MWth
United Kingdom	28 vppm	80 vppm	>50MWth
Japan (Tokyo)	28 vppm	No limits	Not stated
USA (California)	9 ppm	Not stated	Not stated

Among the different techniques to control emissions for achievement of lower pollutants, lean premixed (LPM) combustion is the most popular technique which significantly reduces NOx formation. Contrary to the diffusion combustion for the LPM combustors, fuel and air are mixed in an initial stage resulting in a uniform and lean mixture of fuel/air. For safety reasons, the use of perfectly premixed combustion in industrial machines is not common and fuel is injected just at a short distance upstream of the combustion chamber. This unburned mixture is then delivered to the secondary stage where reaction takes place. The majority of modern gas turbines use lean-premixed staged combustion turbines. Gas turbines using staged combustion are also referred to as Dry Low NO_X (DLN) combustion systems, in which the need for costly water usage to reduce the NO_X emissions is eliminated. Figure 1-2 shows the dependence of main pollutants generated by the LPM combustion of methane and air on the temperature and equivalence ratio [2]. As it can be seen in the figure, CO and NO_X emissions follow the opposite trends. While low temperature is favorable for NO_X reduction, the CO formation exhibits a rapid increase. To meet the low emission targets, the combustion system should operate within the range of equivalence ratio, where the CO and NO_X emissions are kept below the imposed limits by the legislation.

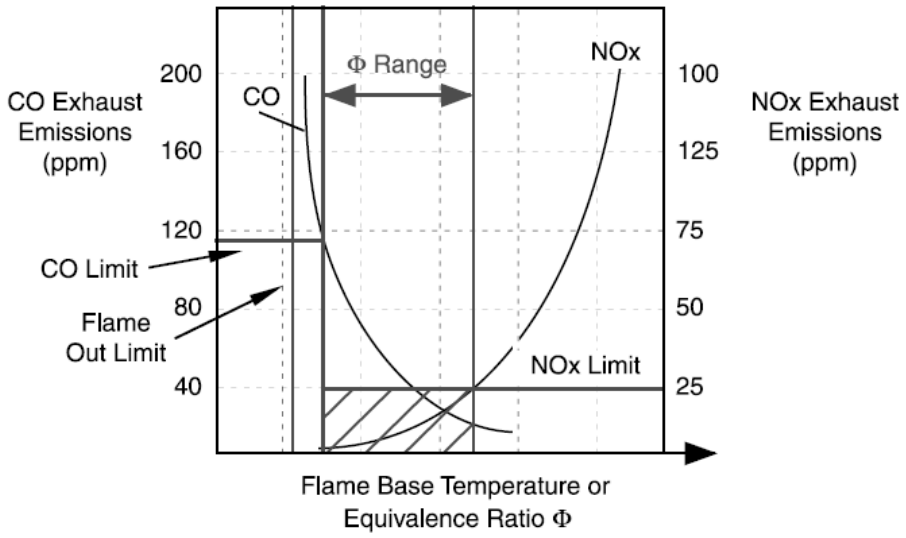

Figure 1-2: Influence of the flame base temperature/ equivalence ratio on CO and NO_X emissions (adapted from reference [2])

However, the resulting absence of diffusive mixing times in the LPM systems leaves the flames sensitive to acoustic excitation from sound waves with flame response which is affiliate to the amplitude, frequency and nature of acoustic wave impingement [3]. Therefore these systems are prone to thermoacoustic instabilities [4], which can lead to the limit cycle of high amplitude pressure oscillation (LCO) in the combustor. This condition is the result of the resonant interaction between aerodynamics, combustion and acoustics in the combustion system [5, 6], which can cause severe damage to the combustion system reducing the life time and efficiency of the combustor [7, 8]. In reality, flow oscillations can be seen even during the stable mode of the combustion. Combustion with small amplitude pressure oscillations, for instance less than about 5% of mean pressure is defined as stable combustion [7], while combustion with large amplitude pressure fluctuations is called unstable or oscillatory combustion. The latest is also referred to as combustion instability which may correspond to an oscillation of the pressure having a frequency as low as 10-20 Hz or as high as several tens of kilohertz. According to Krebs et al. [9], low frequency instabilities occurring at a frequency below 50 Hz are referred to as the Helmholtz mode of oscillations. Intermediate frequency instabilities observed in the range of 50-1000 Hz usually correspond to

the longitudinal acoustic modes of the combustor; while high frequency dynamics, taking place at frequency at above 1000 Hz, correspond to the tangential acoustic modes. Generally, in industrial gas-turbine combustors the first natural modes, vary in the range of 50 -300 Hz based on the geometry and temperature [10]. While the unstable flames are characterized by large amplitude oscillations with a distinct characteristic frequency, the stable flames are mostly accompanied by turbulent flow noise without having any significant frequency in the spectrum [11]. Not only the amplitude of the pressure oscillation has made the unstable combustion distinguishable from the stable one, the position and shape of the flame can also determine on which condition combustion is taking place. Broda et al. [12] conducted an experimental study on combustion instabilities in a premixed swirl stabilized combustor, in which it is indicated that the onset of instabilities can cause significant change in flame structure, and during certain periods of the oscillation cycle it can even cause near extinction of the flame. Lee et al. [13] investigated the local flame structure of a lean premixed gas turbine combustor operating at high pressure and temperature during combustion instability. They observed significant differences in the flame structure during different phases of the combustion instability, and substantial change of the heat release flow field at the corner and inner faces of the dump plane.

However, small changes in the operating parameters (like: chamber pressure, inlet temperature, equivalence ratio, etc. [11, 14]) or geometrical configuration (like chamber dimensions, inlet and exit configurations, fuel injection system, etc. [15, 16]) as well as the change in the fuel composition [17] may turn the combustion from stable to unstable condition. Therefore the possibility of instabilities, which may occur must be anticipated and recognized in the design stage of a LPM gas turbine combustor. For this reason and to find countermeasures applicable to real configurations in the later stage, a deeper understanding of the complex interactions involved in combustion instabilities is essential. To investigate the combustion driven instabilities, the used numerical approaches should address the three basic characteristics: 1- The frequency of the oscillations, 2- Conditions under which the oscillations occur, and 3- The limit cycle amplitude. A short overview, explaining how this thesis contributes to the above mentioned task will be given in the section 1.4.

1.2 Driving mechanisms of combustion instability and Limit Cycles

In general, the oscillatory flow can acquire the energy through different sources. In a combustion system, unsteady heat release from chemical reactions is the main source of energy, driving the periodic motions [7]. The heat release depends on the local equivalence ratio, mass flow rate and also the instantaneous pressure and temperature. Therefore oscillations in the mass flow rate, fluctuations in equivalence ratio, variation in the flame surface or the vortex shedding due to hydrodynamic instabilities [18, 19] may result in heat release fluctuations, which generate acoustic perturbations. The gained energy from the chemical reaction can be exchanged with the background turbulent motions or it can be dissipated into thermal energy due to viscous damping. In general, these instabilities can only sustain in the system if the special relationship (so-called Rayleigh criterion [20]) between heat release fluctuations and acoustic (pressure oscillations) is satisfied. According to this criterion, the pressure fluctuation increases in amplitude if heat release is in phase with pressure oscillation, while it is attenuated if heat release and pressure fluctuation are out of phase[2]. The instabilities can be self-excited as pressure oscillations grow spontaneously within the system or they can be initiated as the flame is excited by any perturbation external to the system [11, 21-25]. The first case, which is referred to as self-excited oscillations is of interest in this dissertation. The dynamics of this flame, even in the absence of external acoustic excitation, involves complex interactions between the aerodynamics, combustion and structure, which bring research into investigation of complex mechanisms such as turbulence, chemical reactions, acoustics and vibration. However, either in a self-excited system or in an acoustically perturbed system, the ampitude of pressure oscilations grows with time only if the energy gain from the comustion to the periodic flow is greater that the energy losses. The limit cycle is reahced when they are in equlibruim meaning that losses are equal to the gain [26]. Figure 1-3 represents the schematic diagram of interaction between energy losses and energy gain as a function of acoustic velocity for a nonlinear system. The black line represents the losses within the system like losses through the boundaries or by turbulence, while the gray line stands for the gain corresponding to the flame dynamics. As it can be seen the losses are linearly dependent on $|u'|^2$, as suggested by Dowling [27], whereas the dependence of the gain is linear in the region I and

[2] Mathematical explanation of Rayleigh criterion is given in chapter 3.

nonlinear in region II. This figure shows that LC is sustained within the nonlinear region and its amplitude (A_{LC}) corresponds to the intersection of two curves.

To quantify the response of the flame to the unsteady inlet velocity and/or equivalence ratio resulting from the impinging acoustic waves, many researches have been conducted using the concept of the flame transfer function [22, 23, 28-30]; however this is not of our interest in this dissertation.

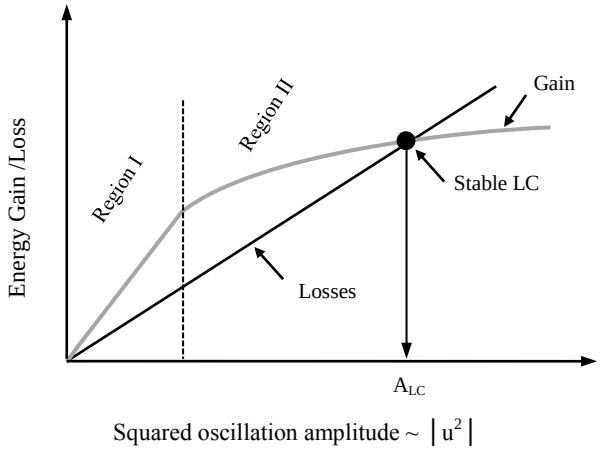

Figure 1-3: Energy gain (gray) and loss (black) as a function of the acoustic velocity (adapted from [26])

1.3 Research objective

The work presented in this dissertation is done within the EU-funded Marie Curie project, LIMOUSINE (**Lim**it cycles of thermo-ac**ous**tic oscillations in gas turb**ine** combustors). The LIMOUSINE project, which is motivated by the need for lean combustion technologies and reduced emissions, represents a multidisciplinary initiative to strengthen the fundamental scientific work in the field of thermo-acoustic instabilities. The objective of the LIMOUSINE project is to investigate the limit cycle behavior of the unstable pressure oscillations which leads to mechanical vibrations and materials fatigue in combustion systems. The research team in this

project consists of 6 academic partners, 2 research institutions and 5 industrial partners.

The main objective of this thesis as a particular work package of the LIMOUSINE project is to predict numerically the limit cycle behavior of the thermo-acoustic instability which appears in a laboratory-scaled partially premixed flame, operating at a range of power of 20-80 kW and air factor 0.8-2 and to develop the coupled thermal/mechanical model of the fluid-structure interactions. When the combustion-driven thermo-acoustic instabilities arise in the combustion system, on the one hand the unsteady pressure oscillation is responsible for the generation of mechanical vibrations and hence the premature failure of the device. On the other hand the oscillating heat transfer to the liner is responsible for the thermo-mechanical materials fatigue. Therefore analysis of such coupled phenomena is demanded for the assessment of the mechanical integrity of gas turbine engines. The research presented in this dissertation addresses the following research questions:

- What are the requirements for an accurate prediction of an unstable regime of a combustor using URANS?
- What are the origin and the driving mechanisms of the Limit cycle pressure oscillation?
- What is the sensitivity of models to the input parameters?
- What are effective parameters in the structure liner which are playing a role in determining the magnitude of the pressure fluctuations?
- How important is the role of heat transfer on the development of instabilities?
- What are the consequences of the high pressure oscillations on the liner vibration and vice versa?

1.4 Outline

The Introduction chapter is followed by **Chapter 2** "On Characteristics of a Non-Reacting and a Reacting Turbulent Flow over a Backward Facing Step (BFS)", in which the main objective is to validate the combined numerical approaches for the combustion prediction. First, results of the transient non-reacting calculations using various turbulence models are compared with the available experimental data in literatures. Moreover calculations are extended for the reacting flow, to verify the accuracy of the chemical models.

Chapter 3 is devoted to the numerical simulation of self-excited combustion pulsation for the LIMOUSINE combustor, in which the simulation becomes unsteady by itself, developing a limit cycle of pressure oscillations. Therefore no separate forcing on boundaries is required. Investigation of the sensitivity and accuracy of the reactive flow field prediction is conducted with regard to choices in computational mesh and turbulent combustion model. Results are presented for different mesh sizes of unstructured and structured grids to identify the grid-independency of the solution. A qualitative validation of the CFD-results and experimental data for the cold flow field is given. To investigate the possibility of studying the thermo-acoustic instabilities, pressure fluctuations are compared between numerical results from a structured mesh, and unstructured mesh as well as with experimental data. A frequency analysis and a mode analysis are carried out. Next comparisons between pressure time signals and pressure FFT spectra are made using different combustion models. The numerical predicted values are compared to experimental data and to eigenmodes obtained from a FEM analysis of the combustor fluid volume. The study shows, that fundamental aspect can be obtained but further development is required. The effective parameters and required developments are implemented into the model and presented in **Chapter 4**. It is indicated that modeling of heat losses through the liner is very important in controlling the magnitude of the thermoacoustic instability. In order to take into account the actual position of the pressure node, end correction is performed by adding an extra length to the resonating duct.

In **Chapter 5**, a Conjugated Heat Transfer approach (CHT) will be applied to represent the transient heat transfer between the turbulent lean partially premixed flame and the walls of the combustor. Targeted will be the prediction of sensitivity of the combustion instabilities to the unsteady heat transfer and its role on characterization of the limit cycle of high amplitude pressure oscillations. Here, the coupled equations for both solid and fluid domain are solved together using the ANSYS-CFX code and defining the same time scales for both fluid and solid regions. The solid mesh resolution needs to be adapted to the thermal penetration depth of the surface temperature oscillations. The importance of the meshing strategy and size of the grid in the solid part of the domain on the accuracy of the predicted magnitude for the pressure fluctuations will also be discussed in this chapter. Furthermore, a comparative analysis based on the predicted frequency and magnitude of instability is done for this approach and the zero-way method presented in chapter 4.

Chapter 6 deals with fluid structure interaction (FSI) focusing on the development of numerical models for interaction between combustion, acoustics and flexural waves on the combustor liners. The main objective will be the prediction of the liner deformation that results from limit-cycle pressure waves, as well as the liner vibration effect on emitting the acoustic waves to the surrounding gases and hence resulting enhanced/damped pressure oscillations. For this reason a partitioned approach is used to model the mutual interaction between the flue gases and the liner. In order to model the flame dynamics ANSYS-CFX code is used, while ANSYS Mechanical is used to determine the dynamic response of a structure under unsteady pressure loads. These two solvers are coupled using system coupling in ANSYS Workbench. To understand the dynamics of the liner, a modal analysis is also performed to determine the natural frequencies and their respective mode shapes. Comparison work between two-way and zero-way interactions is conducted to evaluate the effects of structural deformation on characterizing of the thermoacoustic instabilities. In addition, the influence of the chosen CFD domain on the predicted stability condition of the combustor is discussed, and it is shown how this choice can lead to a deviation between the numerical results and the measurements.

Finally, **Chapter 7** is devoted to the conclusions which are drawn based on the research objectives. Moreover, recommendations for future research are presented in this chapter.

It is important to mention that the core chapters of this thesis, i.e. Chapters 2–6, are self-contained as they have been or are in the process of being published in scientific journals. There may be therefore some repetition of fundamental concepts and references.

References

[1] Docquier, N., and Candel, S., 2002, "Combustion control and sensors: a review," Progress in Energy and Combustion Science, 28(2), pp. 107–150.
[2] Brown, D. M., 1995, "Combustion control apparatus and method " European Patent Application No. 0 677 706 A1, 95/42, General Electeric Company.
[3] Syred, N., 2006, "A review of oscillation mechanisms and the role of the precessing vortex core (PVC) in swirl combustion systems," Progress in Energy and Combustion Science, 32(2), pp. 93-161.

[4] Lieuwen, T., and McManus, K., 2003, "Introduction: Combustion Dynamics in Lean-Premixed Prevaporized (LPP) Gas Turbines," Journal of Propulsion and Power, 19(5), pp. 721-721.
[5] Dowling, A. P., 1995, "The calculation of thermoacoustic oscillations," Journal of Sound and Vibration, 180(4), pp. 557-581.
[6] Lieuwen, T., and Yang, V., 2006, Combustion Instabilities in Gas Turbine Engines: Operational Experience, Fundamental Mechanisms and Modeling., Volume 210, American Institute of Aeronautics and Astronautics (AIAA).
[7] Huang, Y., and Yang, V., 2009, "Dynamics and stability of lean-premixed swirl-stabilized combustion," Progress in Energy and Combustion Science, 35(4), pp. 293-364.
[8] Lieuwen, T., 2003, "Modeling premixed combustion–acoustic wave interactions: a review," Journal of Propulsion and Power, 19(5).
[9] Krebs, W., Bethke, S., Lepers, J., Flohr, P., Prade, B. , "Thermoacoustic Design Tools and Passive Control: Siemens Power Generation Approaches," in Combustion Instabilities in Gas Turbine Engines, T. Lieuwen and V. Yang, Editors. 2005, AIAA: Washington D.C. p. 89-112.
[10] Caraeni, M., Devaki, R. K., Aroniz, M., Oswaldx, M., Srikanth, K., and Caraen, D., "Efcient Acoustic Modal Analysis for Industrial CFD," 47th AIAA Aerospace Sciences Meeting , 5 - 8 January 2009, Orlando, Florida.
[11] Hernández, I., Staffelbach, G., Poinsot, T., Román Casado, J. C., and Kok, J. B. W., 2013, "LES and acoustic analysis of thermo-acoustic instabilities in a partially premixed model combustor," Comptes Rendus Mécanique, 341(1–2), pp. 121-130.
[12] Broda, J. C., Seo, S., Santoro, R. J., Shirhattikar, G., and Yang, V., 1998, "An experimental study of combustion dynamics of a premixed swirl injector," Symposium (International) on Combustion, 27(2), pp. 1849-1856.
[13] Lee, S. Y., Seo, S., Broda, J. C., Pal, S., and Santoro, R. J., 2000, "An experimental estimation of mean reaction rate and flame structure during combustion instability in a lean premixed gas turbine combustor," Proceedings of the Combustion Institute, 28(1), pp. 775-782.
[14] Kim, M.-K., Yoon, J., Park, S., Lee, M.-C., and Youngbin, Y., 2013, "Effects of unstable flame structure and recirculation zones in a swirl-stabilized dump combustor," Applied Thermal Engineering, 58(1–2), pp. 125-135.
[15] Katsuki, M., and Whitelaw, J. H., 1986, "The influence of duct geometry on unsteady premixed flames," Combustion and Flame, 63(1–2), pp. 87-94.
[16] Li, G., and Gutmark, E. J., 2005, "Effect of exhaust nozzle geometry on combustor flow field and combustion characteristics," Proceedings of the Combustion Institute, 30(2), pp. 2893-2901.
[17] Richards, G. A., McMillian, M. M., Gemmen, R. S., Rogers, W. A., and Cully, S. R., 2001, "Issues for low-emission, fuel-flexible power systems," Progress in Energy and Combustion Science, 27(2), pp. 141-169.
[18] Poinsot, T. J., Trouve, A. C., Veynante, D. P., Candel, S. M., and Esposito, E. J., 1987, "Vortex-driven acoustically coupled combustion instabilities," Journal of Fluid Mechanics, 177, pp. 265-292.
[19] Fureby, C., 2000, "A computational study of combustion instabilities due to vortex shedding," Proceedings of the Combustion Institute, 28(1), pp. 783-791.
[20] Rayleigh, J., 1878, "The explanation of certain acoustic phenomena," Nature, 18, pp. 319-321.

[21] Krediet, d. H. J., 2012, "Prediction of limit cycle pressure oscillations in gas turbine combustion systems using the flame describing function," Enschede.
[22] Polifke, W., and Lawn, C., 2007, "On the low-frequency limit of flame transfer functions," Combustion and Flame, 151(3), pp. 437-451.
[23] Palies, P., Schuller, T., Durox, D., and Candel, S., 2011, "Modeling of premixed swirling flames transfer functions," Proceedings of the Combustion Institute, 33(2), pp. 2967-2974.
[24] Kim, D., and Park, S. W., 2010, "Forced and self-excited oscillations in a natural gas fired lean premixed combustor," Fuel Processing Technology, 91(11), pp. 1670-1677.
[25] Meier, W., Weigand, P., Duan, X. R., and Giezendanner-Thoben, R., 2007, "Detailed characterization of the dynamics of thermoacoustic pulsations in a lean premixed swirl flame," Combustion and Flame, 150(1–2), pp. 2-26.
[26] lieuwen, T., Bellows, B. D., Bobba, M. K., and Seitzman, J. M., 2007, "Nonlinear flame transfer function charasteristics in a swirl stabilized combustor," Journal of Engineering for Gas Turbines and Power, 129, pp. 954-961.
[27] Dowling, A. P., 1997, "Nonlinear self-excited oscillations of a ducted flame," Journal of Fluid Mechanics, 346(1), pp. 271-290.
[28] Kim, D., Kim, K., Srinivasan, S., Lee, J. G., Quay, B. D., and Santavicca, D. A., 2009, "Effect of Flame Structure on the Flame Transfer Function in a Premixed Gas Turbine Combustor," Journal of Engineering for Gas Turbines and Power, 132(2), pp. 021502-021502.
[29] Biagioli, F., Paikert, B., Genin, F., Noiray, N., Bernero, S., and Syed, K., 2013, "Dynamic Response of Turbulent Low Emission Flames at Different Vortex Breakdown Conditions," Flow Turbulence Combust, 90(2), pp. 343-372.
[30] Duchaine, F., Boudy, F., Durox, D., and Poinsot, T., 2011, "Sensitivity analysis of transfer functions of laminar flames," Combustion and Flame, 158(12), pp. 2384-2394.

2

On Characteristics of a Non-Reacting and a Reacting Turbulent Flow over a Backward Facing Step (BFS)

Mina Shahi, Jim. B.W.Kok, Artur Pozarlik.

University of Twente, Faculty of Engineering Technology, Laboratory of Thermal Engineering, Enschede, the Netherlands

Submitted to Int Commun Heat Mass

Abstract

The turbulent reacting flow over a backward facing step shares some essential characteristics of premixed combustion occurring in a typical gas turbine combustor, while it is a simpler configuration to observe and model. For this reason and to explore the characteristics of the turbulent flow, in this study the combustion and flow dynamics in a backward facing step as a most elementary part of a combustor is studied numerically in atmospheric conditions. Two different configurations representing two laboratory devices are considered. As a first necessary step, the accuracy of predicted results is validated through the detailed comparison of numerical predictions and experimental measurements for a non-reacting flow. First, based on these non-reacting calculations, the turbulent model is selected and then the reacting simulations are done using a standard combustion model (available in CFX). Calculations are well supported with experimental data available from literature. Among the investigated turbulence models ($k-\omega$, SST and SAS-SST), SAS-SST model showed the best agreement with the experimental data. The chosen turbulence model was used for the calculation of well documented case of turbulent flow over a back ward facing step with the heated wall, showing satisfactory results compared

to experimental data. For modeling of the reacting flow, the BVM combustion model was used. The predicted results using this model showed accurate results with an error about 2% on prediction of reattachment length.

Keywords: *backward facing step, premixed turbulent combustion, reacting flow, non-reacting flow.*

2.1 Introduction

The boundary layer separation of turbulent flow and its subsequent reattachment to a solid surface occurs in many engineering systems, and it has attracted many researchers due to its practical applications. Flows over air foils, in a channel with a sudden area increase, in gas turbines and many heat transfer devices are some of these applications [1, 2]. With the abundance of literature and experimental data, the flow past a backward facing step is often used as a benchmark test case for CFD codes and turbulence models. RANS, LES and DNS codes have all been used to simulate this flow in both 2D and 3D domains [3-6]. However in the present work, the main goal is to predict the exothermic effects on the flow and the combustion dynamics leading to thermoacoustic instabilities in a backward facing step stabilized premixed flame. The combustor of a typical gas turbine represents some similarities with the turbulent flow over a backward facing step as the flame is stabilized by the recirculating area. Besides, due to the blockage, the sudden expansion also occurs; Regardless of whether these blockages are squares or cylinders, a wake-like flow behind the obstacle will be formed which is characterized by a slow inner flow in the recirculating area and fast outer flow of reactants. This recirculation area plays a critical role to sustain the stable combustion, because it acts as an ignition source for reactants traveling into the shear layer at the edge of the step. Since in many circumstances the occurrence of instability is related to the behavior of this recirculation zone or the wake region during the combustion [7-10], the generated data in the combustible flow over a backward facing step can be used in the subsequent investigation of flame characteristics in more complex configurations of a real gas turbine. To understand the elementary process of interaction between combustion and flow perturbation, it is important to access to comprehensive numerical tools which can carefully take into account all aspects of turbulent combustion flow. Here the backward facing step due to its simple geometry and availability of well documented experimental data is considered for the further investigation. Indeed, the location of the reattachment zone and its flow structure determine the local heat and mass transport properties of the flow. Furthermore the characteristics of backward facing

step flow allow to exam several important aspects of turbulent flows. These aspects include separation of a turbulent boundary layer, reattachment of the boundary layer, recirculation, and the occurrence of secondary separation regions, in which the reattachment zone determines the initial conditions for the recovery process downstream of the step. When the fluid flows over a step, the flow separation can cause alternating shedding of vortices from the body, inducing fluctuating forces which may result in structural vibrations and noise. This can even lead to structural failure. This subject has been of great interest and a lot of efforts have been done into studying the size of the recirculating zone under various conditions as well as vortex interactions during blow off or unstable conditions [9, 11, 12].

As it has been mentioned above in order to assess the available numerical tools, this paper is devoted to characterize the turbulent flow over the backward facing step in two different configurations defined based on the test rigs used by Pitz et al. [13] and Vogel et al. [14]. Prior to the results section, the used numerical approaches are described in detail. Then the mean velocity field of a mixing layer formed at the edge of the step in the first configuration is studied under both reacting and non-reacting conditions; the effectiveness of the used turbulence model on the characteristics of the turbulent flow over the step in the absence of the reaction is discussed. Next, calculations are performed for the reacting flow using the turbulence model, which presented the best agreement with the experiment, together with the Burning Velocity combustion Model (BVM). Thereafter, in the second configuration, the transient heat transfer between the working flow (i.e. air) and the wall is investigated in absence of other complicated processes like combustion, and swirling flow. In this case a heat source is embedded on the wall behind the step. To verify the accurate prediction of the flow and thermal boundary layer, the mean velocity and temperature profiles are compared with the available experimental data; in all calculations, the size of recirculating area is compared to the measurements, giving the good consistency.

2.2 Problem definition

The schematic of a backward facing step is shown in Figure 2-1. The flow coming from the left separates at the sharp corner of the step and then reattaches itself to the lower wall at a distance L, behind the step. A recirculation region is subsequently produced directly behind the step. The reattachment length, L, is a function of the Reynolds number, and the expansion ratio H2:H1 [15]. Depending on the Reynolds number, secondary recirculation regions may occur further

downstream past the main recirculation bubble. Flow separation may also occur on the upper wall [15, 16].

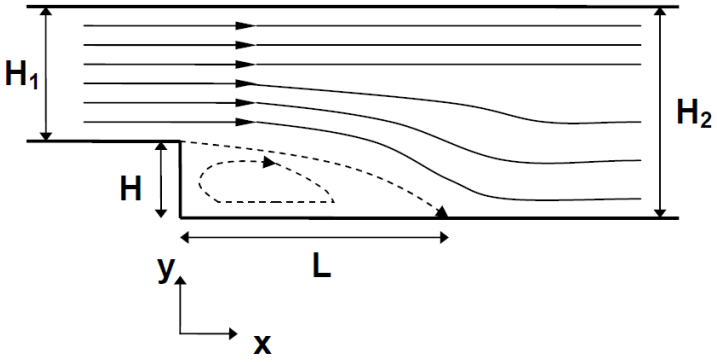

Figure 2-1: Geometry and flow pattern for the backward-facing step calculations

2.3 Numerical approach

In this paper, two different configurations are considered for simulations which respectively are chosen in accordance to the experimental setup of Pitz et al. [13] and Vogel et al [14]. The computational domains consist of unstructured elements. A grid refinement study is performed to determine whether the resolution is accurate enough to capture certain mean flow parameters. The information of the chosen grid is summarized in Table 2-1. The mesh density is increased in vicinity of the step and walls. The numerical simulations were made here by using ANSYS- CFX V12.1. It uses an implicit finite volume formulation to construct the discretized equations representing the Reynolds Averaged Navier-Stokes (RANS) equations. The model consists of a compressible solver with a co-located (non-staggered) finite volume method, such that the control volumes are identical for all transport equations [17]. The basic set of balance equations solved by ANSYS-CFX comprises the Navier-Stokes, species and energy transport equations which are summarized in the following section. A coupled algebraic multi-grid solver is used to give robust solutions for the governing system of linearized equations representing the differential transport equations in discretized form. Convective terms are discretized using a high resolution scheme. It provides high spectral resolution and both low numerical diffusion and dispersion. While shape functions are used to evaluate spatial derivatives for all the diffusion terms. A second order

backward Euler discretization is used for time accuracy. In the time implicit compressible methods, the full compressible equations are solved implicitly to remove the CFL constraint. However to keep the results more precise the solver must be run for constrained CFL values [18]. Therefore the calculations are performed with the time steps (Δt) of 1e-5 s. Boundary conditions which are selected according to [13, 14] will be explained later in the respective sections.

Table 2-1: Grid information

	Configuration 1 Pitz et al. [13]	Configuration 2 Vogel et al [14]
Number of elements	164785	48498

2.4 Mathematical formulation

The full numerical solution of the Navier-Stokes equations is limited to very simple cases, where not a large range of turbulent length and time scales are involved. Therefore to overcome these difficulties, an additional step is introduced by averaging the transport equations. In the Reynolds average, each quantity (ϕ) is split into a mean ($\bar{\phi} = {}^{1}/_{T} \int_{T} \phi(t)\, dt$) and a deviation from mean (turbulent fluctuating component) denoted by ($\phi' = \phi - \bar{\phi}$). The Favre average is defined as the density-weighted average by which the flow variables will be decomposed into mean, $\tilde{\phi} \equiv \overline{\rho\phi}/\rho$, and fluctuating parts, $\phi'' \equiv \phi - \tilde{\phi}$. After time-averaging the equations, extra terms appear in the flow equations which are associated with the interactions between various turbulent fluctuations [19]. Decomposing the velocity, u_i, total energy (non-chemical) e_0 and chemical species Y_k into their Favre average and the corresponding fluctuations and taking the Reynolds average of the conservation equations gives:

- Conservation of mass

$$\frac{\partial \bar{\rho}}{\partial t} + \frac{\partial (\bar{\rho}\tilde{u}_i)}{\partial x_i} = 0 \qquad 2\text{-}1$$

- Momentum

$$\frac{\partial (\bar{\rho}\tilde{u}_i)}{\partial t} + \frac{\partial (\bar{\rho}\tilde{u}_i\tilde{u}_j)}{\partial x_i} = -\frac{\partial \bar{p}}{\partial x_i} + \frac{\partial}{\partial x_i}\left(\overline{\tau_{ij}} - \overline{\rho u_i'' u_j''}\right) \qquad 2\text{-}2$$

τ is the stress tensor which is related to the strain rate by:

$$\overline{\tau_{ij}} = \tilde{\tau}_{ij} + \overline{\tau_{ij}^{''}} \quad 2\text{-}3$$

- Chemical species

$$\frac{\partial(\bar{\rho}\tilde{Y}_k)}{\partial t} + \frac{\partial(\bar{\rho}\tilde{Y}_k\tilde{u}_i)}{\partial x_i} = -\frac{\partial\left(\bar{\rho}\widetilde{u_i''Y_k''}\right)}{\partial x_i} - \frac{\partial(\overline{V_{k,i}Y_k})}{\partial x_i} + \bar{\dot{\omega}}_k \quad 2\text{-}4$$

The source term in the species transport equations is shown by $\dot{\omega_k}$; V_k is the diffusive velocity of the *k*th species.

- Energy equation

$$\frac{\partial(\bar{\rho}\widetilde{e_0})}{\partial t} + \frac{\partial}{\partial x_j}\left(\bar{\rho}\tilde{u}_i\widetilde{e_0} + \tilde{u}_j\bar{p} + \overline{u_j^{''}p} + \overline{\rho u_j^{''}e_0^{''}} + \overline{q_j} - \overline{u_i\tau_{ij}}\right) = \bar{\dot{\omega}}_T \quad 2\text{-}5$$

$\bar{\dot{\omega}}_T$ is a chemical source term, and $\widetilde{e_0}$is given by:

$$\widetilde{e_0} \equiv \tilde{e} + \tilde{u}_k\,\tilde{u}_k\,/2\text{+k} \quad 2\text{-}6$$

q_j is the heat flux which represents heat conduction and transport through species gradients given by ($q_j = -\lambda\frac{\partial T}{\partial x_j} + \rho\sum_{k=1}^{N} V_{k,j}Y_k\,h_{s,k}$).

The turbulent energy, k, is defined by:

$$k = \frac{\widetilde{u_k''u_k''}}{2} \quad 2\text{-}7$$

The objective of turbulent combustion modeling is to propose closures for the unknown quantities (e.g. $\overline{\rho u_i''u_j''}$, $\bar{\rho}\widetilde{u_i''Y_k''}$ and $\bar{\rho}\widetilde{u_i''h_k''}$). Species fluxes, $\bar{\rho}\widetilde{u_i''Y_k''}$, and enthalpy turbulent fluxes, $\bar{\rho}\widetilde{u_i''h_k''}$, are generally closed with the use of the classical gradient assumption using a classical gradient assumption.

2.4.1 Turbulence Modeling

In this work in order to describe the highly turbulent reactive flow behavior, $k-\omega$ [20, 21], SST [22] and SAS-SST [23] turbulent models are implemented.

k- ω Turbulence Model

The k-ω model [20], was developed to improve the predictions in the near wall region and reduce the errors in adverse pressure gradient calculations. The major advantage of the k-ω model is the robust and elegant way how the near wall region is handled. In order to define the turbulent eddy viscosity, the k-ω model uses a frequency scale (ω) called also specific turbulent dissipation rate. Both turbulent

kinetic energy (k) and specific dissipation rate (ω) are obtained from the solution of the following transport equation:

$$\frac{\partial}{\partial t}(\bar{\rho}k) + \frac{\partial}{\partial x_i}(\bar{\rho}\tilde{u}_i k) = \frac{\partial}{\partial x_i}\left[\left(\mu + \sigma_k \frac{\bar{\rho}k}{\omega}\right)\frac{\partial k}{\partial x_i}\right] + P_k - \beta^* \bar{\rho} k\omega \quad 2\text{-}8$$

$$\frac{\partial}{\partial t}(\bar{\rho}\omega) + \frac{\partial}{\partial x_i}(\bar{\rho}\tilde{u}_i \omega) = \frac{\partial}{\partial x_i}\left[\left(\mu + \sigma_\omega \frac{\bar{\rho}k}{\omega}\right)\frac{\partial \omega}{\partial x_i}\right] + \alpha \frac{\omega}{k} P_k - \beta \bar{\rho}\omega^2 + \frac{\bar{\rho}\sigma_d}{\omega}\frac{\partial k}{\partial x_i}\frac{\partial \omega}{\partial x_i} \quad 2\text{-}9$$

Where

$$P_k = \tau_{ij}\frac{\partial \tilde{u}_i}{\partial x_j} \quad 2\text{-}10$$

$$\tau_{ij} = 2\,\mu_t \tilde{S}_{ij} - \frac{2}{3}\bar{\rho}k\delta_{ij} \quad 2\text{-}11$$

$$\tilde{S}_{ij} = \frac{1}{2}\left(\frac{\partial \tilde{u}_i}{\partial x_j} + \frac{\partial \tilde{u}_j}{\partial x_i}\right) - \frac{1}{3}\frac{\partial \tilde{u}_k}{\partial x_k}\delta_{ij} \quad 2\text{-}12$$

The eddy viscosity in this model is defined as Equation 2-13.

$$\mu_t = \bar{\rho}\frac{k}{\widehat{\omega}} \quad 2\text{-}13$$

Where $\widehat{\omega} = \max[\omega, C_{lim}\sqrt{\frac{2\tilde{S}_{ij}\tilde{S}_{ij}}{\beta^*}}]$. β^*, α, β, σ_k , σ_d , σ_ω and C_{lim} are constants or auxiliary functions which are given in [20].

The SST (Shear Stress Transport) Turbulence Model

The $k-\varepsilon$ model has two main weaknesses which are: over predicting the shear stress in adverse pressure gradient flows due to too low dissipation and requirement for near wall modification. The $k-\omega$ model is better in predicting adverse pressure gradient flow and it does not use any damping functions. However it is dependent on the value of ω in free stream flow. In order to improve these models, the SST model suggested by Menter [22] was developed. The SST is an eddy-viscosity model which is using a combination of k$-\varepsilon$ and $k-\omega$ models for the core flow and boundary layer, respectively. For this a blending function F1 is introduced which is equal to one in the near wall region and equal to zero for the flow domain in the outer region. It smoothly switches from the $k-\omega$ model in the

near wall region to the $k-\varepsilon$ model for the rest of the flow. In this way, the near-wall performance of the $k-\omega$ model can be used without the potential errors resulting from the free stream sensitivity of that model. The modelled equations for the turbulent kinetic energy k and the turbulence frequency ω can be written as follows:

$$\frac{\partial \bar{\rho}\mathrm{k}}{\partial \mathrm{t}}+\frac{\partial \bar{\rho}\tilde{\mathrm{u}}_{\mathrm{j}}\mathrm{k}}{\partial \mathrm{x}_{\mathrm{j}}}=(2\mu_{\mathrm{t}}\tilde{S}_{ij}-\frac{2}{3}\bar{\rho}k\delta_{ij})\frac{\partial \tilde{u}_i}{\partial x_j}-\beta^{*}\bar{\rho}\omega\mathrm{k}+\frac{\partial}{\partial \mathrm{x}_{\mathrm{j}}}\left((\mu+\sigma_{\mathrm{k}}\mu_{\mathrm{t}})\frac{\partial \mathrm{k}}{\partial \mathrm{x}_{\mathrm{j}}}\right) \quad 2\text{-}14$$

$$\frac{\partial \bar{\rho}\omega}{\partial \mathrm{t}}+\frac{\partial \bar{\rho}\tilde{\mathrm{u}}_{\mathrm{j}}\omega}{\partial \mathrm{x}_{\mathrm{j}}}=\frac{\gamma}{\mathrm{v}_{\mathrm{t}}}(2\mu_{\mathrm{t}}\tilde{S}_{ij}-\frac{2}{3}\bar{\rho}k\delta_{ij})\frac{\partial \tilde{u}_i}{\partial x_j}-\beta\bar{\rho}\omega^{2}+\frac{\partial}{\partial \mathrm{x}_{\mathrm{j}}}\left((\mu+\sigma_{\omega}\mu_{\mathrm{t}})\frac{\partial \omega}{\partial \mathrm{x}_{\mathrm{j}}}\right)+(1-\mathrm{F}_1)2\bar{\rho}\sigma_{\omega 2}\frac{1}{\omega}\frac{\partial \mathrm{k}}{\partial \mathrm{x}_{\mathrm{j}}}\frac{\partial \omega}{\partial \mathrm{x}_{\mathrm{j}}} \quad 2\text{-}15$$

Each of the constants is blend of an inner (1) and outer (2) constant as:

$$\emptyset=F_1\emptyset_1+(1-F_1)\emptyset_2 \quad 2\text{-}16$$

Where $\emptyset_1$ stands for constant 1 and $\emptyset_2$ represents constant 2. (e.g. $\sigma_{\omega}=F_1\sigma_{\omega 1}+(1-F_1)\,\sigma_{\omega 2}$).

Additional functions can be obtained from:

$$F_1=tanh(arg_1^4) \quad 2\text{-}17$$

$$arg_1=min(max\left(\frac{\sqrt{k}}{\beta^{*}\omega y},\frac{500v}{y^2\omega}\right);\frac{4\rho\sigma_{\omega 2}k}{CD_{k\omega}y^2}) \quad 2\text{-}18$$

$$CD_{k\omega}=max\left(2\bar{\rho}\sigma_{\omega 2}\frac{1}{\omega}\frac{\partial k}{\partial x_j}\frac{\partial \omega}{\partial x_j},1.0e-10\right) \quad 2\text{-}19$$

$$\mu_t=min[\frac{\bar{\rho}k}{\omega},\frac{a_1\bar{\rho}k}{SF_2}] \quad 2\text{-}20$$

ρ is density, μ_t is the turbulent viscosity, μ is the molecular dynamic viscosity, y is the distance from the field point to the nearest wall, and S is the vorticity magnitude.

and the blending function F_2 can be obtained from:

$$F_2=\tanh(arg_2^2) \quad 2\text{-}21$$

$$arg_2=\max(\left(\frac{2\sqrt{k}}{\beta^{*}\omega y},\frac{500\tilde{\nu}}{y^2\omega}\right)) \quad 2\text{-}22$$

$$\gamma_1=\frac{\beta_1}{\beta^{*}}-\frac{\sigma_{\omega 1}\lambda^2}{\sqrt{\beta^{*}}}\quad,\gamma_2=\frac{\beta_2}{\beta^{*}}-\frac{\sigma_{\omega 2}\lambda^2}{\sqrt{\beta^{*}}} \quad 2\text{-}23$$

The constants are taken from the ref. [22]:

$\beta^* = 0.09, a_1 = 0.31, \lambda=0.41$

$\beta_1 = 0.075, \sigma_{\omega 1} = 0.5, \sigma_{k1} = 0.85$

$\beta_2 = 0.0828, \sigma_{\omega 2} = 0.856, \sigma_{k2} = 1.0$

The SAS Turbulence Model

The Scale-Adaptive Simulation (SAS) is an advanced URANS model which allows better resolution of the turbulent spectrum in unstable flow conditions. This model can change smoothly between LES-like behavior in regions where the turbulence structure is well resolved and the SST model where the unsteady flow is not well resolved. The starting point of the transformation to the SST model is the k-vt formulation as given by Menter et al.[23].

The following equations have been derived there for the variables k and $\Phi = \sqrt{k}L$:

$$\frac{\partial \bar{\rho} k}{\partial t} + \frac{\partial \tilde{u}_j \rho k}{\partial x_j} = P_k - c_\mu^{\frac{3}{4}} \bar{\rho} \frac{k^2}{\Phi} + \frac{\partial}{\partial y}\left[\frac{\mu_t}{\sigma_k}\frac{\partial k}{\partial y}\right] \quad 2\text{-}24$$

$$\frac{\partial \bar{\rho} \Phi}{\partial t} + \frac{\partial u_j \bar{\rho} \Phi}{\partial x_j} = \zeta_1 \frac{\Phi}{k} P_k - \zeta_2 \mu_t S|u''| \frac{\Phi^2}{k^{3/2}} - \zeta_3 \bar{\rho} k + \frac{\partial}{\partial y}\left[\frac{\mu_t}{\sigma_\Phi}\frac{\partial \Phi}{\partial y}\right] \quad 2\text{-}25$$

$$P_k = \nu_t S^2, \ \nu_t = c_\mu^{1/4} \Phi \quad 2\text{-}26$$

with

$$|u''| = \sqrt{\frac{\partial^2 \tilde{u}_i}{\partial x_j^2}\frac{\partial^2 \tilde{u}_i}{\partial x_j^2}} \quad 2\text{-}27$$

Where S is the absolute value of strain rate. Constant used in the SAS model (i.e. ζ_1, ζ_2, ζ_3, cμ and κ) are given in [24].

Indeed these formulations, contrary to standard URANS models, provide a turbulent length scale, which is proportional to the local flow structure and not to the thickness of the turbulent layer. Since the second derivative term, |u"|, in the equation for Φ is the SAS-relevant term, the length scale predicted by the above model is largely proportional to the von Karman length scale as:

$$L_{vK} = \kappa \left| \frac{\frac{\partial \bar{u}}{\partial y}}{\frac{\partial^2 \bar{u}}{\partial y^2}} \right| \quad 2\text{-}28$$

The L_{vK} adjusts to the already resolved scales in a simulation and provides a length-scale, proportional to the size of the resolved eddies.

In order to add the SAS capability into the SST model, the Φ-equation is transformed to the k − ω framework using this relation: $\Phi = \frac{\mathbf{1}}{\mathbf{c_\mu^{1/4}}} \frac{\boldsymbol{k}}{\boldsymbol{\omega}}$.

The resulting ω-equation is:

$$\frac{\partial \bar{\rho}\Phi}{\partial t} + \frac{\partial \bar{\rho}\tilde{u_j}\omega}{\partial x_j} = \alpha\bar{\rho}S^2 - \beta\bar{\rho}\omega^2 + \frac{\partial \omega}{\partial x_j}\left(\frac{\mu_t}{\sigma_\omega}\frac{\partial \omega}{\partial x_j}\right) + \frac{2\bar{\rho}}{\sigma_\Phi}\left(\frac{1}{\omega}\frac{\partial k}{\partial x_j}\frac{\partial \omega}{\partial x_j} - \frac{k}{\omega^2}\frac{\partial \omega}{\partial x_j}\frac{\partial \omega}{\partial x_j}\right) + \tilde{\xi}_2\bar{\rho}\kappa S^2\frac{L}{L_{vK}} + \left[\frac{\bar{\rho}\omega}{k}\frac{\partial}{\partial x_j}\left(\frac{v_t}{\sigma_\omega}\frac{\partial k}{\partial x_j}\right)\left(\frac{1}{\sigma_k} - \frac{1}{\sigma_\Phi}\right)\right] \quad 2\text{-}29$$

The first three terms, on the RHS of the Equation 2-29, are the standard terms of the original Wilcox model. The second term, $\frac{2\bar{\rho}}{\sigma_\Phi}\left(\frac{1}{\omega}\frac{\partial k}{\partial x_j}\frac{\partial \omega}{\partial x_j}\right)$, is the cross diffusion term, which is also included in the SST model helping to prevent the free stream sensitivity. The last term including $\left(\frac{1}{\sigma_k} - \frac{1}{\sigma_\Phi}\right)$ is equal to 0. The remaining term is the $F_{SST-SAS}$ term, $\frac{-2\bar{\rho}}{\sigma_\Phi}\left(\frac{k}{\omega^2}\frac{\partial \omega}{\partial x_j}\frac{\partial \omega}{\partial x_j}\right) + \tilde{\xi}_2\bar{\rho}\kappa S^2\frac{L}{L_{vK}}$, which is meant to preserve the SST model in the RANS regime and to activate the SAS capability in the URANS regions. This term is modeled as follows:

$$F_{SST-SAS} = \bar{\rho}F_{SAS}max.\left[\tilde{\xi}_2\kappa S^2\frac{L}{L_{vK}} - \frac{2}{\sigma_\Phi}k.\max\left[\frac{1}{\omega^2}\left(\frac{\partial \omega}{\partial x_j}\frac{\partial \omega}{\partial x_j}\right), \frac{1}{k^2}\frac{\partial k}{\partial x_j}\frac{\partial k}{\partial x_j}\right], 0\right] \quad 2\text{-}30$$

F_{SAS}, $\tilde{\xi}_2$, and σ_Φ are constants value.

2.4.2 Combustion Model

The full numerical simulation of a combusting turbulent flow field without any assumptions is still not feasible. Due to limitations of the code and hardware (computational expense), the simulations have been carried out with the help of the Burning Velocity Model (BVM) model which is standard available in the ANSYS-CFX code. The basic principles and features of this model are discussed below [24-26]:

Burning Velocity Model

In premixed and partially premixed flames, the flamelets have a discontinuity between the burnt and the un-burnt regions; to analyze these kinds of flames, two important scalar variables (a mixture fraction and a progress variable) have been introduced which are defined in terms of a normalised fuel mass fraction. In this model the scalar reaction progress variable subdivides the flow field in two different areas, the burnt and the un-burnt mixture. Unlike the reactant and product mass fractions which vary continuously through the field, the progress variable as a convenient marker for both premixed and non-premixed zones is constrained to take values close to zero or unity everywhere except in the flamelets. Therefore burnt regions are treated similar to a diffusion flame whereas the un-burnt region is represented by the cold mixture. The mass fractions in the non-reacted fraction of the fluid, $Y_{i,fresh}$, are obtained by linear blending of fuel and oxidiser compositions. The species mass fractions in the burned fraction of the fluid, $Y_{i,burned}$, are computed by applying the flamelet model.

If a simple global reaction rate mechanism can be assumed, and ignoring the pressure variation, the thermochemistry of premixed combustion can be described in terms of two composition variables (e.g. mixture fraction $Z(x,t)$ and a reactant/product mass fraction$Y_i(x,t)$):

$$\frac{\partial(\rho Z)}{\partial t} + \nabla.(\rho u Z) = \nabla.(\rho D \nabla Z), \qquad 2\text{-}31$$

$$\frac{\partial(\rho Y_i)}{\partial t} + \nabla.(\rho u Y_i) = \nabla.(\rho D \nabla Y_i) + \dot{\omega}_i \qquad 2\text{-}32$$

$D(x,t)$ is the molecular diffusion coefficient, which is assumed to be applicable for all species. These two equations are applicable irrespective of whether combustion takes place premixed, partially premixed or non-premixed flames. However it is more convenient to replace the Y_i by a normalized quantity (i.e. progress variable $c(x,t)$), which is defined as:

$$Y_i(x,t) = Y_i(c(x,t), Z(x,t)) \qquad 2\text{-}33$$

Where $c(x,t) = 0$ in reactants and $c(x,t) = 1$ in equilibrium combustion products. By substitution of Equation 2-33 in to Equation 2-32 the instantaneous equation can be written as:

$$\frac{\partial(\rho c)}{\partial t} + \nabla.(\rho u c) = \nabla.(\rho D \nabla c) + \frac{1}{\partial \rho Y_i / \partial c}.\left[\dot{\omega}_i + \frac{\partial^2 Y_i}{\partial c^2}\rho\chi_c + \frac{\partial^2 Y_i}{\partial Z^2}\rho\chi_Z + \frac{\partial^2 Y_i}{\partial c \partial Z}\rho\chi_{Z,c}\right] \quad 2\text{-}34$$

The dependency of Y_i and Z leads to the appearance of three additional terms which will be absent in the fully premixed case. These terms contain the following scalar dissipation quantities:

$$\chi_Z = D\nabla Z.\nabla Z \quad 2\text{-}35$$

$$\chi_c = D\nabla c.\nabla c \quad 2\text{-}36$$

$$\chi_{Z,c} = D\nabla Z.\nabla c \quad 2\text{-}37$$

Equation 2-34 can be applied for the all modes of combustion, while without the above mentioned scalar dissipation terms it is only applicable for the fully premixed combustion. The correct consideration for the partially premixed and non-premixed modes is depended on the dissipation terms. More detailed information about the chemical and molecular terms in the transport equations is given in [26].

For use in Favre-averaged turbulent combustion simulations, the scalars have to be Favre-averaged. As explained before, at any given time and position in space the fluid is considered to be either fresh materials or fully reacted. Then, the averaged reaction progress variable, $\tilde{c}$, is the probability for the instantaneous state of the fluid being reacted. The mean species composition of the fluid is computed according to:

$$\widetilde{Y_i} = (1-\tilde{c})\widetilde{Y}_{i,fresh} + \tilde{c}\widetilde{Y}_{i,burned} \quad 2\text{-}38$$

And

$$\tilde{F} = \tilde{Z}.(1-\tilde{c}) \quad 2\text{-}39$$

Which F and Z are weighted reaction progress and mixture fraction, respectively.

The reaction progress variable is computed from the following transport equation:

$$\frac{\partial(\bar{\rho}\tilde{c})}{\partial t} + \frac{\partial(\bar{\rho}\widetilde{u_j}\,\tilde{c})}{\partial x_j} = \frac{\partial}{\partial x_j}\left[(\overline{\rho D} + \frac{\mu_t}{\sigma_F})\frac{\partial \tilde{c}}{\partial x_j}\right] + \bar{\omega}_c \quad 2\text{-}40$$

The weighted reaction progress variable is computed by solving a transport equation:

$$\frac{\partial(\bar{\rho}\tilde{F})}{\partial t}+\frac{\partial(\bar{\rho}\widetilde{u_j}\,\tilde{F})}{\partial x_j} = \frac{\partial}{\partial x_j}\left[(\overline{\rho D}+\frac{\mu_t}{\sigma_F})\frac{\partial\tilde{F}}{\partial x_j}\right]+2(\overline{\rho D}+\frac{\mu_t}{\sigma_F})(\frac{\partial\tilde{Z}}{\partial x_j}.\frac{\partial\tilde{c}}{\partial x_j})-\tilde{Z}\overline{\omega_c} \quad 2\text{-}41$$

The default value of the turbulent Schmidt number for the weighted reaction progress variable is $\sigma_F = 0.9$.

The burning velocity model (BVM) is used to close the combustion source term for reaction progress.

$$\overline{\omega}_c = \bar{S}_c - \frac{\partial}{\partial x_j}\left((\overline{\rho D})\frac{\partial\tilde{c}}{\partial x_J}\right) \quad 2\text{-}42$$

$$\bar{S}_c = \bar{\rho}_u S_T|\nabla\tilde{c}| \quad 2\text{-}43$$

Where $\bar{\rho}_u$ is the density of the unburnt mixture. The diffusive exchange of species and energy, which makes the flame proceed in space, is already accounted for by the source term $\overline{S}_c$. the turbulent burning velocity is calculated using the Zimont model [24].

2.5 Results and discussion

2.5.1 Configuration 1: Back ward facing step according to Pitz and Daily set up

This test case deals with the turbulent premixed propane/air flame stabilized at a backward facing step which has been studied experimentally by Pitz et al.[13]. The test rig is shown in Figure 2-2. The air and propane are combined using three parallel venturi tubes and then mixed in a one meter long premixed section. The flow converges over the backside of the profile step with a 2:1 area ratio. The premixed flame is stabilized in a turbulent mixing layer at the edge of a 25 mm high step. The geometry shown in the Figure 2-2, is completely described in [13]. Here, the simulations are performed for the non-reacting (ϕ=0) and reacting (ϕ=0.57) premixed propane/air flow at a Reynolds number equal to 22,000. The Reynolds number ($\mathrm{Re_h} = \frac{U_0 H}{\upsilon}$) is defined based on the step height, H, average inlet velocity, U_0, and kinetic viscosity, υ. The chosen computational domain which excludes the premixed section is 347 mm long, 51 mm high and has a third dimension in a span-wise direction with a thickness equal to the size of one numerical element. The velocity field at the inlet is specified as that of a fully-

developed turbulent channel flow at the equivalent Reynolds number. A pressure-based outlet boundary condition is used for the outflow. The other boundaries are considered as adiabatic and no-slip velocity boundary conditions, whereas the side walls are symmetric.

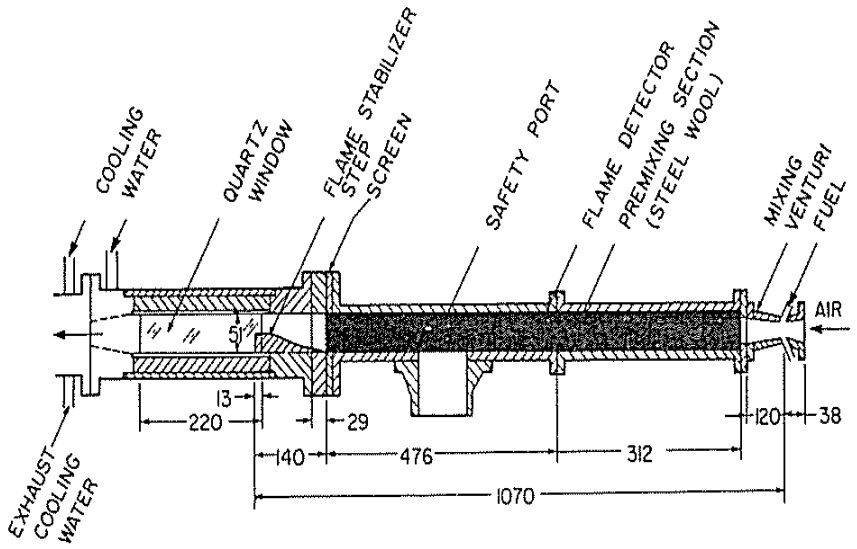

(a)

(b)

Figure 2-2: (a) the experimental set up (from [13]) (b) simplified CFD domain including the flame stabilizer step (i.e. configuration 1)

For the presentation of the results we first start with the general description of the two-dimensional flow field presented for a non-reacting condition. Calculations are done by using various turbulence models. The issues related to each model are addressed and the best model is selected for the further calculations. The reacting case is next simulated by using the chosen turbulence model from previous calculations. Figure 2-3 compares the results for velocity profile at the step (i.e. X/H=0) and X/H=3 for non-reacting flow. Here, three different turbulence models

are used. Numerical predictions of streamwise mean velocity using various turbulence models show a similar trend of flow over the step. The velocity profiles indicate that the flow separated at the step, resulting in recirculation regions behind the step, and then redeveloped along the channel which agrees well with the experimental results. The turbulence model which gave the best prediction in the non-reacting configuration is SAS-SST, while there is still some tendency to over-predict the velocity. Furthermore, the size of the mean recirculation region can be used as a comparative tool for determining the accuracy of backward facing step computations. The size of the recirculation vortex is defined by the reattachment length, L, which is the distance from the step face to the point of zero wall shear stress. It can be also estimated from the velocity field. The predicted value of the reattachment length is reported in Table 2-2. The SST turbulence model predicted the reattachment length with an error as small as about 5%. More significant error is observed for the $k-\omega$ model with the predicted reattachment length at the position of 6.54 H. While the predicted mean reattachment point by using the SAS-SST model is computed to 6.78 H which gives just about 3% deviation from the measured value of 7H.

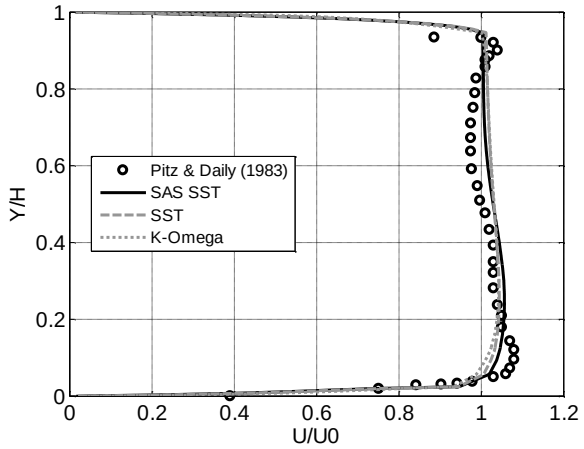

(a)

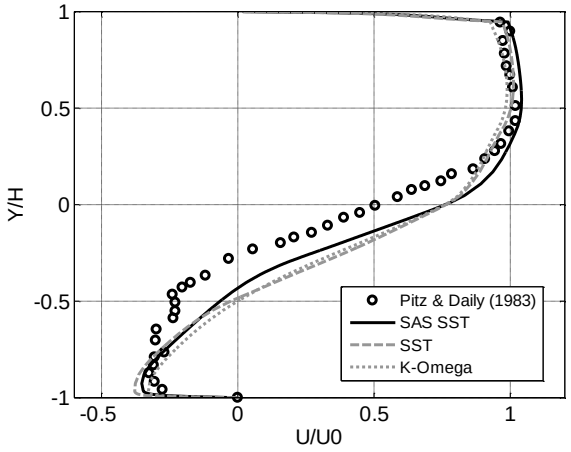

(b)

Figure 2-3: Predicted velocity profile of Configuration 1 at (a) X/H=0 (b) X/H=3 for non-reacting flow (ϕ=0)

Table 2-2: Reattachment lengths calculated at Re_h=22,000 for non-reacting flow (ϕ=0)

	L/H	
	Present work	Error (%)
SAS SST	6.78	3.14
SST	6.67	4.71
$k-\omega$	6.54	6.57
Experiment [13]	7	---

To assess the effect of the combustion processes on the mean flow field, transient average stream-wise velocity profiles for the reacting flow are presented in Figure 2-4 at three different sections using the BVM combustion model. BVM uses a RIF flamelet library [24] for the 'burnt' mixture; this mechanism involves a 35 species 108 reactions scheme for the propane-air gas mixture. Based on the previous results for non-reacting flow, the SAS-SST model, which gives the best non-reacting flow prediction, is used to model the turbulence effects. Overall, one can say this model yields satisfactory results for the mean velocity profile of the reacting flow. Just behind the step at X/H=1 the flow is almost stagnant and not very turbulent. In this location at the step height (i.e. Y/H=0), there is a large velocity gradient while further downstream where the hot reactants are penetrating into the cold flow at the center of the channel, velocity changes gradually. The maximum reverse velocity in the non-reacting flow at X/H=3 was 0.31 U_0; while as seen in Figure 2-4, in the reacting flow it is about 0.47 U0 meaning that the maximum reverse velocity in the reacting flow is higher which is due to the heat release. The important observation is that within the height of the step (Y/H<0), the reverse velocity is underpredicted by the model pointing to the fact that the strength of the predicted recirculation zone is less than the measurements. While above the step height (i.e. center channel), velocity profiles are in good agreement with the measurements. That can be explained due to the deviation from two-dimensional behavior which can affect the size and strength of the vortexes formed behind the step.

Table 2-3 shows reattachment lengths calculated for the reacting flow. Here, as a result of the expansion due to combustion, the reattachment length decreases 35% compared to the non-reacting flow (L/H=7). In this case, the reattachment length is numerically predicted with an error about 2% which is fairly acceptable.

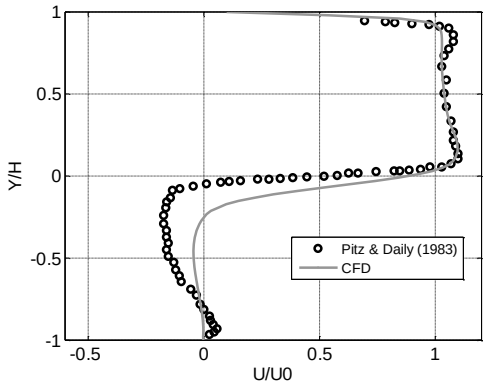

(a)

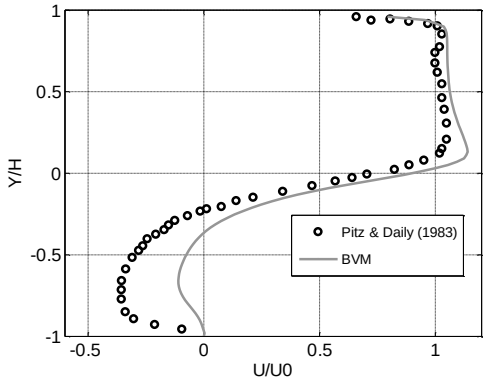

(b)

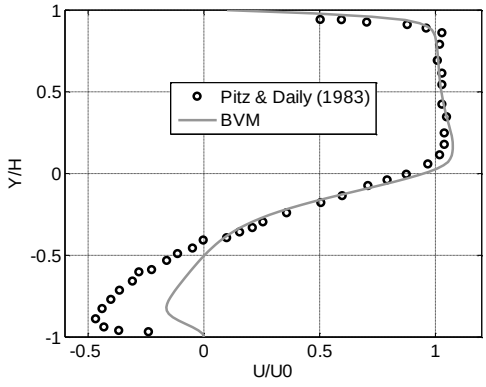

(c)

Figure 2-4: Predicted stream-wise velocity profile in configuration 1 at (a) X/H=1 (b) X/H=2 (c) X/H=3 for reacting flow (ϕ=0.57)

Table 2-3: Reattachment lengths calculated at Re_h=22000 for Reacting flow (ϕ=0.57)

	L/H		
	Present work	Experiment [13]	Error (%)
Reacting flow	4.4	4.5	2.2

2.5.2 Configuration 2: Back ward facing step with heated wall

Due to the thermal interaction between hot gases and the colder liner wall, and also the correlation between gas temperature, density and speed of sound, correct prediction of the heat transfer is of high importance. The effects of the enhanced heat transfer between hot gases and the liner during the unstable regime of the combustor may result in damage of the liner where there is interaction between the flame and the wall. For this reason and to verify the accuracy of the models to predict the heat transfer, in this section simulations are done for the case of stationary flow across a backward facing step with a heat source embedded across the bottom wall downstream the step. Geometric details of the control volume and the coordinate system applied in this section follows the setup as used by Vogel et al.[14]; the length of the domain is 40 H, the height upstream and downstream of the step are respectively equal to 4 H and 5 H for an expansion ratio $ER = \frac{W}{(W-H)}$ of 1.25, while the value of H is taken as 3.8 cm. Similar to the configuration 1, the CFD domain in this configuration has a third dimension with a thickness equal to the size of one numerical element. Definition of the boundary condition relies on the properties of the physical condition known through the experimental data. Therefore, a constant heat flux, $q''=270 W/m^2$ is embedded across the bottom wall, downstream of the step. To make a comparison in this case the Reynolds number (Re_h) is fixed to 28,000 and air at ambient temperature is selected as a working fluid. The chamber is subjected to an external air flow at room temperature entering the computational domain upstream of the step expanding downstream and forms a recirculation region as it is shown in Figure 2-5. The velocity field at the inlet is specified as that of a fully-developed turbulent channel flow at a similar Reynolds number. However the reference free stream velocity is equal to 11.3 m/s. A pressure-based outlet boundary condition is used for the outflow. The other boundaries are considered as adiabatic and no-slip velocity boundary conditions.

Based on the previous calculations done on the configuration 1, the SAS-SST model is chosen for modeling the turbulence effects.

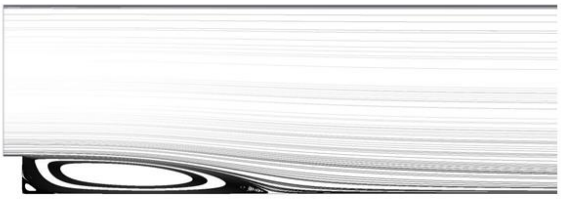

Figure 2-5: Stream function of mean flow averaged in space

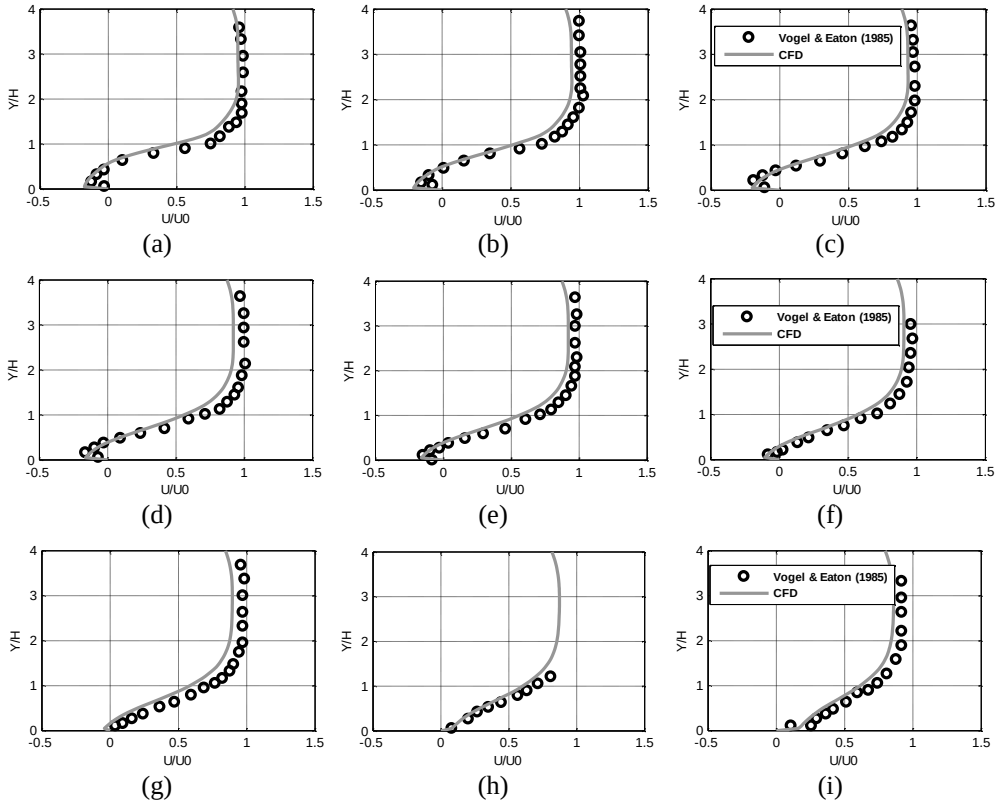

Figure 2-6: Velocity profiles at various locations (a) X/H=2.3, (b) X/H=3, (c) X/H=3.73, (d) X/H=4.46, (e) X/H=5.20, (f) X/H=5.94, (g) X/H=6.67, (h) X/H=7.4, (i) X/H=8.87

According to Figure 2-6, the main bulk of the flow field away from the wall was modelled fairly well. Velocity profiles showed good agreement with the experiments. The main differences are observed near the bottom wall, especially in vicinity of the centre of the recirculating zone. Here, the velocity gradients are under predicted. The reattachment length is predicted to be 6.8 H which gives an error of 1.9% compared to the measured value of 6.67 H. Generally velocity profiles demonstrate the growth of the shear layer, and the subsequent contact of flow with the wall at the reattachment point.

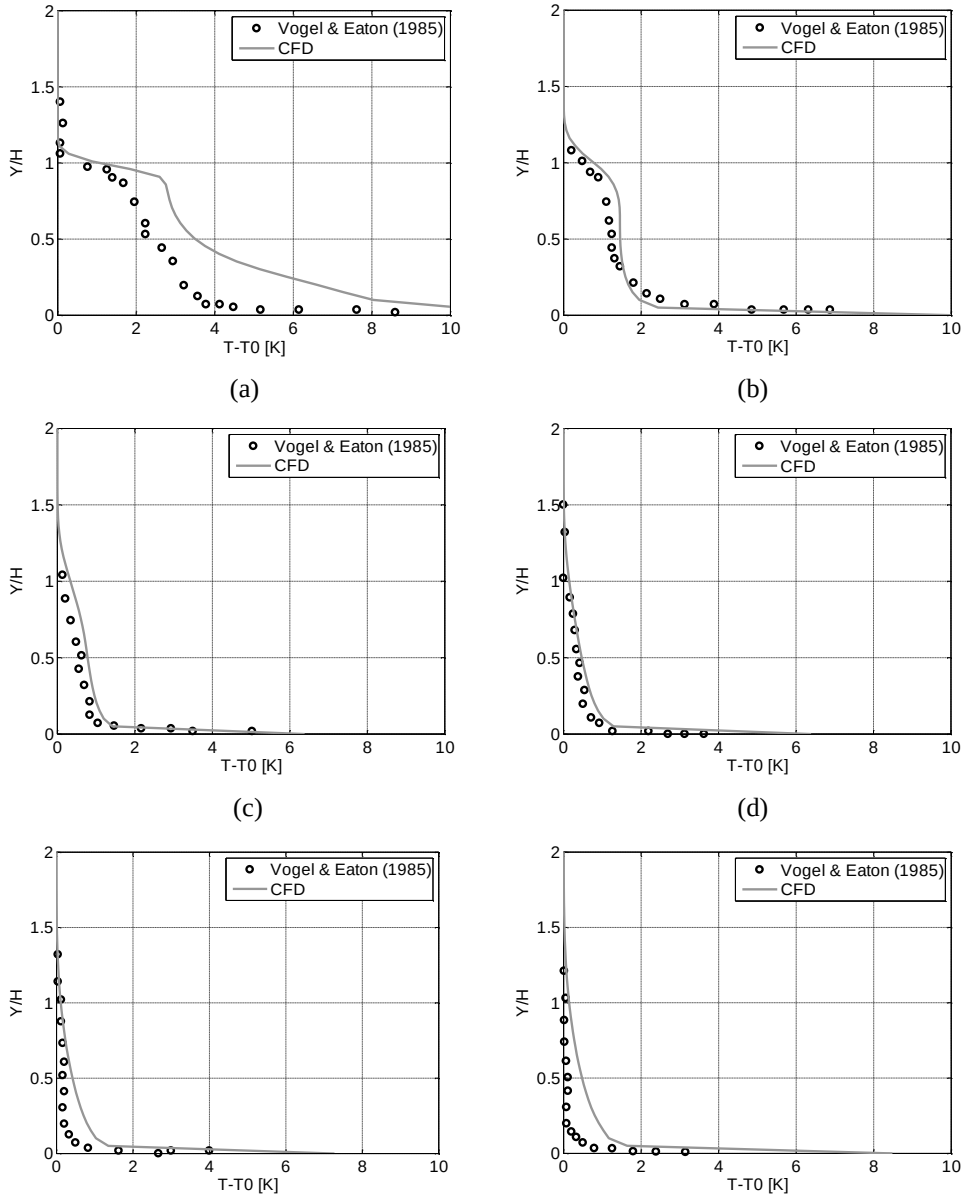

Figure 2-7: Temperature profiles at different locations (a) X/H=0.33, (b) X/H=1.7, (c) X/H=4.3, (d) X/H=7, (e) X/H=9.7, (f) X/H=15

Figure 2-7 shows the comparison of the temperature profiles at different streamwise positions downstream of the step. Significant gradients in the temperature are observed in the near wall region along the length of the downstream section. The only exception, (i.e. the only region far from the wall where significant temperature gradients occur) is immediately behind the step. This is due to the presence of the secondary bubble as well as the larger recirculating zone squeezing the induced flow. The spread of the mean temperature gradients downstream the reattachment location clearly shows the growth of the thermal boundary layer.

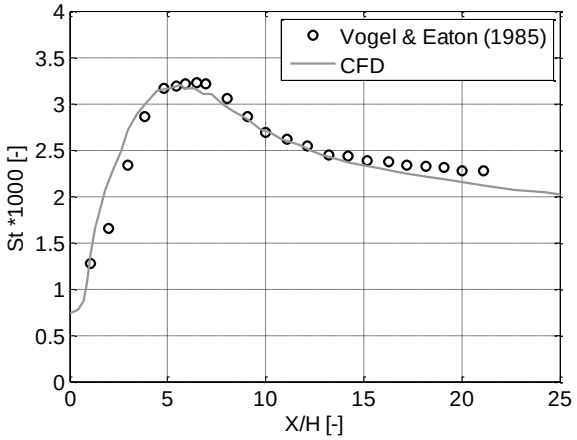

Figure 2-8: Predicted and measured Stanton number along the bottom line of the BFS

Figure 2-8 compares the predicted and measured Stanton number (St); this dimensionless number represents the ratio of heat which is transferred into the fluid to the thermal capacity of the fluid, as:

$$St = \frac{h_c}{\rho u c_p} \qquad 2\text{-}44$$

where h_c is the convection heat transfer coefficient, equal to the ratio of heat flux (q″) to temperature difference between wall temperature (T_w) and external boundary temperature (T_0); ρ , c_p and u are the density, the specific heat and speed of the fluid , respectively.

According to the Figure 2-8, both Stanton number profiles show the same feature. The position of the maximal Stanton number peak and also the peak magnitude are

precisely predicted which are in consistence with experiments. Keeping in mind that the location of X/H=0 corresponds to the step location, it can be observed that the low heat transfer rate occurs in the recirculation region which is followed by a steep increase. The maximum value of Stanton number is achieved approximately slightly upstream of reattachment point which is equal to 6.8 H. Compared to Figure 2-7, it can be concluded that the decrease in wall temperature (T-T0) is accompanied by an increase in convective heat transfer till its maximum value near the reattachment point, while downstream the reattachment the Stanton number decreases as the wall temperature is increased.

Conclusion

In this work, numerical investigation of turbulent flow with regions of separation behind a Back ward facing step have been carried out for both reacting and non-reacting flow. Among the investigated turbulence models ($k-\omega$, SST and SAS-SST), SAS-SST model showed the best agreement with the experimental data. The chosen turbulence model was used for the calculation of well documented case of turbulent flow over a back ward facing step with the heated wall, showing satisfactory results compared to experimental data. For modeling of the reacting flow, the BVM combustion model was used. The predicted results using this model showed accurate results with an error about 2% on prediction of reattachment length.

Acknowledgements

The authors would like to acknowledge the support of the EC in the Marie Curie Actions – Networks for Initial Training, under call FP7-PEOPLE-2007-1-1-ITN, Project LIMOUSINE with project number 214905.

References

[1] Abbott, D. E., and Kline, S. J., 1962, "Experimental Investigation of Subsonic Turbulent Flow Over Single and Double Backward Facing Steps," Journal of Basic Engineering, 84(3), pp. 317-325.
[2] Adams, E. W., and Johnston, J. P., 1988, "Effects of the separating shear layer on the reattachment flow structure part 2: Reattachment length and wall shear stress," Experiments in Fluids, 6(7), pp. 493-499.

[3] Friedrich, R., and Arnal, M., 1990, "Analysing turbulent backward-facing step flow with the lowpass-filtered navier-stokes equations," Journal of Wind Engineering and Industrial Aerodynamics, 35(0), pp. 101-128.
[4] Avancha, R. V. R., and Pletcher, R. H., 2002, "Large eddy simulation of the turbulent flow past a backward-facing step with heat transfer and property variations," International Journal of Heat and Fluid Flow, 23(5), pp. 601-614.
[5] Armaly, B. F., Durst, F., Pereira, J. C. F., and Schönung, B., 1983, "Experimental and theoretical investigation of backward-facing step flow," Journal of Fluid Mechanics, 127, pp. 473-496.
[6] Pozarlik, A. K., and Kok, J. B. W., 2012, "Numerical Simulation of a Turbulent Flow Over a Backward Facing Step With Heated Wall: Effect of Pulsating Velocity and Oscillating Wall," Journal of thermal science and engineering applications, 4(4), p. 041005.
[7] Lee, S. Y., Seo, S., Broda, J. C., Pal, S., and Santoro, R. J., 2000, "An experimental estimation of mean reaction rate and flame structure during combustion instability in a lean premixed gas turbine combustor," Proceedings of the Combustion Institute, 28(1), pp. 775-782.
[8] Schadow, K. C., and Gutmark, E., 1992, "Combustion instability related to vortex shedding in dump combustors and their passive control," Progress in Energy and Combustion Science, 18(2), pp. 117-132.
[9] Emerson, B., O'Connor, J., Juniper, M., and Lieuwen, T., 2012, "Density ratio effects on reacting bluff-body flow field characteristics," Journal of Fluid Mechanics, 706, p. 219 250.
[10] Rees, S. J., 2009, "Hydrodynamic instability of confined jets & wakes and implications for gas turbine fuel injectors," PhD thesis, University of Cambridge.
[11] Pozarlik, A. K., 2010, "Vibro-acoustical instabilities induced by combustion dynamics in gas turbine combustors," PhD, University of Twente, Enschede, The Netherlands.
[12] Altay, H. M., Speth, R. L., Hudgins, D. E., and Ghoniem, A. F., 2009, "Flame–vortex interaction driven combustion dynamics in a backward-facing step combustor," Combustion and Flame, 156(5), pp. 1111-1125.
[13] Pitz, R. W., and Daily, J. W., 1983 "Experimental study of combustion in a turbulent free shear layer formed at a rearward facing step," AIAA Journal, 21(11), pp. 1565-1570.
[14] Vogel, J. C., and Eaton, J. K., 1985, "Combined Heat Transfer and Fluid Dynamic Measurements Downstream of a Backward-Facing Step," Journal of Heat Transfer, 107(4), pp. 922-929.
[15] Biswas, G., Breuer, M., and Durst, F., 2004, "Backward-facing step flows for various expansion ratios at low and moderate Reynolds numbers," Journal of Fluids Engineering, 126(3), pp. 362-374.
[16] Lee, T., and Mateescu, D., 1998, "Experimental and numerical investigation of 2-D backward-facing step flow," Journal of Fluids and Structures, 12(6), pp. 703-716.
[17] Patankar, S. V., 1980, Numerical Heat Transfer and Fluid Flow, Hemisphere, New York.
[18] L.Y.M. Gicquel, G. Staffelbach, and Poinsot, T., 2012, "Large Eddy simulations of gaseous flames in gas turbine combustion chambers," Progress in Energy and Combustion Science, 38(6), pp. 782–817.
[19] Versteeg, H. K., and Malalasekera, W., 2007, An Introduction to Computational Fluid Dynamics: The Finite Volume Method, Pearson Education Limited.

[20] Wilcox, D. C., 2006, Turbulence modeling for CFD, DCW Industries, Inc., , La Canada CA.
[21] Wilcox, D. C., 2008, "Formulation of the k-omega turbulence model revisited," AIAA Journal, 46(11), pp. 2823-2838.
[22] Menter, F. R., 1994, "2-Equation Eddy-Viscosity Turbulence Models for Engineering Applications," Aiaa Journal, 32(8), pp. 1598-1605.
[23] Menter, F. R., and Egorov, Y., 2010, "The Scale-Adaptive Simulation Method for Unsteady Turbulent Flow Predictions. Part 1: Theory and Model Description," Flow Turbulence and Combustion, 85(1), pp. 113-138.
[24] ANSYS, December 2006, "ANSYS CFX-Solver Theory guide," ANSYS CFX Release 11.0.
[25] Zimont, V. L., 2000, "Gas premixed combustion at high turbulence. Turbulent flame closure combustion model," Experimental Thermal and Fluid Science, 21(1–3), pp. 179-186.
[26] Bray, K., Domingo, P., and Vervisch, L., 2005, "Role of the progress variable in models for partially premixed turbulent combustion," Combustion and Flame, 141(4), pp. 431-437.

3

Sensitivity of the Numerical Prediction of Turbulent Combustion Dynamics in the LIMOUSINE Combustor

Mina Shahi, Jim. B.W.Kok, Artur Pozarlik. J.C. Roman Casado, Thomas Sponfeldner

University of Twente, Faculty of Engineering Technology, Laboratory of Thermal Engineering, Enschede, the Netherlands
Department of Mechanical Engineering, Imperial College London, London, UK

Published in J. Eng. Gas Turbines Power 136(2) 2014

Abstract

The objective of this study is to investigate the sensitivity and accuracy of the reaction flow field prediction for the LIMOUSINE combustor with regard to choices in computational mesh and turbulent combustion model. The LIMOUSINE combustor is a partially premixed bluff body stabilized natural gas combustor designed to operate at 20-80 kW and atmospheric pressure and used to study combustion instabilities. The transient simulation of a turbulent combusting flow with the purpose to study thermo-acoustic instabilities is a very time consuming process. For that reason the meshing approach leading to accurate numerical prediction, known sensitivity, and minimized amount of mesh elements is important. Since the numerical dissipation (and dispersion) is highly dependent on, and affected by, the geometrical mesh quality, it is of high importance to control the mesh distribution and element size across the computational domain. Typically, the structural mesh topology allows using much less grid elements compared to the unstructured grid, however an unstructured mesh is favorable for flows in complex geometries. To explore computational stability and accuracy, the numerical dissipation of the cold flow with

mixing of fuel and air is studied first in the absence of the combustion process. Thereafter the studies are extended to combustible flows using standard available ANSYS-CFX combustion models. To validate the predicted variable fields of the combustor's transient reactive flows, the numerical results for dynamic pressure and temperature variations, resolved under structured and unstructured mesh conditions, are compared with experimental data. The obtained results show minor dependence on the used mesh in the velocity and pressure profiles of the investigated grids under non-reacting conditions. More significant differences are observed in the mixing behavior of air and fuel flows. Here the numerical dissipation of the (unstructured) tetrahedral mesh topology is higher than in the case of the (structured) hexahedral mesh. For that reason, the combusting flow, resolved with the use of the hexahedral mesh presents better agreement with experimental data and demands less computational effort. Finally in the paper the performance of the combustion model for reacting flow is presented, and the main issues of the applied combustion modeling are reviewed.

Keywords*: structured mesh, unstructured mesh, RANS solver, partially premixed combustion.*

3.1 Introduction

The first step for the CFD calculation is the generation of a mesh in the domain of interest, on which the governing partial differential transport equations can be discretized. Nowadays, many different element and grid types are available; however the choice highly depends on the problem and the solver capabilities, because every method has advantages and disadvantages. One category of meshes are the structured meshes. A structured mesh is a mesh which uses a uniform element shape. The topology of the cells in a structured mesh is specified for the mesh as a whole, and is not deduced from the nodes. Another type of mesh is the unstructured mesh. Unlike a structured mesh, unstructured grids employ an irregular mesh to cover a volume, using geometry mesh entities like faces, edges and nodes [1, 2]. An overview of unstructured mesh techniques for computational fluid dynamics is given by Mavriplis [3] and Kikuchi[4].

In general, structured grid approaches are often used with implicit formulations [5], while unstructured methods seem to be more conveniently used with the explicit formulations [6]. In general, implicit methods used on structured grids seem to be more stable, accurate and converge faster, at least for a large class of practical test cases [7]. In this specific context, to the best knowledge of the authors there is no literature directly evaluating the impact of using

fully structured versus unstructured flow solvers on RANS modeling of combustible flows.

Hansen et al. [8] investigated the performance of unstructured grids for turbulence resolving calculations in the application of flow over a circular cylinder at Reynolds numbers 3,900-140,000. They came to the conclusion that good comparison with experimental data was obtained with the use of structured grids for variables like the Strouhal number, time-averaged drag, back pressure, and recirculation zone length. For simulations of flows at a Reynolds number of 140,000, the time-averaged coefficient of pressure and drag fell within two separate sets of experiments and closely match a similar set of computations on structured grids using a high order of discretization solver.

Studies done by Hua et al. [9] on the flow near a spur-dike indicate that the precision with unstructured grids is higher than that with structured grids in spite that the CPU time required is slightly more with unstructured grids.

Studies done by Tomita et al. [10] showed the strong influence of mesh type on the flow quantities. However they proved that for both structured and unstructured mesh types, the SST turbulence model presented good prediction compared to experiments, while for simulations with other turbulence models like (RSM) results using the structured mesh were superior.

Hence it can be concluded that on basis of the literature the accuracy of the flow simulation is sometimes, but not always, best with a structured solver and it seems to be dependent on the flow geometry and the quality of the mesh generator. For this reason our purpose in this study is to explore the performance and limitations of certain structured and unstructured grids to investigate the numerical dissipation of the fuel/air mixture flow specifically for the bluff body flow in the LIMOUSINE combustor. All experimental data used for validation of this study is taken from [11]. The experimental configuration and computational domain are first introduced in the section “combustor setup”. The next Section “numerical method” provides the details about the numerical methods, meshes and sets of boundary conditions used for CFD calculations. The applied physical models for turbulence and combustion are presented in the section “modeling of turbulence and combustion”. Due to the importance of the mixing as a determining factor in the combustion modeling, the first part of the result section is devoted to the analysis of the mixture flow in the absence of the combustion process. CFD predictions obtained by using a fully structured and a fully unstructured solver are

discussed and compared to experiments. Subsequently, studies are extended to flows with combustion using combustion models standard available in ANSYS-CFX.

3.2 Combustor setup

The experiment, which is used as a basis for modeling studies, is performed on a test rig which is shown in Figure 3-1 [11]. It is located at the University of Twente and 4 other laboratories, within the framework of the European Marie Curie Initial Training Network project "LIMOUSINE". The set-up is designed to study limit cycles of combustion rate oscillations due to thermo-acoustic instability. The combustor consists of two sequentially coupled rectangular ducts with different widths, with the burner in between the two ducts. The duct upstream of the burner has a 25x150 mm^2 cross section and is 275 mm long, whereas the duct downstream the burner has a cross sectional area enlarged to 50x150 mm^2, to partly compensate the volume expansion due to the combustion. In the transition between the ducts the burner is mounted, that creates a flow recirculation pattern that stabilizes the flame, by means of a triangular bluff body. In this configuration which is the third design version of the combustor (V3), the total length of the combustor is 1050 mm (see Table 3-1 for dimensions). Therefore the width (150 mm) of the combustor is much larger than the depth (50 mm), but much less than the height, and the system approximates in behavior a two dimensional combustor. Details about dimensions of the model combustor are summarized in Table 3-1. Air as the oxidizer is injected at the upstream end. The flow recirculation that stabilizes the flame is in this case created by a wedge, which is placed at the point where the small duct is attached to the large duct. From the side surfaces of the wedge gaseous fuel is injected through 62 holes. The fuel used here is methane at room temperature. All pieces, except the brass bluff body, are made from heat resistant stainless steel S310. The only cooling of the combustor is by natural convection and radiation at the outside surfaces. The burner can operate at a range of power of 20-80 kW and air factor 0.8-2.

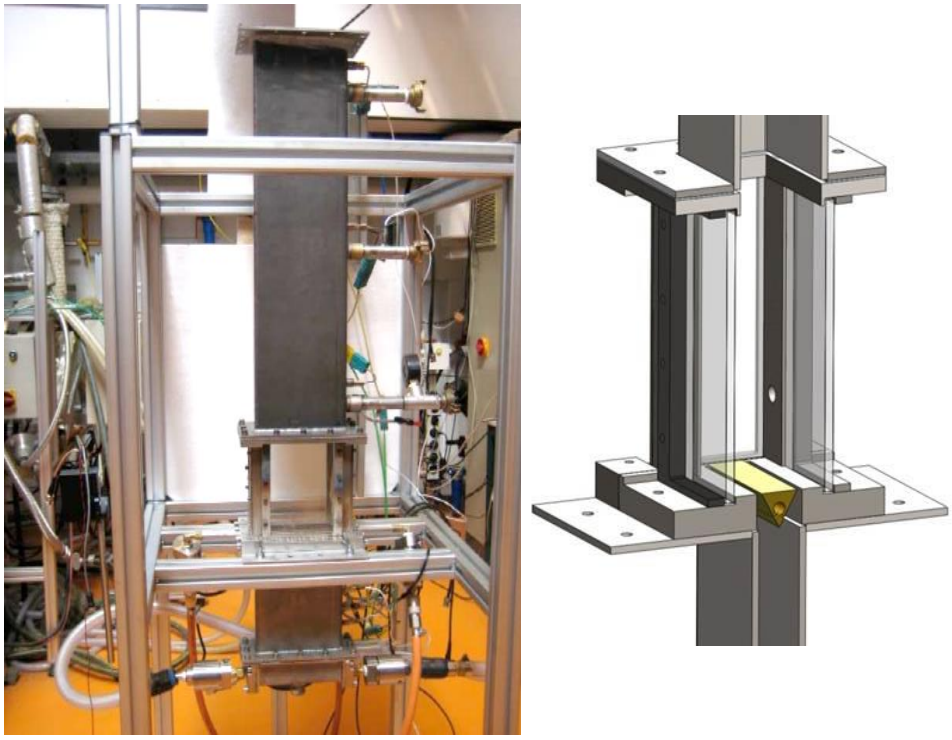

(a) (b)

Figure 3-1: (a) experimental set up (b) limousine burner

Table 3-1: Dimensions of the model combustor

Location	Dimension (mm)
Upstream height	220
Upstream width	25
Downstream height	780
Downstream width	50
Width of the combustor in the third direction	150

3.3 Numerical method

The CFD code employed here is ANSYS-CFX 14.0. It uses an implicit finite volume formulation to construct the discretized equations representing the Reynolds Averaged Navier-Stokes equations for the fluid flow. The model consists of a compressible solver with a co-located (non-staggered) finite volume method, such that the control volumes are identical for all transport equations [12]. To avoid the decoupling of the pressure field, CFX uses the Rhie-Chow [13] discretization method for the mass terms, as modified by Majumdar [14]. A coupled algebraic multi-grid solver is used to give robust solutions for the governing system of linearized equations representing the differential transport equations in discretized form. For the discretization of the governing equations a high resolution advection scheme spatial method and a second order backward Euler discretization for time accuracy is used. The computational geometry used in the solution process is illustrated in Figure 3-2.

Details about boundary conditions imposed on the domain are summarized in Table 3-2. The flow parameters are set consistent with the experimental conditions depicted in Table 3-3. The closed acoustic inlet boundary condition at the upstream end was implemented by prescribing a uniform and steady inlet velocity profile at the air inlet, which ensured an acoustically closed inlet. The mass flow rate of fuel per unit cross sectional area was specified at the fuel inlet. At the combustor outlet the pressure was set to a constant value of 1 atm, which represents the open acoustic boundary condition. In order to take in to account the effect of heat losses through the walls, the walls were treated as convective boundaries where an outside heat transfer coefficient and outside temperature were specified.

In this work the effects of turbulence are simulated by using the Shear Stress Transport Turbulence Model (SST) in the steady state calculations, while for the transient calculations the Scale-Adaptive Simulation model (SAS) is used. Reacting flow simulations are carried out on the model combustor using different combustion models which are standard available in ANSYS-CFX. In the following sections the used turbulence and combustion models are described briefly.

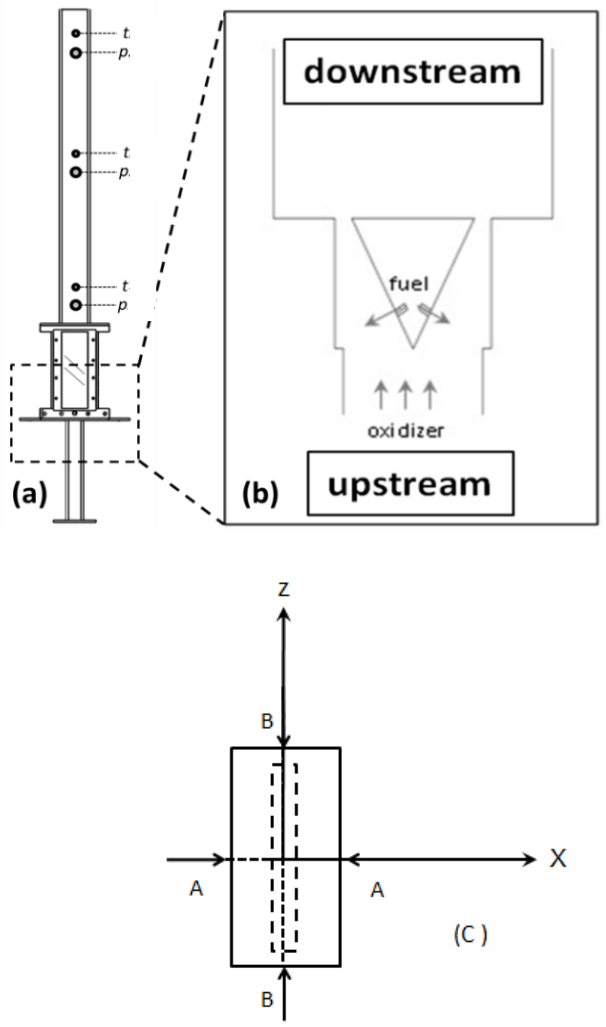

Figure 3-2: A schematic representation of the model combustor: (a) computational domain in CFD calculation (b) an enlarged view around the wedge (c) cross sectional area of the combustor (view from the top)

Table 3-2: Details about boundary condition

Location	B.C
Air Inlet	Normal speed
Fuel Inlet	Mass flow rate
Outlet	Average static pressure
Walls	Non-slip

Table 3-3: Operating condition

Power (kW)	Air factor	Fuel mass flow rate [g/s]	Air mass flow rate [g/s]
40	1.4	0.8	19.152
60	1.2	1.2	24.624

3.3.1 Modeling of Turbulence and combustion

The SST (shear stress transport) turbulence model

The $k-\varepsilon$ turbulence model has two main weaknesses as: over predicting the shear stress in adverse pressure gradient flows, due to too low dissipation, and requirement for wall modification. The $k-\omega$ model is better in predicting the adverse pressure gradient flow and it does not use any damping functions. However, it is dependent on the value of ω in the free stream flow. In order to improve these models, the SST model suggested by Menter [15] was developed. The SST is an eddy-viscosity model which is using a combination of $k-\varepsilon$ and $k-\omega$ models for the core flow and boundary layer, respectively. For this a blending function F1 is introduced which is equal to one in the near wall region and equal to zero for the flow domain in the outer region. It smoothly switches from the $k-\omega$ model in the near wall region to the $k-\varepsilon$ model for the rest of the flow. In this way, the near-wall performance of the $k-\omega$ model can be used without the potential errors resulting from the free stream sensitivity of that model.

The SAS turbulence model

The Scale-Adaptive Simulation (SAS) is an advanced URANS model which allows better resolution of the turbulence spectrum in unstable flow conditions. This model can change smoothly between LES-like behavior in regions where the turbulence structure is well resolved and the SST model where the unsteady flow is not well resolved. The starting point of the transformation to the SST model is the k-vt formulation as given by Menter et al.[16].

3.3.2 Modelling of the combustion

The simulations here have been carried out with the help of four different combustion models (available in ANSYS-CFX code), depending on suitability in terms of time and available computer capacity. Their basic principles and features were given in [17].

3.4 Results and discussions

3.4.1 Part I: Meshing Effects

All the meshes used in this study were generated using the meshing tool ANSYS Workbench 14.0. The grid which represents the flow domain can be unstructured (composed of hexahedra, tetrahedral, wedges, and pyramid control volume shapes) or structured. In general, structured meshes offer easy data access, while unstructured meshes offer more convenient mesh adaptivity and better fit to complex geometries. The big advantage of using the structured hexa meshes applications is, that one can align the mesh relatively nicely with the flow direction, therefore reducing numerical diffusion and aiding convergence, and less elements are demanded to fill the considered domain. However it should be noticed that in each approach the mesh adjacent to the wall should be fine enough to resolve the boundary layer flow. In boundary layers, quadrilateral, hexahedron, and prism/wedge cells are preferred over triangles, tetrahedrons, or pyramids.

Considering that all important turbulent structures and stresses are generated close to the wall, it is very important to control the distance of the first element from the wall surface, because different turbulence models have different requirements for mesh treatments to guarantee accurate results. For the unstructured mesh, it is possible to define the smaller and larger element sizes to control this distance from the wall surface. For the structured mesh generation the control of the elements distribution near the wall is more robust and the smoothing process as well as the

use of different functions is possible. Since the resolution of the grid has significant effects on the accuracy of results, in this work each mesh type was used for three different mesh sizes in each structured and unstructured approach, and the final mesh chosen for simulation is shown in Table 3-4. Figure 3-3 demonstrates the influence of the number of elements in the present configuration based on the vertical component of velocity profile at three different lines along the length of the combustor for structured and unstructured meshes. The velocity profiles on the final chosen grids are compared for three different lines taken from two different planes: plane A-A and plane B-B which are respectively shown in Figure 3-4 and Figure 3-5. As it is obvious, in the plane A-A, the unstructured grid predicts higher value of velocity in each location while the trend is not the same for the second plane (i.e. B-B) (see Figure 3-5); this points to the fact that the mass flow rate remains the same using any type of grids.

Table 3-4: Number of elements for each mesh

	Structured Mesh	Unstructured Mesh
Number of elements	4,000,822	6,200,000

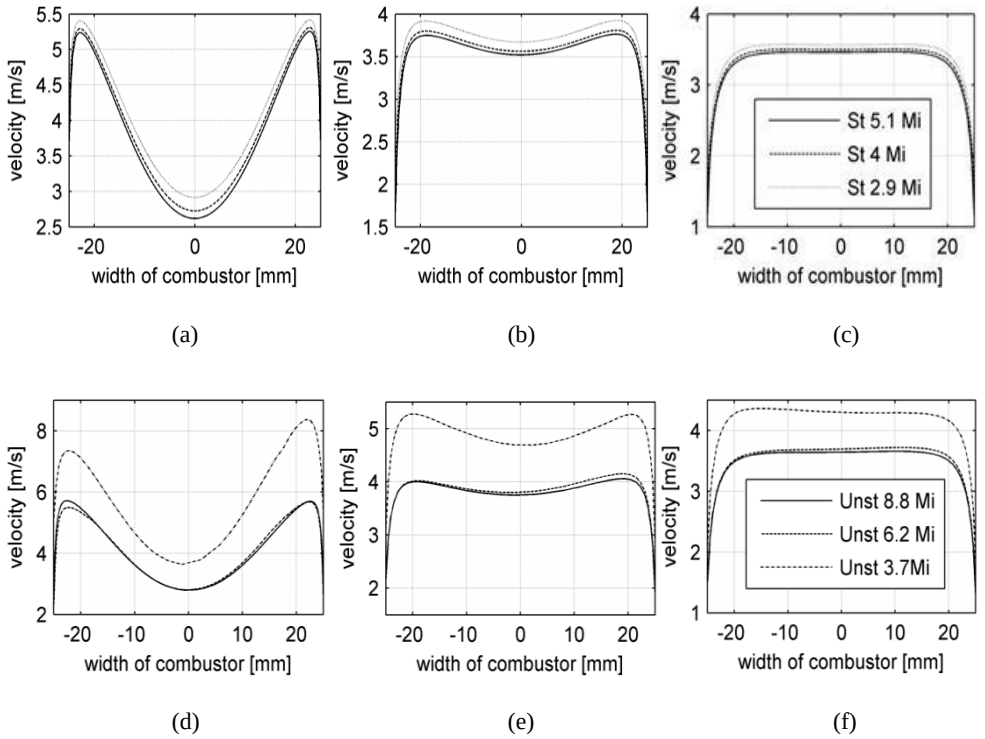

Figure 3-3: Mesh-dependency studies of structured grid (st) at different locations: (a) y=20 cm, (b) y=40 cm, (c) y=60 cm and unstructured mesh (unst): (d) y=20 cm, (e) y=40 cm, (f) y=60 cm based on the streamwise velocity.

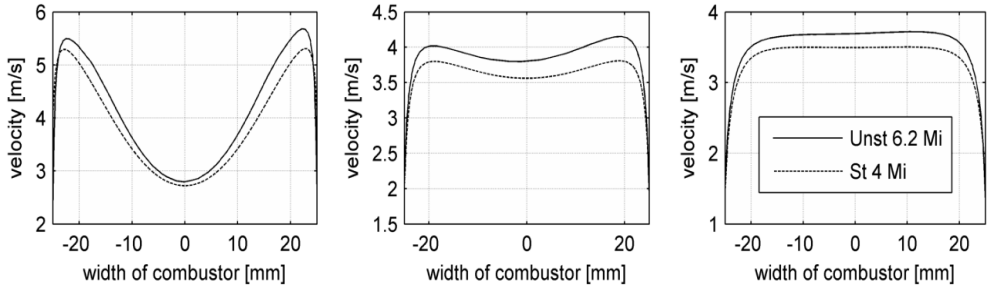

Figure 3-4: Comparison of streamwise velocity for the chosen grids taken from cross section A-A at: (a) y=20 cm, (b) y=40 cm, (c) y=60 cm

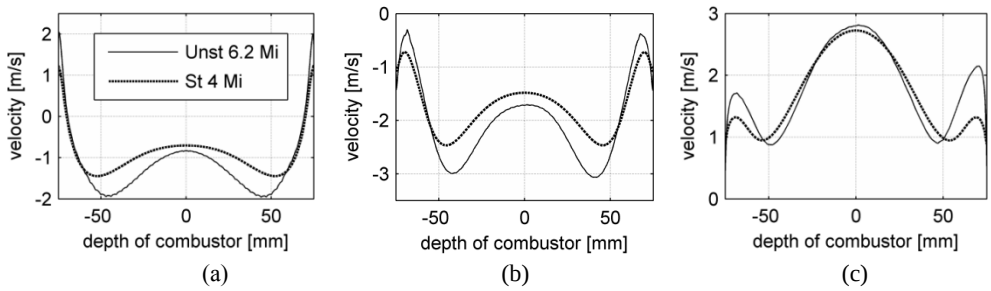

Figure 3-5: comparison of streamwise velocity for the chosen grids taken from cross section B-B at: (a) y=0.5 cm, (b) y=10 cm, (c) y=20 cm

Mechanisms of mixing

In the Reynolds-averaged approach, a model for the turbulent mass flux, $\overline{u_j' c'}$, is required to calculate averaged scalar fields; where u_j' and c' are fluctuating components of instantaneous velocity and instantaneous concentration of species, respectively. The gradient diffusion model [18] can be used to model $\overline{u_j' c'}$ given by:

$$\overline{u_j' c'} = -K_{jj} \frac{\partial \bar{c}}{\partial x_j} \qquad 3\text{-}1$$

Where K_{jj} is the eddy diffusivity of the scalar concentration, and is generally calculated from $K_{jj} = \vartheta_t / Sc_t$. ϑ_t stands for the turbulent viscosity and Sc_t is a turbulent Schmidt number.

By ignoring reactions, sources and molecular diffusion, similarly to molecular models, the following transport equation must be satisfied:

$$\frac{\partial \bar{c}_i}{\partial t} + \bar{u}_j \frac{\partial \bar{c}_i}{\partial x_j} = \frac{\partial}{\partial x_j}\left(K_{jj} \frac{\partial \bar{c}_i}{\partial x_j}\right) \qquad 3\text{-}2$$

The Eddy diffusivity is a matrix expression that may vary in space.

In this study, we measure the CH_4 concentration as well as the eddy viscosity in the absence of chemical reaction to investigate the effect of the chosen mesh on the gradient diffusion model. Figure 3-6 represents the effect of the chosen grid on the mixing behavior. The CH_4 mass concentration obtained by using each grid type is shown in three different cross sectional planes along the length of the combustor. It can be assumed that in this combustor turbulent diffusion is several orders of magnitude larger than molecular diffusion, and therefore, ideally prediction of turbulent mixing should not be affected by numerical diffusion [19]. However, much stronger mixing is predicted by the unstructured mesh, probably because of the strong numerical diffusion inherent to these grids (numerical artifact resulting from the use of a first order upwind for discretizing the convection terms). Indeed in the structured mesh, cells are aligned with the general flow direction giving lower numerical dissipation and lower cell count.

The obtained mixing results in the unstructured grid as well as the velocity profile presented in Figure 3-3 are slightly asymmetric with respect to the center, which is not expected from a physical point of view.

Figure 3-7 shows the calculated turbulent eddy viscosity on two different types of grids. Although higher rate of mixing and therefore smaller gradient of concentration was predicted by the unstructured grid, the turbulent eddy viscosity and therefore the eddy diffusion is less in this case, confirming the existence of higher numerical diffusion attached to this grid which leads to higher mixing. Overall not only these results show how numerical diffusion affects the distribution of species, they also demonstrate how numerical diffusion can cause an unphysical asymmetric velocity profile.

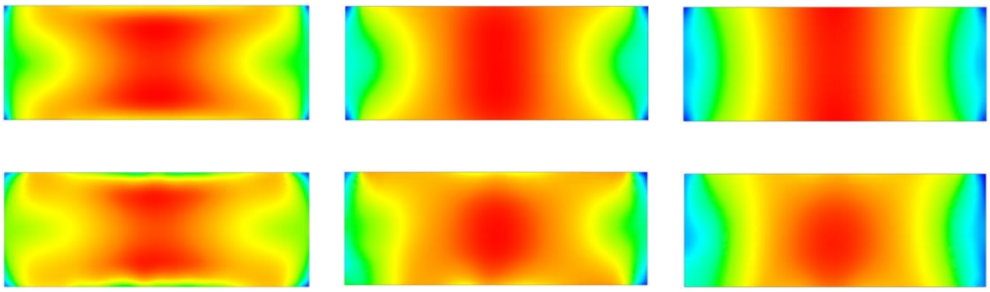

(a) (b) (c)

Figure 3-6: Comparison of structured (st) (on top) and unstructured mesh (unst) (on bottom) on the mixing behavior of CH4 concentration at: (a) y=10 cm, (b) y=20 cm, (c) y=30 cm

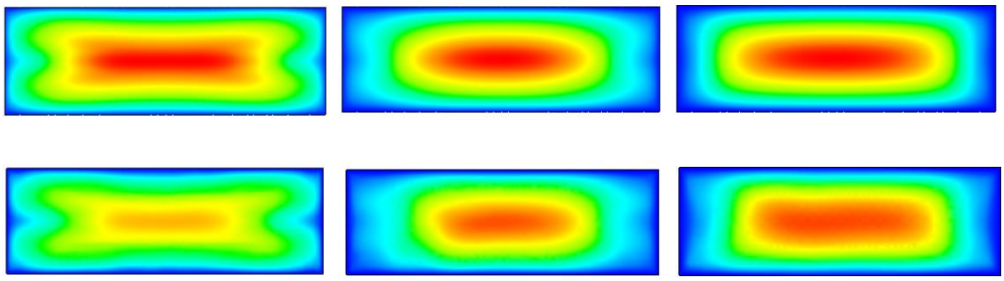

(a) (b) (c)

Figure 3-7**:** Comparison of turbulent eddy viscosity calculated by structured (st) (on top) and unstructured mesh (unst) (on bottom) at: (a) y=10 cm, (b) y=20 cm, (c) y=30 cm

Flow characteristics

Figure 3-8 shows a time averaged transient solution of the vertical velocity component, v, in the cold flow simulation, as well as velocity measurements obtained with the Particle Image Velocimetry method (PIV) averaged over 100 images, measured at Imperial College London. In each part of this figure, isocontours of v = 0 are shown which are representing the location of the recirculation zones (labeled in with 0). Recirculation occurs in three regions: in the central recirculation zone (referred as CRZ) which is stabilizing the flame, and

also in two regions between the fresh fuel gas jets and near the liner of the downstream duct referred as (ORZ: outer recirculation zone).

The predictions compare quite well with the measurements in the center and outer recirculation regions, while the velocity magnitude in profiles close to the wall is overpredicted: especially in the case of using the unstructured grid. This can be due to the near-wall treatment used in the simulations and the resulting cell size very close to the wall. A second explanation is that in measurements very close to the walls, reflections from the laser beam tend to under predict the velocity, due to bright spots or deposition of particles etc. And lastly, at downstream positions of around 25 mm the PIV data shows a region of lower velocities. This is due to reflections from the rear window causing under predictions of the velocity similar to the regions close to the side walls. Furthermore the core of the CRZ is more squeezed compared to measured data. However, the current predictions are able to capture the essential characteristics of the flow (i.e stagnation points etc.). Although there are some differences between simulations and experiments, the predicted pressure fluctuations which will be discussed later show very good agreement with experimental data.

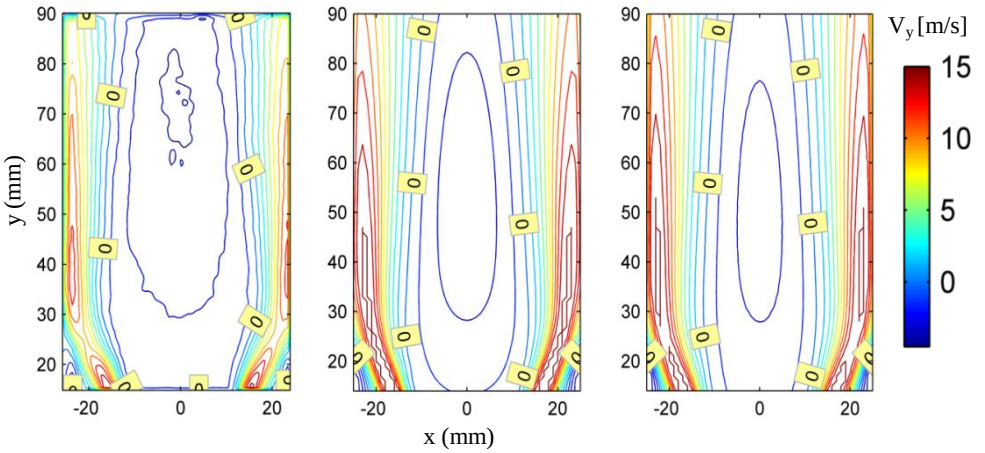

Figure 3-8: Stream wise velocity component for 40 kW thermal power and air factor 1.4: experiment (left), structured mesh (middle), unstructured mesh (right)

Figure 3-9 shows the average velocity profiles on the chosen grids taken from the plane B-B (see Figure 3-2) at mid-pitch (x=0) across the entire stream and span. Calculations done on the structured grid show more uniform velocity profile in the streamwise direction compared to the unstructured grid confirming the prediction of higher turbulent eddy viscosity in the structured mesh as presented in Figure 3-7. Considering the fact that the first and the last fuel injectors on the side surfaces of the wedge are far from the side walls in the spanwise direction (z), the presence of two corner recirculating zones (CORZ) is expected. These CORZs can squeeze the main flow and create a big recirculation zone in the middle acting like a blockage where the flow expands around it. Under reacting conditions, this effect of blockage on the spanwise direction should be less because of higher acceleration of flow and thermal expansion (see Figure 3-10).

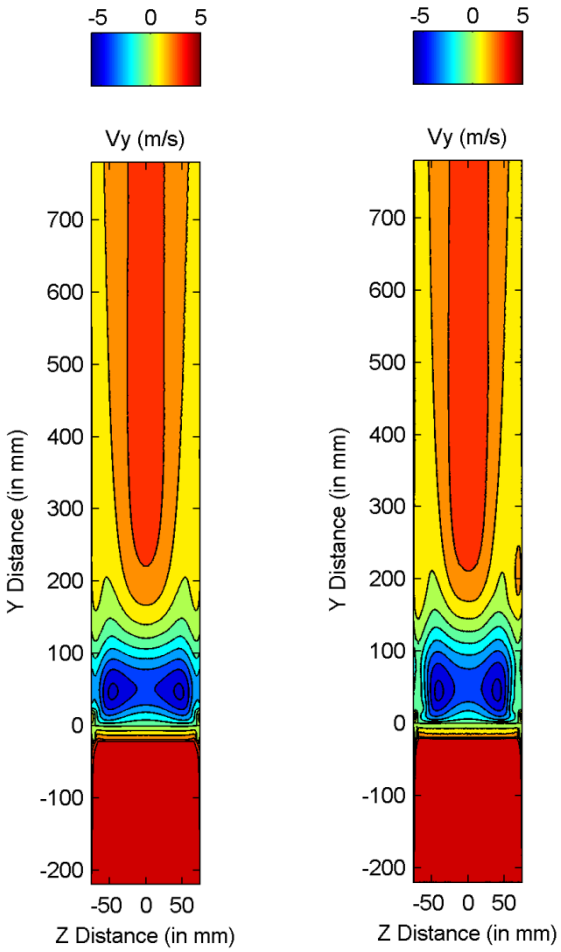

(a) (b)

Figure 3-9**:** Stream wise velocity component on the cross sectional area B-B: (a) structured mesh, (b) unstructured mesh

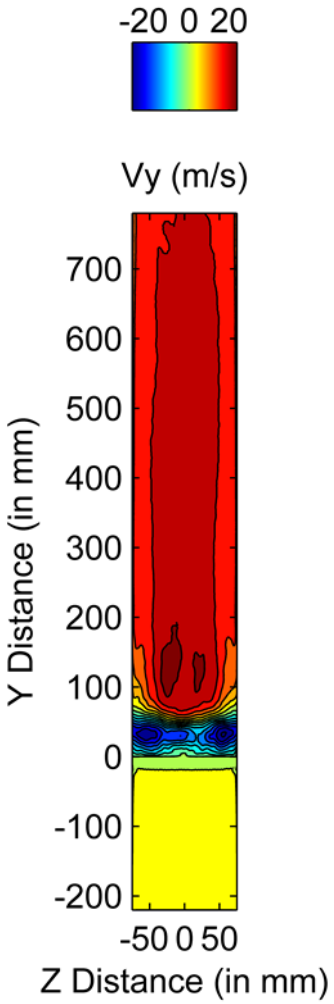

Figure 3-10: Stream wise velocity component on the cross sectional area B-B using BVM model power = 60 kW and λ=1.2

Figure 3-11 and Figure 3-12 show the enlarged view of the mesh around the wedge for the structured and unstructured grids, respectively. Due to having very small scales in the geometry (i.e. 1mm fuel holes and 3 mm burner passage slots), generating a mesh with good quality and without massive jumps in the element size or introducing high aspect ratios is very difficult. Despite these difficult

aspects of the combustor design, care was taken to keep the aspect ratio, expansion factor and orthogonality angle in the desired range.

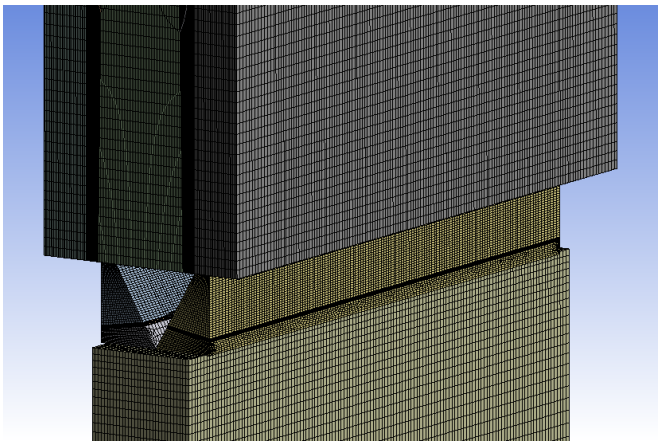

Figure 3-11: Details of mesh around the bluff body for structured mesh

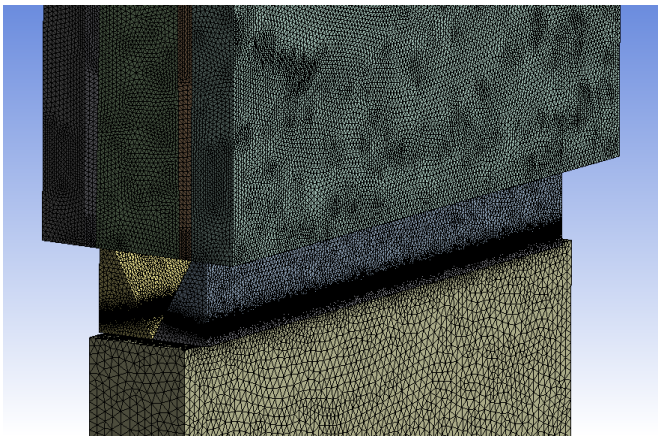

Figure 3-12: Details of mesh around the bluff body for unstructured mesh

Figure 3-13 presents the conserved variables residues history in the simulation process for both mesh methods. It is important to mention that, in the case of the unstructured grid, the numerical procedure started oscillating around residues value

of 1e-5. Therefore a dissipative scheme is set up using a first-order discretization for the Navier-Stokes advection terms to avoid numerical instabilities, and then after 100 iterations the discretization order of advection terms in momentum equations was changed back to second order.

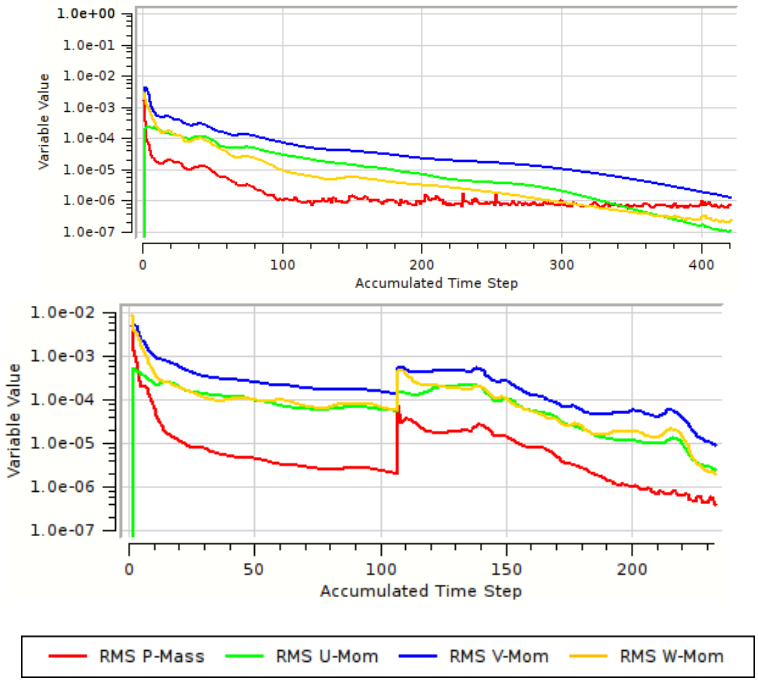

Figure 3-13: Numerical residuals using structured (top) and unstructured mesh (bottom)

3.4.2 Part II: non-reacting flow

The acoustic phenomenon in a gas turbine combustor can originate from different sources. Vibrating mechanical structures, regions of turbulent flow, mixing of fluids with different temperatures are some examples for sound generation mechanisms. However, earlier performed analyses on different types of noise sources in the combustor chamber, showed that the acoustic noise induced by the unsteady combustion process is the strongest acoustic source [20]. This is of course missing in non-reacting calculations. To determine the exothermic effects on the

flow in the model combustor, a non-reacting flow was first simulated as a reference by using different mesh types. The main parameters which were analyzed are: pressure fluctuations, streamwise velocity and also temperature in the case of hot flow. To observe the pressure fluctuations inside the combustion chamber, several locations along the length of the combustor are monitored, which are shown in Figure 3-14. In this figure, P1 to P6 are representing the location of both CFD monitor points and test rig pressure transducers, while T1 to T4 stand for thermocouple locations.

The measurement errors for the pressure transducers as reported in [11] are 12% for a single sample and for measurements in order of 4,000 Pa. However the data acquisition system combines the results of several samples to reduce this value to value of 2.6%.

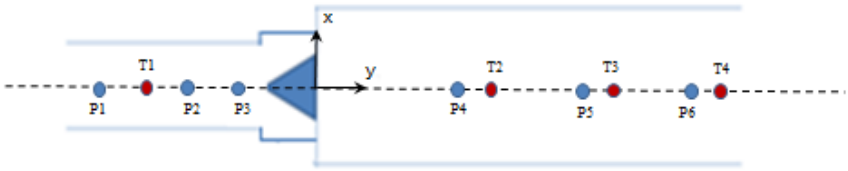

Figure 3-14: Pressure and temperature monitoring points in the CFD domain: upstream and downstream of the wedge

Figure 3-15 shows the pressure spectra of the isothermal flows in the combustor with **non-reacting** mixture measured and calculated at three pressure transducer locations mounted downstream the bluff body (numbers 4 to 6 in Figure 3-14). To have better visualization of the plots, the pressure data obtained from the unstructured grid has been scaled down by a factor 5. The combustor shows a self-excited acoustic mode at about 90 Hz. Other peaks of lower magnitude can be observed at multiple times the main frequency. The comparison between the calculated and measured mean velocity on structured and unstructured meshes (Figure 3-8) showed a minor dependence on the used mesh. The comparison of pressure data shows however an overprediction of a factor of 5 in the amplitude of oscillations by the unstructured mesh simulation in comparison with both measured data and structured mesh simulation data. In addition the first mode calculated using the unstructured grid is under predicted by 20 Hz. The higher harmonics are more damped and not so clear in this scheme.

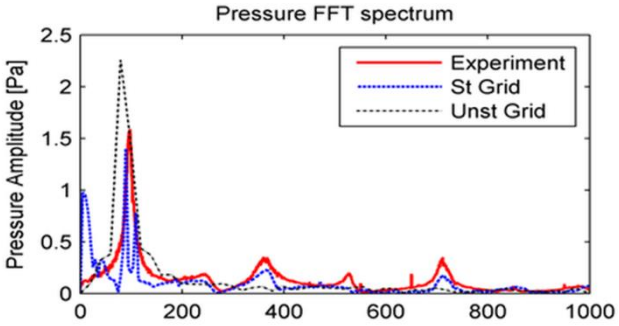

(a)

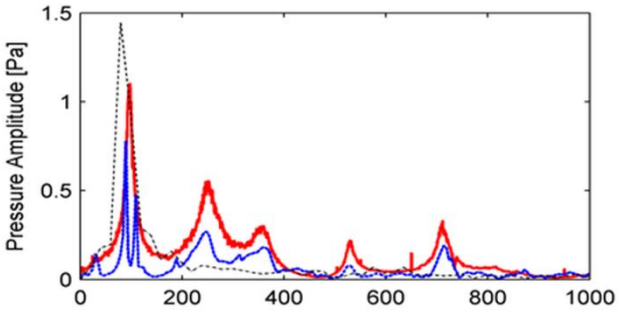

(b)

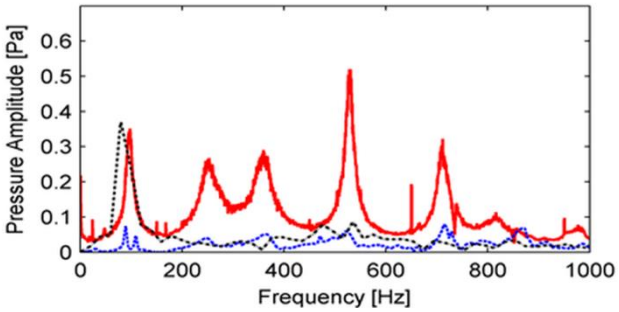

(c)

Figure 3-15: FFT for 40 kw thermal power and air factor 1.4: experiment, structured mesh, unstructured mesh for different locations: (a) p4, (b) p5, (c) p6

The multi microphone method (MMM) is applied on the pressure data obtained from the CFD calculations (at the locations of pressure transducers P1 to P6) to reconstruct the acoustic pressure and velocity fields. Figure 3-16 shows the amplitude of pressure as well as velocity fluctuations, measured at the first and the second peak frequencies against the length of the combustor. The origin of the axial axis in this case is taken at the center of the exit plane. Therefore zero in the x-axis corresponds to the exit of the burner, and the vertical thick line at (-0.78) shows the position of the bluff body. The pressure anti-node at the inlet and the node at the outlet of the combustor confirm that the open-closed acoustic boundary condition is established well by the numerical method. The pressure amplitude decreases along the combustor and the maximum pressure occurs right above the bluff body, which matches the theoretical location of the maximum pressure for the first quarter wave. The pressure profile obtained at the second resonance peak (at about three times the first fundamental frequency) is consistent with the ¾ wavelength resonant mode of an acoustic pipe.

Table 3-5 represents the values of reflection coefficients at the exit plane, obtained from the simulation based on the structured grid and also from the experiment at the University of Twente for the same operating condition. Quite good agreement can be seen between experiments and CFD data for the values of the reflection coefficients (R*)*. These results prove that the combustor is acoustically open as *R* tends to unity.

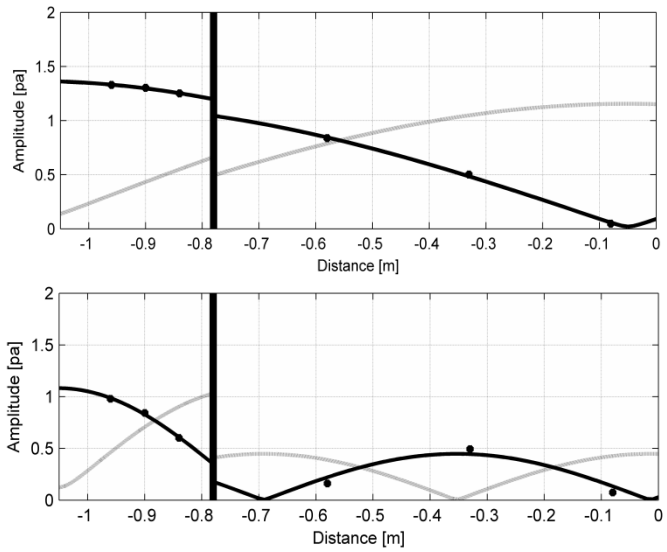

Figure 3-16: Pressure (black line) and velocity (gray line) mode shape at the first fundamental frequency (top) and at the third quarter wave mode (bottom) for the structured grid calculations

Table 3-5: Reflection coefficients calculated at the exit of the combustor

CFD		Experiment	
|R|	Φ	|R|	Φ
0.98	-3.00	0.99	$-\pi$

3.4.3 Part III: Reacting flow- Combustion modeling effect

The reacting premixed flow is studied experimentally and also with 4 different combustion models. Results are presented in Figure 3-17 for air flow rate 19 g/s and a thermal power of 40 kW. For this flow, three clear self-excited modes are found experimentally at the University of Twente test rig which are around 240 Hz, 480 Hz and 720 Hz. To identify the nature of these modes, a FEM analysis has been done with the average temperature field, given by the experimental data, to obtain the acoustic eigenmodes. As Heckl [21] proposed, due to the area blockage

of the burner, it can be assumed that the upstream and the downstream part of the combustor are acoustically decoupled, therefore only the downstream duct has been taken into account in the FEM calculation. The obtained results confirm that the first and the third frequencies observed in the experiment are the first two acoustic modes of the combustor. The measured pressure signal shows limit cycle behavior with strong non-linearities with a peak at twice the fundamental frequency [22]. Besides these modes there are more peaks observed experimentally which correspond to vibrational eigen frequencies of the liner presented in [23]. Pressure fluctuation time history and FFT as obtained from simulations using different combustion models (all available in ANSYS- CFX) are presented in Figure 3-17. Failure of the Eddy Dissipation /Finite Rate Chemistry model can be concluded on basis of its prediction of a stable flame (which is not the case for the investigated operating condition).

The PDF Flamelet model in CFX is originally designed for modeling of non-premixed flames. Although testing this model for the LIMOUSINE combustor shows the model is able to predict the instability correctly, it failed in prediction of self-excited modes. The Burning velocity model (BVM) is found to over- predict mean temperature and the rate of conversion to product species. The predicted temperature profiles are consistent with the over-prediction of the molar fraction of major product species.

Fourier analysis of the pressure signal obtained from the BVM model yields two distinct peaks appearing at frequencies of about 319 and 638 Hz. Among the combustion models tested in this paper, that is the only model able to predict the frequency doubling of the first self-excited mode. These peaks were present in the experiment, but with different amplitude and frequencies. Since in this paper the mutual interaction between flow and the vibrating liner (due to the high amplitude thermo-acoustic instabilities) for the numerical computations has been neglected, the effect of the vibrating walls on the combustible flow is only visible in the experimental data. Numerical simulation by using Large Eddy Simulation (LES) at CERFACS in the current combustor also predicted a dominant peak at 305 Hz and also the secondary peak 617Hz, see [24], which is close to the value calculated by the BVM model. Nevertheless, some discrepancies between numeric and experiment, in the prediction of fundamental frequency in this Bluff body stabilized combustor, the use of the BVM model for other applications on a swirl stabilized flame computations shows promising results compared to the experimental data [25].

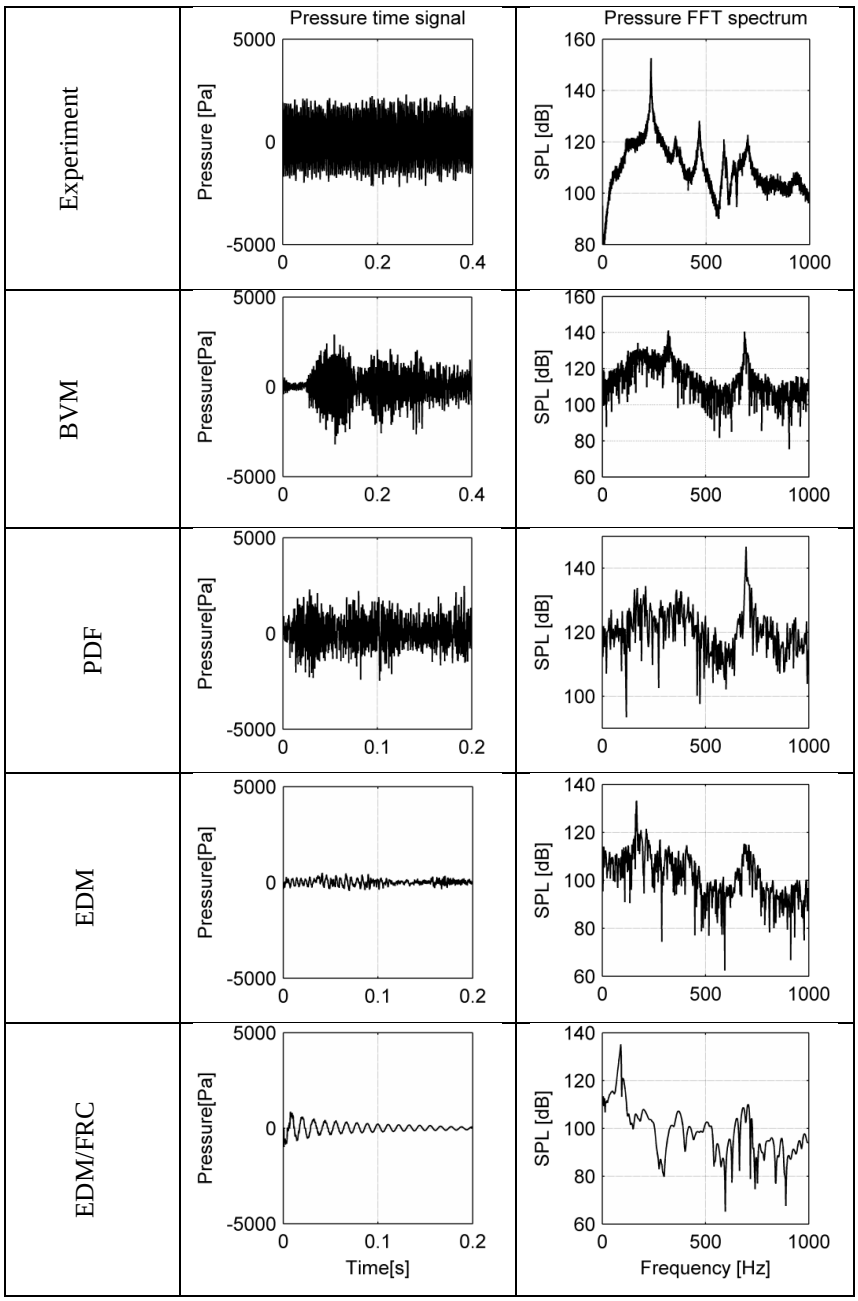

Figure 3-17: Pressure fluctuations time history (left column) and FFT (right column) at power = 40 kW and λ=1.4 measured at a location 200 mm downstream the wedge

3.5 Conclusion and Future work

In the paper, two structured-unstructured grid techniques in a finite volume method are used to simulate reacting and non-reacting flow in a partially premixed bluff body stabilized model combustor. This paper has presented the performance of the combustion model for reacting configuration, and the main issues of the performed combustion modeling were reviewed. The following conclusions can be drawn from the present study:

- The obtained velocity fields resolved under structured and unstructured mesh conditions show minor dependence on the used mesh in the mean velocity compared to the PIV data, while the pressure fluctuations were found to depend heavily on the investigated grids.
- The unstructured mesh showed larger rates of mixing as compared to the structured mesh and hence this hints at significant numerical diffusion caused by the unstructured mesh discretization.
- Using the Eddy Dissipation/Finite Rate Chemistry combustion model results in an unphysical stable flame (also flash back was observed). Although the PDF Flamelet model is able to predict the instability within the investigated combustion system, it failed in prediction of the frequency of the self-excited modes.
- The Burning velocity model (BVM) is found to over-predict the mean temperature and rate of conversion to product species. However this model is able to predict the frequency doubling of the first self-excited mode. To overcome the former problem, it is important to improve the boundary condition imposed to the liner. Of significance may be the influence of the prescribed liner boundary condition on the predictions. This influence is likely to be larger than in the stable combustion processes. In order to assess the energy transfer from the combustor to the ambient, besides considering the convection from the liner, heat transfer due to radiation (emission) from the quartz glass windows should be also taken into account.

Acknowledgments

The authors would like to acknowledge the funding of this research by the EC in the Marie Curie Actions Networks for Initial Training, under call FP7-PEOPLE-2007-1-1-ITN, Project LIMOUSINE with project number 214905. Special thanks go to Dr. Phil Stopford for the support in the use of ANSYS-CFX.

References

[1] Weatherill, N. P., 1988, "A method for generating irregular computational grids in multiply connected planar domains," International Journal for Numerical Methods in Fluids, 8(2), pp. 181-197.
[2] Koomullil, R., Soni, B., and Singh, R., 2008, "A comprehensive generalized mesh system for CFD applications," Mathematics and Computers in Simulation, 78(5–6), pp. 605-617.
[3] Mavriplis, D. J., 1997, "Unstructured grid techniques," Annual Review of Fluid Mechanics, 29, pp. 473-514.
[4] Kikuchi, N., 1986, "Adaptive grid-design methods for finite element analysis," Computer Methods in Applied Mechanics and Engineering, 55(1–2), pp. 129-160.
[5] Beam RM, and Warming, R., 1982., "Implicit numerical method for the compressible Navier–Stokes and Euler equations," Lecture notes of Von Karman institute for fluid dynamics.
[6] Caughey, D. A., and Hafez, M. M., 1994, "Frontiers of Computational Fluid Dynamics ", John-Wiley & Sons, New York.
[7] Çete, A. R., Yükselen, M. A., and Kaynak, Ü., 2008, "A unifying grid approach for solving potential flows applicable to structured and unstructured grid configurations," Computers & Fluids, 37(1), pp. 35-50.
[8] Hansen, R. P., and Forsythe, J. R., 2003, "A Comparison of Structured and Unstructured Grid Solutions for Flow Over a Circular Cylinder," Proceedings of the 2003 DoD User Group Conference, IEEE Computer Society, p. 104.
[9] Hua, Z.-l., Xing, L.-h., and Gu, L., 2008, "Application of a modified quick scheme to depth-averaged κ–ε turbulence model based on unstructured grids," Journal of Hydrodynamics, Ser. B, 20(4), pp. 514-523.
[10] Tomita, J. T., Silva, L. M. d., and Silva, D. T. d., "Comparison between unstructured and structured meshes with different turbulence models for a high pressure turbine application " Proc. Proceedings of ASME Turbo Expo.
[11] Roman Casado, J. C., and Kok, J. B. W., 2012, "Non-linear effects in a lean partially premixed combustor during limit cycle operation," Proceeding of ASME Turbo Expo 2012, Copenhagen, Denamrk, pp. 837-846.
[12] Patankar, S. V., 1980, Numerical Heat Transfer and Fluid Flow, Hemisphere Publishing Corp.
[13] C.M.Rhie, and W.L.Chow, 1982, "a numerical study of Turbulent Flow Past an Isolated Airfoil with the Trailing Edge Separation," Aiaa Journal, pp. 82-0998.
[14] Majumdar, S., 1988, "Role of underrelaxation in momentum interpolation for calculation of flow with nonstaggered grids," Numerical Heat Transfer, 13(1), pp. 125-132.
[15] Menter, F. R., 1994, "2-Equation Eddy-Viscosity Turbulence Models for Engineering Applications," Aiaa Journal, 32(8), pp. 1598-1605.
[16] Menter, F. R., and Egorov, Y., 2010, "The Scale-Adaptive Simulation Method for Unsteady Turbulent Flow Predictions. Part 1: Theory and Model Description," Flow Turbul. Combust., 85(1), pp. 113-138.
[17] 2011, ANSYS CFX solver manager user's guide. Release 14.0. .

[18] Combest, D. P., Ramachandran, P. A., and Dudukovic, M. P., 2011, "On the Gradient Diffusion Hypothesis and Passive Scalar Transport in Turbulent Flows," Industrial & Engineering Chemistry Research, 50(15), pp. 8817-8823.
[19] Liu, M., 2012, "Age Distribution in the Kenics Static Micromixer with Convection and Diffusion," Industrial & Engineering Chemistry Research 51(20), pp. 7081-7094.
[20] Pozarlik, A., 2010, " Vibro-Acoustical Instabilities Induced by Combustion Dynamics in Gas Turbine Combustors," PhD thesis PhD thesis, University of Twente, Enschede, Netherlands.
[21] Heckl, M., 2010, "the Rijke tube: A green's function approach in the frequency domain," Acta Acustica united with Acustica, 96(4), pp. 743-752.
[22] J.C.Roman Casado, and J.B.W.Kok, 2012, "Non-linear effects in a lean partially premixed combustor during limit cycle operation " Proceeding of ASME Turbo Expo 2012Copenhagen, Denamrk.
[23] A. Can Altunlu, Mina Shahi, Artur Pozarlik, P.J.M. van der Hoogt, J.B.W.Kok, and Boer, A. d., "Fluid-structure interaction on the combustion instability," Proc. ICSV19.
[24] Vera, I. H., 2011, "Soot modeling in flames and Large-Eddy Simulations of thermo-acoustic instabilities," PhD, Universite de Toulouse.
[25] Ozcan, E., 2012, "Tuning the self -excited thermo-acoustic oscilations of a gas turbine combustor to Limit Cycle Operations by means of numerical analysis " Master Thesis, University of Twente.

4

Assessment of Thermoacoustic Instabilities in a Partially Premixed Model Combustor Using URANS Approach

Mina Shahi*, Jim. B.W.Kok, J.C. Roman Casado, Artur Pozarlik

University of Twente, Faculty of Engineering Technology, Laboratory of Thermal Engineering, Enschede, the Netherlands

Published in Appl. Therm. Eng. 71(1) 2014

Abstract

The paper presents a numerical study of the mechanisms deriving thermoacoustic instabilities in a lean partially premixed combustor in conditions representative of gas turbine combustion systems. Various combustion models and modelling approaches able to predict the onset of thermoacoustic instabilities are examined and applied to the experimental test rig in order to assess their validity. The influence of the imposed acoustic and thermal boundary conditions on characterization of the coupling between heat release rate fluctuations and the acoustic field is investigated. Predicted data is used to improve the understanding of mutual interactions between pressure fluctuations and unsteady heat release in the unstable combustors which play an essential role in characterizing limit-cycle behavior. The mean convective time delay between heat release and the perturbation in the flow is used to determine the stability condition of the combustor. The study shows that heat transfer is important parameter regulating pressure oscillations.

Keywords: *Partially premixed combustion, Thermoacoustic instabilities, Combustion modeling, Heat transfer, RANS solver, Limit Cycle of Pressure Oscillations*

4.1 Introduction

Unfortunately the low emission of NOx and CO of the lean premixed combustion of natural gas comes at the cost of a high sensitivity to thermoacoustic instabilities [1-3]. Combustion instabilities are caused by resonant interactions with the acoustic field. Therefore, it is important to understand and explore the elementary processes of interaction between combustion and acoustic perturbations, which may become driving/coupling processes under unstable conditions. Unstable combustors can exhibit significant flow and pressure oscillations which may reach such high amplitudes that they cause flame extinction, structural vibration, flame flashback and ultimately failure of the system [4-6]. Several coupled mechanisms are known to promote such interactions, for example: flame-acoustic wave interactions, flame vortex interactions, thermal-structure interactions, fluid-structure interactions, all of them may be present in a system individually or simultaneously [7-10]. The large amplitude pressure perturbations are indicated as Limit Cycle Oscillations (LCO) of the pressure;

In this paper the goal is to model the thermo-acoustic self-oscillation phenomena in a laboratory-scale lean combustor operating in a partially premixed burning regime by means of CFD tools. This model combustor was built within the European project called LIMOUSINE. The burning conditions of the test rig correspond to a partially premixed flame where strong equivalence ratio variations can be created. Such regimes control auto-ignition problems, flame stabilization in the near field of burners, local quenching or re-ignition mechanisms. Since the classical models developed for premixed or purely diffusion flames should not be used unless specifically adapted, modeling such complex combustion physics numerically is a challenging task. In previous work done by authors [11], the impact of grid types and turbulent combustion modeling on the flow and predicted flame dynamics are evaluated; the BVM model found to be qualitatively in line with the experimental observations. It was also reported that the error in the prediction of the acoustic characterization could be due to the influence of the prescribed liner boundary condition. Here, the extended study aims to improve the CFD model in order to achieve to the quantitative match with the experiments. For this reason, the BVM model with an alternative discretization is implemented. Furthermore, for accurate prediction of the frequency and corresponding magnitude of the thermo-acoustic instability, and also to capture the reacting flow physics within the combustor, the effects of specified thermal and acoustical boundary conditions on characterizing limit-cycle behavior are examined. The predicted data accounts for the fact that a

precise model for predicting the heat losses from the system is essential to access the accurate estimation of instability magnitude.

4.2 Thermoacoustic instability: Limit cycle feedback loop

The acoustic phenomenona in the gas turbine are deriven by various sources; Vibrating mechanical structures, regions of turbulent flow, mixing of fluids with different temperatures are a few examples of sound generation mechanisms. According to the modern theory for sound generation in fluid media, as formulated by Ligthill [12, 13], sources for sound generation can be identified to be of a monopole, dipole or quadrupole nature:

1- Fluctuating fluid volumes (e.g. created by unsteady combustion, piston machines or cavitation)
2- Fluctuating external forces (e.g. created by flow around solid objects)
3- Fluctuating shear of fluid particles; the best known source of this is free turbulence (e.g. in a jet.)

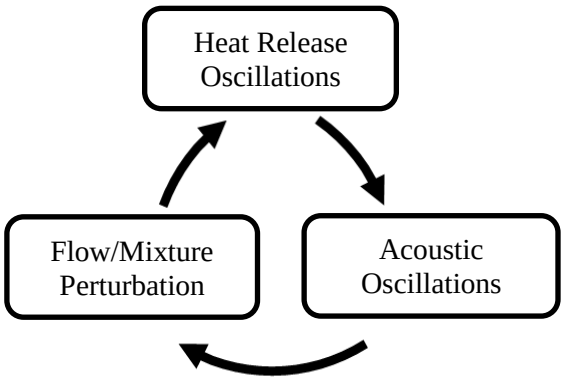

Figure 4-1: The feedback mechanism affecting the appearance of thermoacoustic instabilities in the combustion processes.

In a uniform and stagnant fluid, the Lighthill equation describing these three basic aero-acoustic sources of sound (on the right hand side of Equation 4-1) can be expressed as:

$$\frac{1}{c_0^2}\frac{\partial^2 p'}{\partial t^2}-\frac{\partial^2 p'}{\partial x_i^2}=\underbrace{\frac{\partial^2}{\partial t^2}\left(\frac{p'}{c_0^2}-\rho'\right)}_{\text{monopole source}}-\underbrace{\frac{\partial \mathrm{f_i}}{\partial \mathrm{x_i}}}_{\text{dipole source}}+\underbrace{\frac{\partial^2}{\partial x_i \partial x_j}\left(\rho v_i v_j-\tau_{ij}\right)}_{\text{quadrupole source}} \qquad 4\text{-}1$$

In the combustion chamber, the flame is acting as a monopole acoustic source. Depending on the temporary flame positions and wrinkling, hot gases expand or contract in each direction simultaneously. According to the literatures on the different types of sources in the combustor chamber, the acoustic power from the combustion process is the strongest acoustic source [14, 15]. Fluctuations of velocity, acoustic oscillations (i.e. fluctuation of pressure field), and perturbations in the fuel concentration and in the mixing process may result in heat release perturbations and consequently pressure fluctuations. Perturbations of heat release are part of a self-exciting loop initiating the thermoacoustic instability. This feedback process affects the characteristics of the thermoacoustic instabilities. The involved dynamics results in a resonant coupling between unsteady combustion processes, pressure field in the combustion system and the mixing process. The main phenomena involved in the feedback mechanism process are depicted in Figure 4-1. Depending on the phase shift between these dynamic systems, energy may be fed back into the initial perturbation source and thereby sustaining or damping the instability mechanism. The Rayleigh criterion [16] which recognizes the difference between damped or amplified interaction between pressure and heat release is often used to investigate and predict combustion instabilities. It states that if pressure and heat release fluctuations are in phase, the magnitude of thermoacoustic instabilities are enhanced, whereas the instabilities are damped when the pressure oscillations and heat release are out of phase. This criterion is expressed by the following equation:

$$\iiint_{\Omega} \mathrm{p'q'\,d\Omega} > 0 \qquad 4\text{-}2$$

where $\mathrm{p'}$ and $\mathrm{q'}$ are pressure and heat release fluctuations, respectively, integrated over one cycle of the oscillation in the flow domain Ω. The product of thermal oscillation and sound pressure fluctuation must be positive to enable combustion oscillations, whereas the negative sign indicates a damping process.

Rayleigh's criterion is a necessary but not a sufficient condition for the instabilities to occur [17]. Therefore Equation 4-2 has been extended to Equation 4-3 to include the losses of acoustic energy at the boundaries and entropy effects. According to Equation 4-3, the acoustic energy growth rate depends on the Rayleigh term but

also on the acoustic fluxes; therefore the Rayleigh criterion is only a necessary condition for instability to occur.

$$\frac{\gamma-1}{\gamma\bar{p}}\int_V \int_T p'(x,t)\, Q'(x,t)\, dt\, dV \geq \int_A \int_T p'(x,t)\, u'(x,t)\, dt\, dA \qquad 4\text{-}3$$

As long as the energy flux from the flame to the acoustic field is greater than the losses, the amplitude of the pressure oscillations grows every period. When the acoustic energy losses match the energy gain the amplitude remains constant over time and this unstable regime is referred to as the Limit Cycle of pressure Oscillations (LCO). Since the integrals are also spatial both effects: destabilizing and stabilizing can occur at different locations of the combustor and at different times. The overall stability of the combustor will be then defined by the net acoustical energy added to the combustor domain.

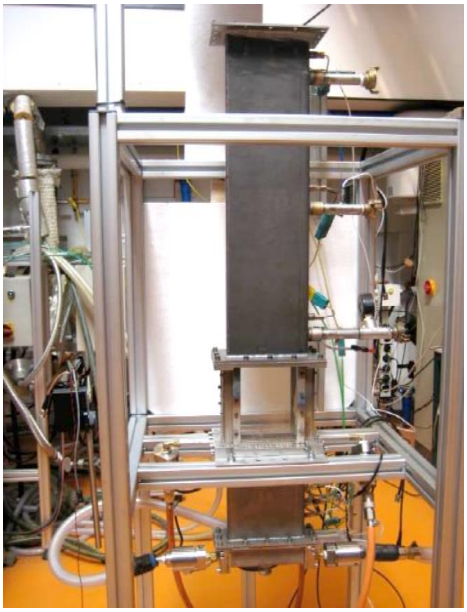

(a)

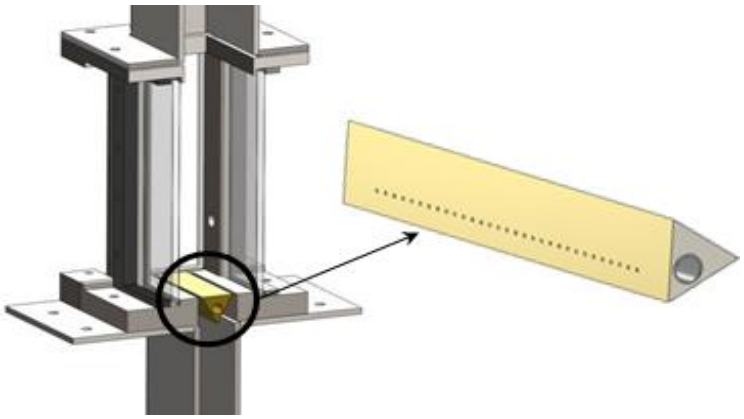

(b)

Figure 4-2 : (a) experimental set up (b) limousine burner

4.3 Burner description

The experiment, which is used as a basis for modeling studies, is performed on a test rig which is shown in Figure 4-2. It is located at university of Twente and 4

other laboratories, within the framework of the European LIMOUSINE project. The set-up is designed to study limit cycles due to thermo-acoustic instability. The combustor consists of two rectangular ducts with different widths, with the burner coupling both ducts. The duct upstream of the burner has a 25x150 mm^2 cross section and is 275 mm long, whereas the duct downstream the burner has a 50x150 mm^2 cross sectional area to compensate the volume expansion due to the combustion. Although there are different approaches possible to stabilize a flame, in this study bluff body stabilization is used. Therefore in the transition between the ducts the burner is mounted that creates a flow recirculation pattern that stabilizes the flame. In this configuration which is the third design version of the combustor (V3), the total length of the combustor is 1050 mm (see table 4-1 for dimensions). Therefore the length of the combustor is much larger compared to the width making it behaves like a two dimensional combustor. Details about dimensions of the model combustor are summarized in Table 4-1. The combustor has large quartz glass windows in every wall to allow optical access to the flame. All pieces, except the brass bluff body, are made from heat resistant stainless steel S310.

Table 4-1 : Dimensions of the model combustor

Location	Dimension (mm)
Upstream height	220
Upstream width	25
Downstream height	780
Downstream width	50
Width of the combustor in the third direction	150

Air as the oxidizer is injected at the upstream end through a custom made air distribution system which has two longitudal pipes with passing holes of 2mm diameter. Fuel is injected through holes at the side of the wedge (see figure 4-2). Fuel used here is 100% methane at room temperature. The flow recirculation that stabilizes the flame is in this case created by the wedge which is placed at the point where the small duct is attached to the large duct. From the side surfaces of the wedge gaseous fuel is injected through 62 holes. The air and fuel flow are

controlled from a PC with control software and mass flow controller valves. The dynamic pressure is measured at 6 points along the combustor with piezoresistant pressure transducers. Three pressure transducers in the plenum are flush mounted in the wall, while the pressure transducers downstream the burner, are mounted in side tubes. Thereby the pressure transducers are protected from high temperatures. Every side tube ends in a long hose connected to a terminal metal pipe filled with an acoustic damping material, to impose anechoic conditions. Pressure signals were measured with a DAQ system linked to a laptop. For every operating condition, 10,000 samples were recorded for each channel at 3,125 HZ.

The only cooling of the combustor is by natural convection and radiation. The burner can operate at a large range of power and air factors. This configuration behaves like a variation of a Rijke tube [18]. It deviates from the standard Rijke tube because it is closed at the bottom end, open to the atmosphere at the downstream end and it has an air flow forced into it.

4.4 Meshing and Numerical approach

To save computational cost, the computational domain is reduced to a slice including just one fuel injector hole at either side of the flame holder. All the meshes used in this study are generated using the meshing tool ANSYS Workbench 14.5. Since the resolution of the grid has significant effects on the accuracy of results, in this work three different mesh sizes have been used and the final mesh chosen for simulation is shown in Table 4-2.

Table 4-2: Number of elements for each mesh

	Number of elements
Original geometry	539,590
Enlarged geometry	695,976

ANSYS-CFX 14.5 uses an implicit finite volume formulation to construct the discretized equations representing the Reynolds Averaged Navier-Stokes equations for the fluid flow. The model consists of a compressible solver with a co-located (non-staggered) finite volume method such that the control volumes are identical for all transport equations [19]. To avoid the decoupling of the pressure field, CFX uses the Rhie-Chow [20] discretization method for the mass terms as modified by

Majumdar [21]. A coupled algebraic multi-grid solver is used to give robust solutions for the governing discrete system of linearized equations. For the discretization of governing equations, a high resolution advection scheme for spatial and second order backward Euler discretization for time accuracy is used. In the time implicit compressible methods, the full compressible equations are solved implicitly to escape the CFL stability limit. However to keep the results more precise the solver must be run for low CFL values [22]. The computational geometry used in the solution process is illustrated in Figure 4-3.

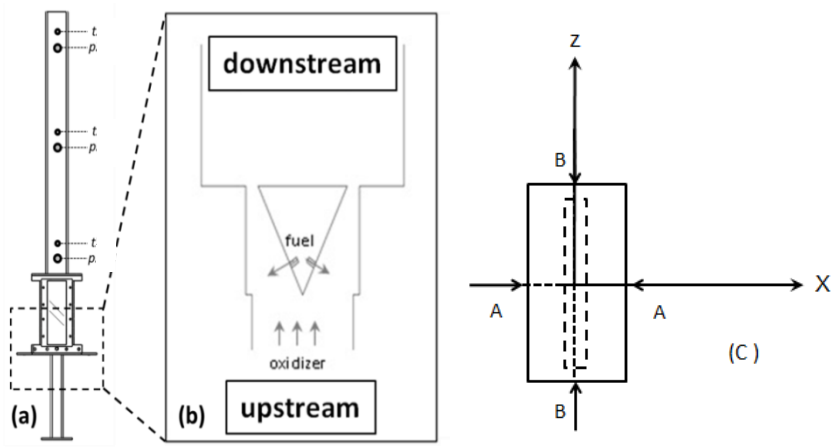

Figure 4-3 : A schematic representation of the model combustor: (a) computational domain in CFD calculation (b) an enlarged view around the wedge (c) cross sectional area of the combustor (view from the top)

4.4.1 Governing equations

The basic set of balance equations solved by ANSYS-CFX comprises the Navier-Stokes, species and energy transport equations. The Favre average mass, momentum and energy conservation equations can be written as following:

- Conservation of mass

$$\frac{\partial \bar{\rho}}{\partial t} + \frac{\partial (\bar{\rho}\tilde{u}_i)}{\partial x_i} = 0 \qquad 4\text{-}4$$

- Momentum

$$\frac{\partial(\bar{\rho}\tilde{u}_i)}{\partial t}+\frac{\partial(\bar{\rho}\tilde{u}_i\tilde{u}_j)}{\partial x_i}=-\frac{\partial \bar{p}}{\partial x_i}+\frac{\partial}{\partial x_i}\left(\overline{\tau_{ij}}-\overline{\rho u_i^{"}u_j^{"}}\right) \quad 4\text{-}5$$

τ is the stress tensor which is related to the strain rate by:

$$\overline{\tau_{ij}}=\widetilde{\tau_{ij}}+\overline{\tau_{ij}^{"}} \quad 4\text{-}6$$

- Chemical species

$$\frac{\partial(\bar{\rho}\tilde{Y}_k)}{\partial t}+\frac{\partial\,(\bar{\rho}\tilde{Y}_k\tilde{u}_i)}{\partial x_i}=-\frac{\partial\left(\bar{\rho}\widetilde{u_i''Y_k''}\right)}{\partial x_i}-\frac{\partial(\overline{V_{k,i}Y_k})}{\partial x_i}+\bar{\dot{\omega}}_k \quad 4\text{-}7$$

V_k is the diffusive velocity of the *k*th species. The source term in the species transport equations is shown by $\dot{\omega_k}$;

- Energy equation

$$\frac{\partial(\bar{\rho}\widetilde{e_0})}{\partial t}+\frac{\partial}{\partial x_j}\left(\bar{\rho}\tilde{u}_i\widetilde{e_0}+\tilde{u}_j\bar{p}+\overline{u_j^{"}p}+\overline{\rho u_j^{"}e_0^{"}}+\overline{q_j}-\overline{u_i\tau_{ij}}\right)=\bar{\dot{\omega}}_T \quad 4\text{-}8$$

$\bar{\dot{\omega}}_T$ is the chemical source term and $\widetilde{e_0}$ is given by:

$$\widetilde{e_0}\equiv\tilde{e}+\tilde{u}_k\,\tilde{u}_k\,/2+k \quad 4\text{-}9$$

Where the turbulent energy, k, is defined by:

$$k=\frac{\widetilde{u_k^{"}u_k^{"}}}{2} \quad 4\text{-}10$$

Note that the term q_j in Equation (4-8) is the heat flux which represents heat conduction and transport through species gradients given by ($q_j=-\lambda\frac{\partial T}{\partial x_j}+\rho\sum_{k=1}^{N}V_{k,j}Y_k\,h_{s,k}$).

The unclosed terms contain products of fluctuating values (e.g. $\overline{\rho u_i^{"}u_j^{"}}$, $\bar{\rho}\widetilde{u_i''Y_k''}$ etc.) which need to be modeled. In this work the effects of turbulence are modeled by using the Shear Stress Transport Turbulence Model (SST) in the steady state calculations, while for the transient calculations the Scale-Adaptive Simulation model (SAS) is used. Reacting flow simulations are carried out on the model combustor using different combustion models which are standard available in ANSYS-CFX.

4.4.2 Boundary conditions

The numerical treatment of the flow boundary condition is of great importance and can result in artificially stable or unstable predictions. Details about boundary conditions imposed on the domain are summarized in Table 4-3. The flow parameters are set consistent with the experimental conditions depicted in Table 4-4. The closed acoustic inlet boundary condition at the upstream end of the combustor was implemented by using a uniform and steady inlet velocity profile at the air inlet, which ensured an acoustically closed inlet. The mass flow rate of fuel was specified at the fuel inlet. A partially reflecting boundary condition was applied at the outlet by setting pressure at that location to a constant value of 1atm, which implements the open acoustic boundary condition.

Table 4-3: Details about boundary condition

Location	B.C
Air Inlet	Normal speed
Fuel Inlet	Mass flow rate
Outlet	Average static pressure
Walls	Non-slip

Table 4-4: Operating condition

Power (kW)	Air factor	Fuel mass flow rate [g/s]	Air mass flow rate [g/s]
40	1.4	0.8	19.152

4.5 Results and discussions

Figure 4-4 represents the measured stability condition of the combustor for all possible combinations of 4 thermal power and 4 air factor settings, allowed by the air and fuel control valves. The most important parameter to characterize the stability condition of the combustor is found to be the air factor. Here the important

observation is that the limit cycle is always present for flames richer than λ = 1.60. The majority of operating points always show the same regime. However there is a small region of operating conditions (including λ = 1.60 & λ = 1.80) that can be either in the stable or unstable regime (detailed in [23]).

Typical results of the predicted temperature field (i.e. a 2D snapshot) from a stable and also an unstable flame are presented in figure 4-5. In both cases, the central recirculating zone (CRZ) forms a flame stabilization region where the incoming mixture of air and fuel are mixed with the hot products before ignition. The recirculated hot combustion products transports momentum and energy back to the further upstream where they mix with the incoming fresh mixture. Furthermore, due to the sudden expansion of the combustor configuration, two corner recirculation zones (CORZ) are formed downstream of the bluff body. Presented temperature fields show that in the unstable flame, natural coherent structures in the shear layers lead to a penetration of the fresh gases to the flame before it burns completely, which also results in a fluctuating heat release rate. Due to the expansion of the flow the flame is pushed outward and simultaneously blocks the inlet flow causing the flame flashbacks periodically in the burner. Unburned mixture segments broken up away from the main stream of the flow, may generate local hot spots further downstream. The flame zone thus reaches the enhanced burning state which is shortened and becomes compact compared to the stable regime.

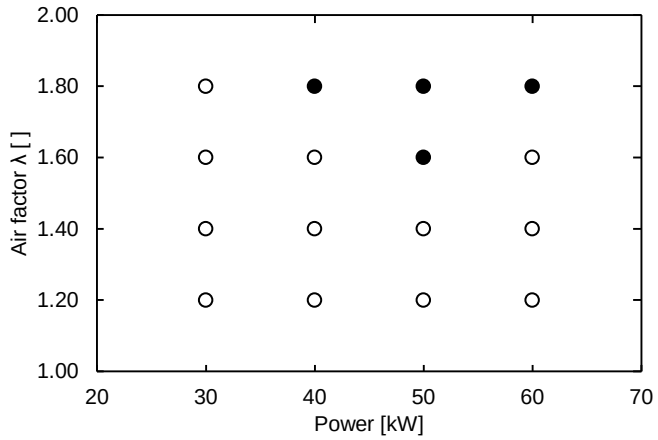

Figure 4-4: Stability map for the limousine burner: ○ unstable combustion, ● stable combustion.

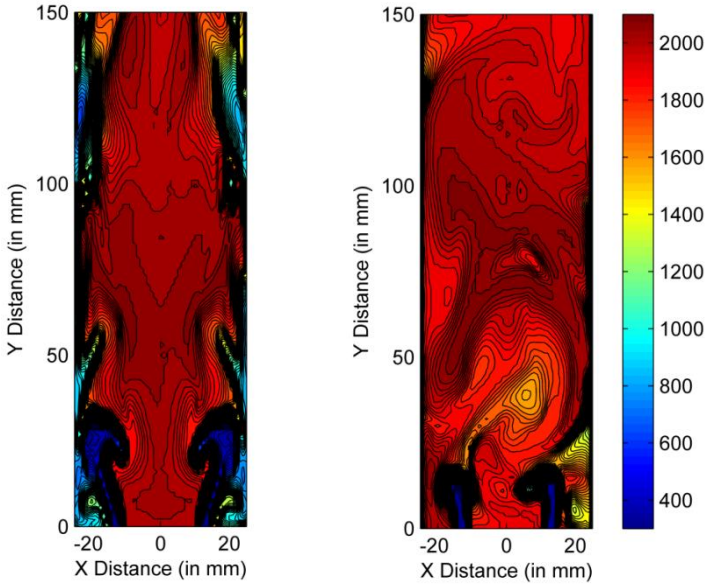

Figure 4-5: A 2D snapshot of temperature field derived from (a) a stable flame (b) an unstable flame

4.5.1 Combustion modeling effect

In simple models of turbulent combustion processes, it is assumed that fuel and oxidizer are either fully premixed prior to entering to the flame zone or they enter the flame zone separately. However, in reality, this is often not the case. Many practical combustion devices, including gas turbine engines often operate in a partially premixed burning regime in which the fuel and oxidizer are partially mixed at the time of combustion. In this section the reacting partially premixed flow is studied experimentally and also with different combustion models (available in ANSYS-CFX code). Here calculations have been done for one specified point: air flow rate 19 g/s (λ = 1.40) and a thermal power of 40 kW. The pressure signals and FFT spectra are respectively presented in Figure 4-6 and Figure 4-7. For this flow, three clear self-excited modes are found experimentally at frequencies around 240 Hz, 480 Hz and 720 Hz. The self-excitation of combustion instabilities is linked to the phase relationship between the acoustic pressure field and the unsteady heat release via Rayleigh's criterion as previously

explained in this paper (also described in [24, 25]). To identify the nature of these modes, a FEM analysis has been done with the average temperature field given by the experimental data to obtain the acoustic eigenmodes. Since the upstream and the downstream part of the combustor are acoustically decoupled, only the downstream duct has been taken into account in the FEM calculation with the pressure node at the wedge location. The obtained results confirm that the first and the third frequencies observed in the experiment are the first two acoustic modes of the combustor [23, 26]. The measured pressure signal shows limit cycle behavior with strong non-linearities with a peak at twice the fundamental frequency (referred to as frequency doubling) [26]. Comparing the amplitude of peaks in the spectrum shows that the relative amplitudes of the main dynamics corresponding to the acoustic modes are higher than the relative amplitudes of secondary peaks pointing to the fact that the non-linear effects for pressure is small. Beside these acoustic modes, there are more peaks observed which are corresponding to eigenfrequencies of the liner as presented in [27]. Pressure fluctuation time signals obtained using different combustion models are presented in Figure 4-6. Failure of the Eddy Dissipation /Finite Rate Chemistry model is assessed based on the prediction of a stable flame (which is not the case for the investigated operating condition). In this model, the methane and the air have been assumed to react in accordance with a two-step reaction mechanism obeying the reactions:

$$CH_4 + 3/2O_2 \rightarrow CO + 2H_2O$$
$$CO + 1/2O_2 \rightarrow CO_2 \qquad \text{4-11}$$

In the ED/FR model both a mixing rate and an Arrhenius rate, as a function of the mean temperature and composition, are evaluated and the smallest rate is chosen as the mean reaction rate for the reacting species. However, the ED/FR model can handle only global kinetic mechanisms, being the turbulent rate the same for all the reactions. Therefore, if detailed chemistry is taken into account, the ED/FR model will likely produce incorrect results since the rate of production/destruction of the species has to be controlled by all the Arrhenius parameters for accurate description of turbulence/chemistry interactions [28].

The PDF Flamelet model in CFX is developed for modeling of non-premixed flames. Whereas testing this model for the LIMOUSINE combustor, it was found that the model is able to predict the instability correctly, but it failed in prediction of self-excited modes.

The Burning velocity model (BVM) is found to over-predict the mean temperature and species concentrations. In this model the combustion process is modeled in terms of a single transport equation for the mean reaction progress variable $\bar{c}$. The source term of the progress variable is defined by [29]:

$$\bar{w}_c = \rho_u s_T |\nabla \bar{c}| \qquad 4\text{-}12$$

Where s_T is the turbulent flame speed, including physico-chemical properties and local turbulence parameters of the combustible mixture. The coupling to the transport equations of the flow field is conducted with the density calculated from the reaction progress variable.

Fourier analysis of the pressure signal obtained from the BVM model yields two distinct peaks appearing at frequencies of about 319 and 638 Hz. Among the combustion models tested in this paper, the BVM model is the only model able to predict the frequency doubling of the first self-excited mode. These peaks were present in the experiment, but with different amplitude and frequencies. Since in this paper the mutual interaction between flow and the vibrating liner (due to the high amplitude thermo-acoustic instabilities) for the numerical computations has been neglected, the effect of the vibrating walls on the combustible flow is only visible during the experiment. Numerical simulation by using Large Eddy Simulation (LES) in the current combustor also predicted a dominant peak at 305 Hz and also the secondary peak 617Hz [11] which is close to the value calculated by BVM model. Nevertheless, some discrepancies between simulations and experiment, in the prediction of fundamental frequency in this bluff body stabilized combustor, use of the BVM model for other applications on a swirl stabilized flame computations shows promising results as compared to experimental data [30]. Although the Burning Velocity Model (BVM) is intended for simulation of premixed or partially-premixed flames, accuracy of results using the BVM becomes unsatisfactory, when the flame is lifted and products are recirculating into the fresh mixture; therefore the results will not be in line with the experiment. Especially the reaction is predicted to start further upstream as compared to the experiment, showing as streaks of high temperature surrounding the fuel jet. Using an alternative discretization will suppress these unphysical artifacts and improves the accuracy of results as presented in Figure 4-7-f.

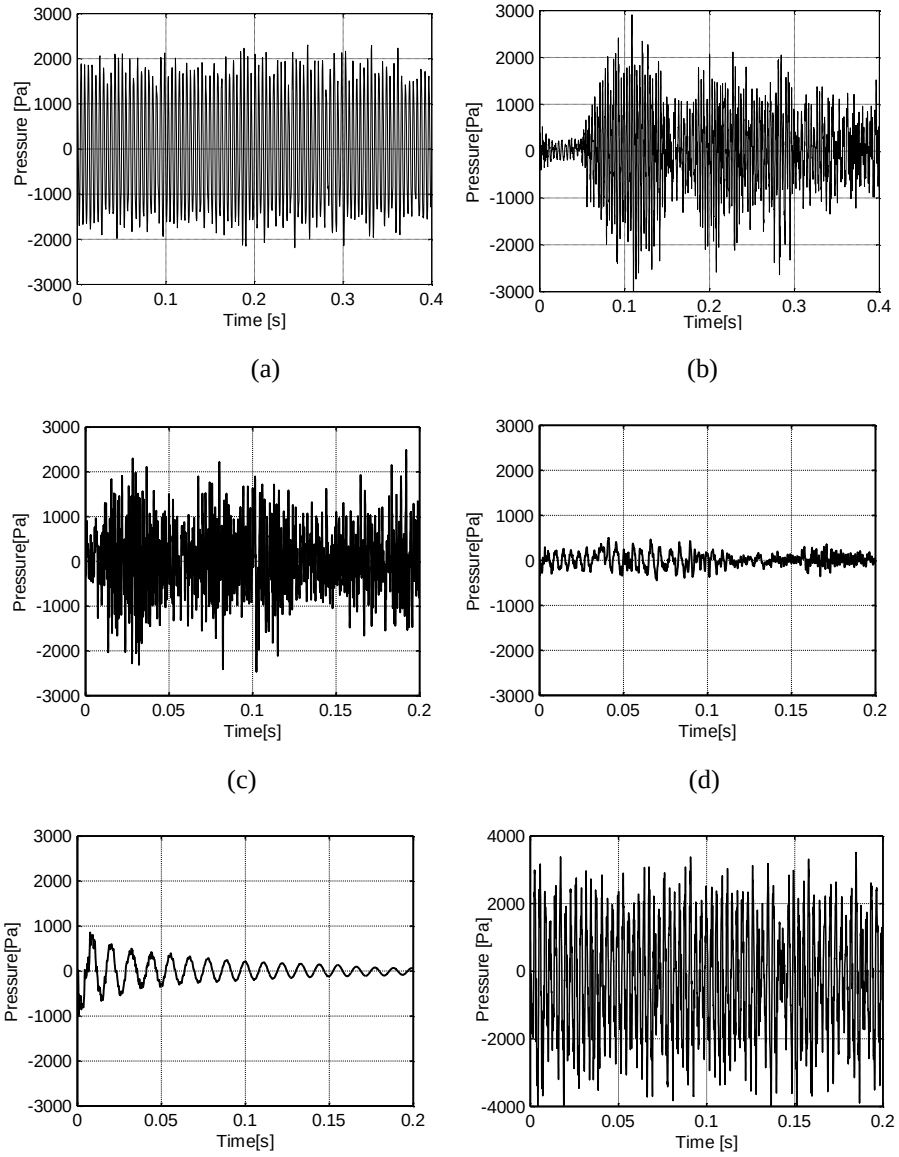

Figure 4-6: Pressure fluctuations time history at power = 40 kW and λ=1.4 measured at a location 200 mm downstream the wedge taken from (a) Experiment (b) BVM (c) PDF (d) EDM (e) EDM/FRC (f) modified BVM

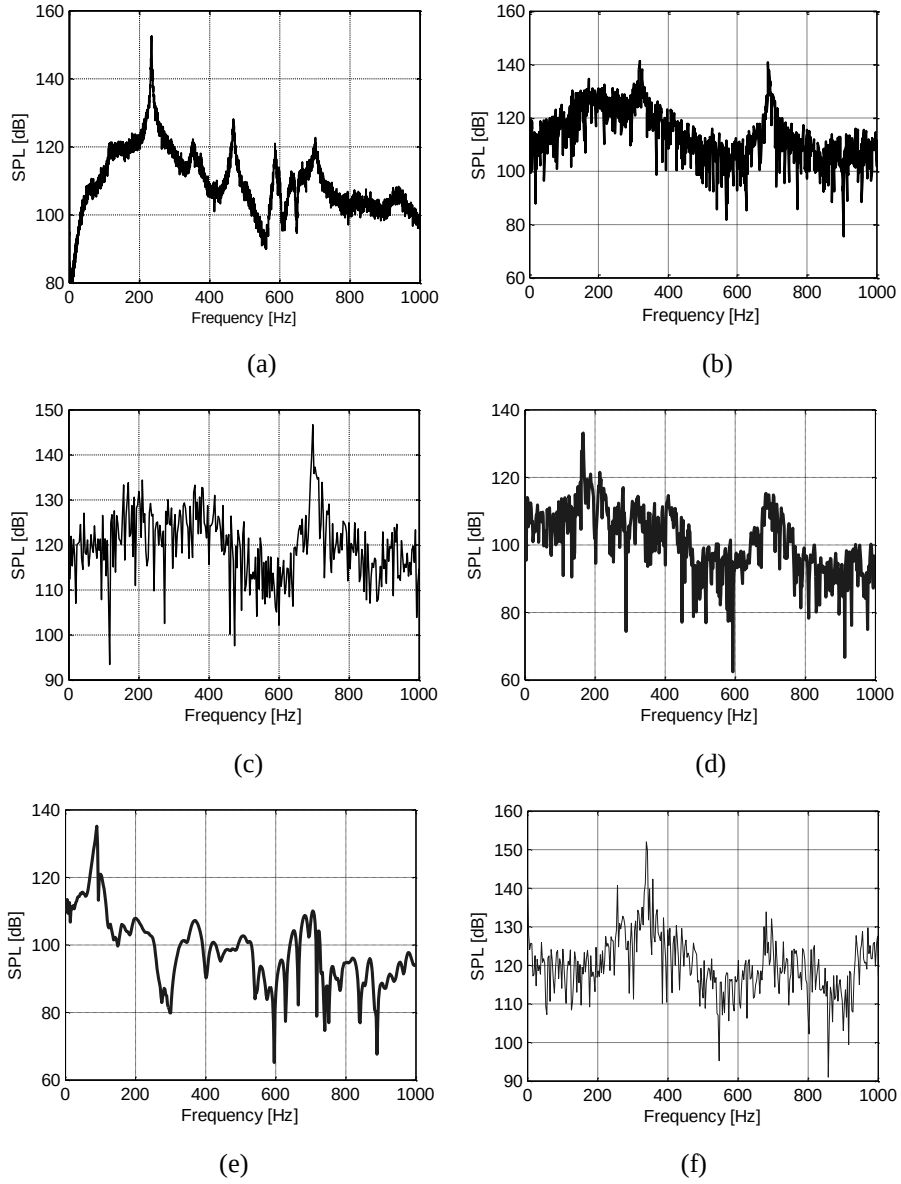

Figure 4-7: Pressure spectrum at power = 40 kW and λ=1.4 measured at a location 200 mm downstream the wedge taken from (a) Experiment (b) BVM (c) PDF (d) EDM (e) EDM/FRC (f) modified BVM

4.5.2 Acoustic boundary condition effect

The acoustic boundaries of a combustor have the important role to characterize the combustion-acoustic instabilities. The flux of acoustic energy through the boundaries is the major component of the acoustic losses. Therefore the imposed acoustic boundary conditions together with the temperature field can define/change the frequencies and amplitudes at which the acoustic modes are in resonance. In the previous calculations it was assumed that the acoustic pressure goes to zero at the open end (outlet). Although the pressure amplitude decreases within the duct, it does not drop to zero, and therefore not all the sound is reflected back down the tube. Indeed some is radiated into the fluid outside. This effect can be taken into account by considering the final layer of fluid at the open end to vibrate back and forth as a piston [31]. In the presence of a mean flow for an un-flanged pipe, the end correction (δ) varies from the value of $\delta/a = 0.61$ at the high Strouhal number limit ($Sr = fL/U$)[3], (a is the pipe radius), to the value of $\delta/a = 0.19$ in the low Strouhal number limit [31, 32]. Therefore the CFD domain downstream the wedge is elongated to represent the complex boundary condition in the form of an end correction. Therefore there is now a pressure node just beyond the original outlet of combustor located at (Dh+ δ) and a velocity node at the position of (- Uh) as presented in Figure 4-8. The reflection of low frequency waves at the outlet (i.e. an open end) occurs with an 180^o degree phase shift. This means that the wave steepening effect is reversed after the reflection.

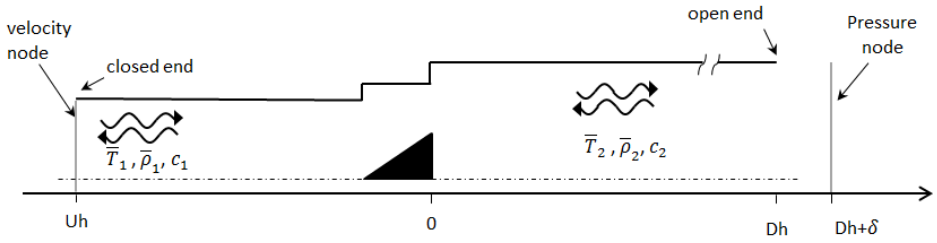

Figure 4-8: The enlarged computation domain

[3] L is a characteristic length (equal to the diameter D in case of a circular cylinder or tube in cross flow) and U the free-stream velocity.

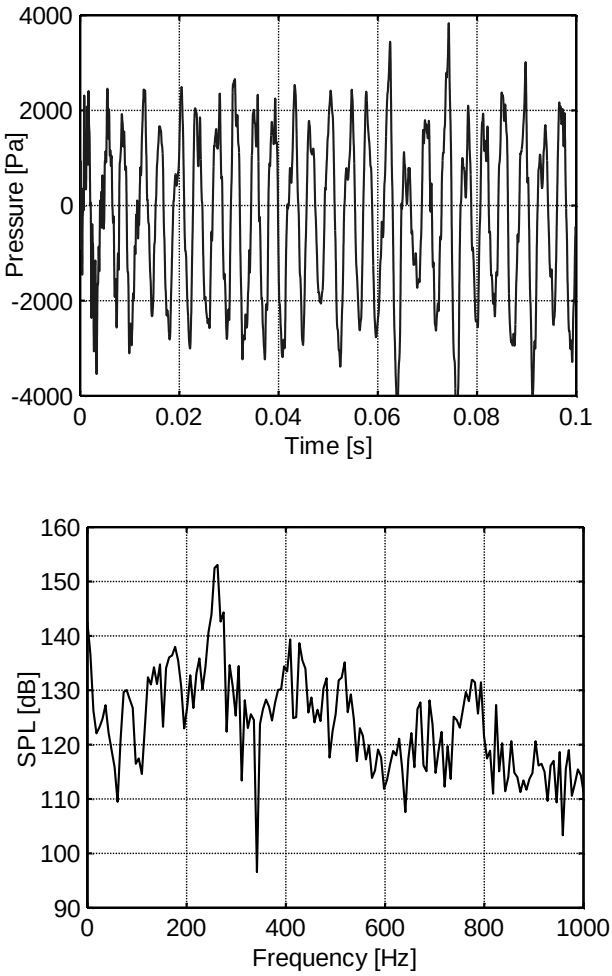

Figure 4-9: Pressure fluctuations time history and FFT at power = 40 kW and λ=1.4 measured at a location 200 mm downstream the wedge by using the modified BVM and implementing the end correction

An overview of the amplitude of the pressure fluctuation in the simulation, as a function of time and frequency is shown in Figure 4-9. It is apparent that by considering the end correction in the CFD domain some acoustic energy has been transferred from the second frequency to the first one. Table 4-5 represents the capability of the present numerical solution to capture the main flow features. The frequency in which the main instability occurs is overpredicted by 9.5% error as

compared to the experimental value. The magnitude of the first mode is also overpredicted about 0.6 dB.

Table 4-5: Calculated and measured self-excited modes

	f1 (Hz)	Amplitude (dB)
CFD	256	153
Experiment	234	152.4

4.5.3 Flow characteristics

The recirculating flow region behind the bluff body contains hot combustion products that ignite the incoming reactants. Considering that the unsteady flow fields in reacting bluff-body flows are mainly dominated by large-scale coherent structures, even a small change in the flow field can modify hydrodynamics at the burner outlet by increasing/decreasing velocity of the oxidizer and fuel and in consequence affect the strength of the recirculation zone. This can play an important role in the mechanisms of the flame stabilization and mixing, which may cause thermo-acoustic instabilities. Particle Image Velocimetry, PIV, is capable of measuring the two-dimensional unsteady flow field inside the combustor. This can be used, e.g. in order to visualize the recirculation zone behind the bluff body, which is an important factor for the flame stabilization mechanism in the LIMOUSINE combustor; as the prediction of the reversal zone behind the bluff body is of a great importance for the subsequent analysis of the flame-flow interaction inside the LIMOUSINE burner. Here the velocity field, measured with PIV at Imperial College London on the twin unit of LIMOUSINE combustor is used as a validating tool for the used numerical methods [33]. The recording frequency was 10Hz. Figure 4-10 shows the mean vertical velocity component (v) downstream of the bluff body for the unstable operating point of the combustor. The experimental data has been averaged over the small number of 327 images which explains the reason for having rather noisy mean velocity fields. The origin of the vertical axis is the burner plane. In each part of this figure, isocontours of v = 0 are shown representing the spatial boundaries of the recirculation zone. The

central recirculating zone (CRZ) forms a flame stabilization region where the incoming mixture of air and fuel are mixed with the hot products before ignition which allows high rate of heat release. The flow in this region is associated with high turbulence intensity. Furthermore, due to the sudden expansion of the combustor configuration, two corner recirculation zones (CORZ) are formed downstream of the bluff body. Overall, the simulation captured the correct trend, but slightly over-predicted the magnitude of the streamwise velocity as well as the extent of the recirculation zone. The main reason for such findings is the slight difference in the predicted axial momentum flux at incoming fresh flow of reactants passing the bluff body. These small flow differences impose changes in the recirculating region which modify the flame stabilization mechanism. Despite these observations, there is fair agreement between the mean flow predictions and the measurements. The current predictions are able to capture the essential characteristics of the flow (i.e. stagnation points etc.), and as presented in Table 4-6 uncertainties do not exceed 11% compared to experimental data (which also contains measurement errors like the reflections from the laser beam).

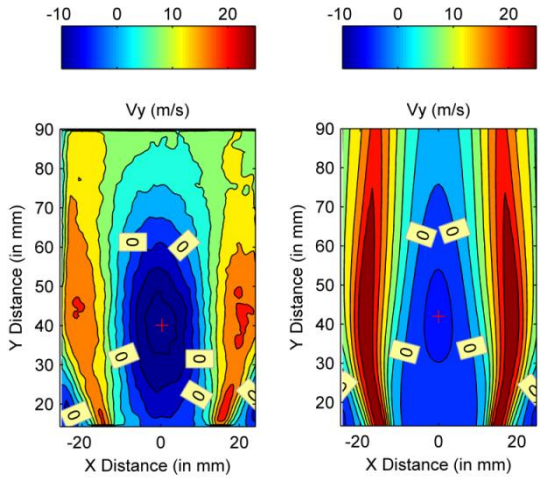

(a) (b)

Figure 4-10: The average stream wise velocity component at power = 40 kW and λ=1.4 for (a) PIV [33] and (b) CFD model

Table 4-6: Calculated and measured reattachment length

	PIV	CFD
Reattachment length (mm)	67.77	75.8
Error (%)	---	11.85

4.5.4 Heat transfer effect on the liner

During the combustion process, heat is transferred from the hot flame by radiation and convection to the liner. However, the radiative heat exchange highly depends on the distance between the flame and the liner and also on the absorption by the colder combustion gases in between. The liner is cooled by the surrounding air at atmospheric condition; hence there is heat transfer from the structure to the environment. The balance between the heat absorption released from the hot gases by convection and radiation and the heat lost to the surrounded air by convection and also radiation defines the increase rate of the liner temperature. Figure 4-11 represents the schemata of the heat transfer process through the liner walls. The radiation heat flux, and the convection heat flux from gas are shown respectively by Q_{rad1} and Q_{conv1}; While Q_{conv2} , Q_{rad2} respectively stand for the convection and radiation heat flux from the liner to the surrounding air, $Q_{cond_{1,2}}$ is the conduction heat flux across the wall thickness and also along the liner. Loss of heat by conduction along the liner is negligible compared to the other terms. Therefore under steady-state conditions, the heat transfer into the wall domain is balanced by the heat transfer out of it.

$$\mathrm{Q_{rad1}} + \mathrm{Q_{conv1}} = \mathrm{Q_{rad2}} + \mathrm{Q_{conv2}} \qquad 4\text{-}13$$

The study of the heat transfer occurring during a cycle of a pressure oscillation in the LIMOUSINE combustor has been numerically investigated in the premixed condition [34], while in this paper, the main purpose is to investigate the effect of the thermal losses on the unstable behavior of the flame in a partially premixed condition. Two numerical simulations are done only for one operative condition, where the limit cycle behavior have been observed (power = 40 kW and λ=1.4). The first simulation is performed assuming the lateral side walls to be adiabatic, while in the second calculations the lateral side walls (liner) are considered as isothermal with a prescribed constant temperature of 1,000 K. The effect of the

thermal losses on the combustion instabilities and the possible limit cycle behavior will be discussed in the following results (Figure 4-12 to Figure 4-18).

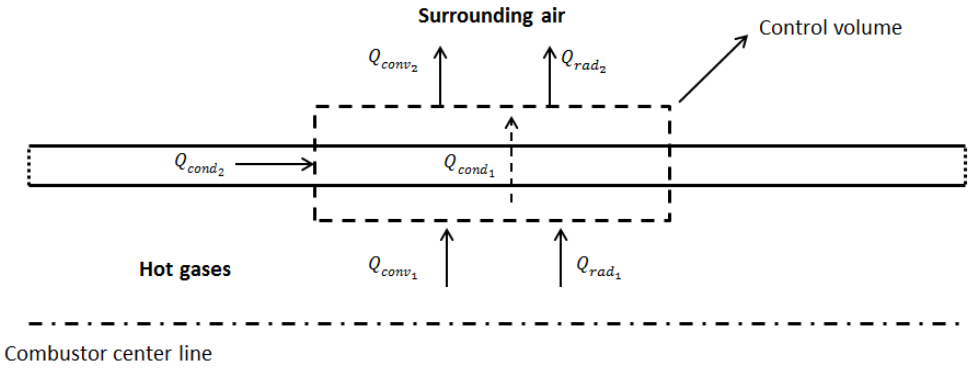

Figure 4-11: Representation of the heat transfer in the combustor

Pressure & Temperature fields

Figure 4-12 represents the pressure signal calculated for the adiabatic and non-adiabatic liner. The evolution of the pressure oscillations for the isothermal case represents for almost the whole simulation an amplitude of about 2,500 Pa, while by considering the adiabatic liner, the pressure can even reach to 5,000 Pa which is much higher than the measured value. As it was previously mentioned, limit cycle oscillations determine an equilibrium point in which the energy flux from the flame to the environment is constant. The adiabatic boundary condition on the liner minimizes the amount of energy that can be dissipated by heat losses and as a consequence the LCO has larger amplitude. Therefore taking into account the heat losses through the liner in the second simulation will lead to the lower pressure amplitudes. Comparing Figure 4-13 and Figure 4-14, it can be observed that the temperature evolution in the case with the isothermal liner is smoother and more uniform, while assuming the adiabatic liner leads to the bigger temperature gradients across the fluid domain. Bigger and stronger temperature gradients are more likely to produce stronger fluctuations in the mass flow rate since bigger temperature fluctuations are expected. Furthermore in the case with the adiabatic liner, it seems that the mixing process of hot gases and the fresh incoming fuel/air mixture takes place over a larger volume compared to the isothermal case, and in

deed the flame is more disturbed by the incoming fresh mixture which also results in a stronger heat release fluctuation. Comparing these two figures also shows that faster reaction occurs in the adiabatic case. Finally this all leads to the higher level of pressure oscillations compared to the isothermal case which was presented in Figure 4-12. In addition in the adiabatic liner case a bubble of cold flow is formed causing the local quenching of the flame close to the bluff body which is acting as a heat sink (Figure 4-13-c). Therefore in this case, there is less contact between hot products and cold mixture leading to slower reaction compared to the second case. While according to Figure 4-14, the incoming fresh jets are surrounded by hot gases trapped in the center and corner recirculating zones; the incoming mixture of air and fuel are mixed with the hot products before ignition and indeed the recirculated hot combustion products transports momentum and energy back to the further upstream where they mix with the incoming fresh mixture; The exchange between the recirculating hot exhaust gases and the fresh methane air mixture supplies the energy required to ignite the fresh gases. The shear layer between the hot exhaust gases and the fresh methane air mixture acts in a way to increase the temperature of the reactants as they are convected into the flame zone. Unburned mixture segments broken up away from the main stream of the flow, will generate local hot spots further downstream. A periodic variation of the temperature field and a spatial motion of the flame can be clearly observed in both cases; however this movement (i.e. the perturbation of the flow rate induced by the standing mode which is controlling the reaction rate in front of the burner) is stronger in the adiabatic liner case compared to the isothermal one. Overall, it can be concluded that the accuracy of pressure results (i.e. acoustic of the system) relies on the thermal loads on the liner. Also both cases regardless of the given error rate in the main frequency of instability over-predicted the magnitude. This means that still more accurate model, able to predict the accurate heat losses is required.

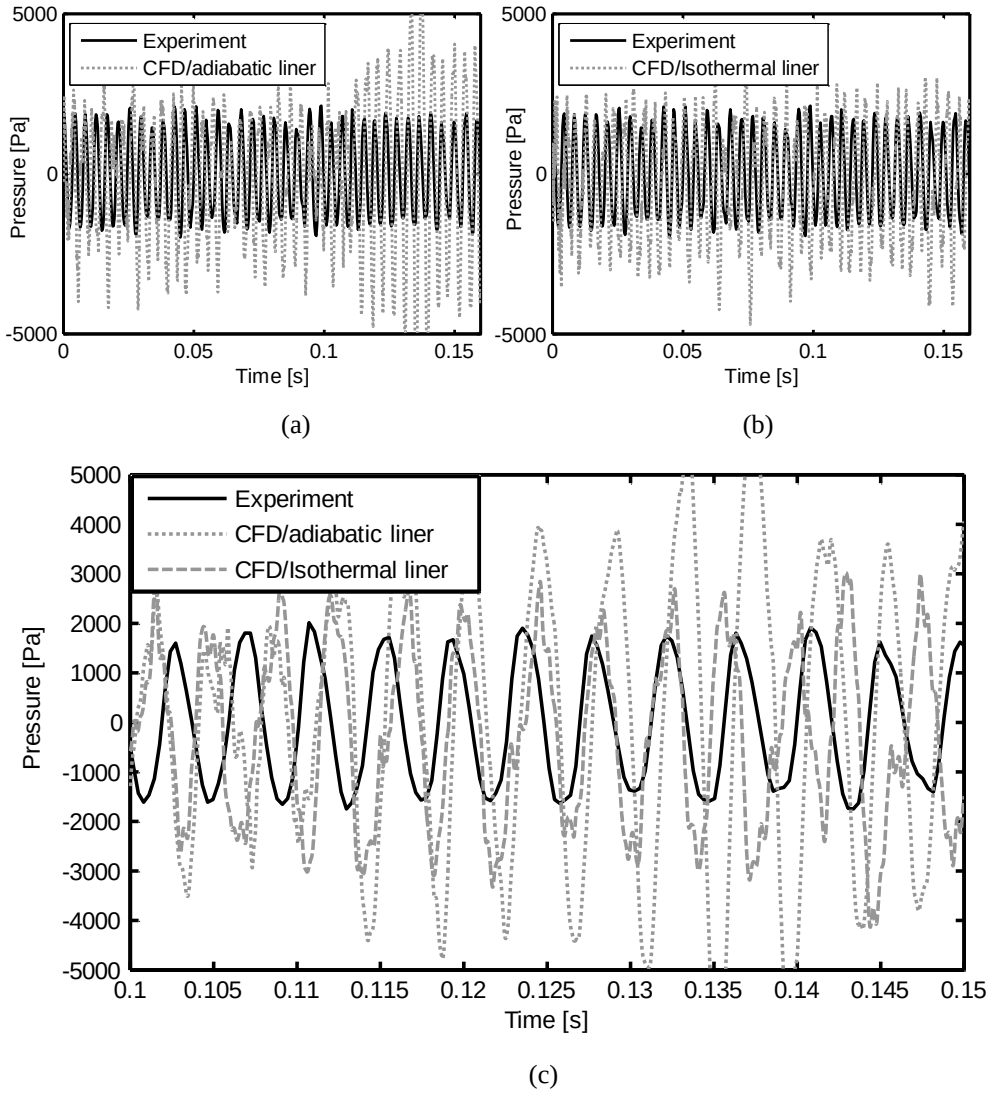

Figure 4-12: Pressure signal over the time for the (a) adiabatic (b) isothermal liner case (c) comparison between cases

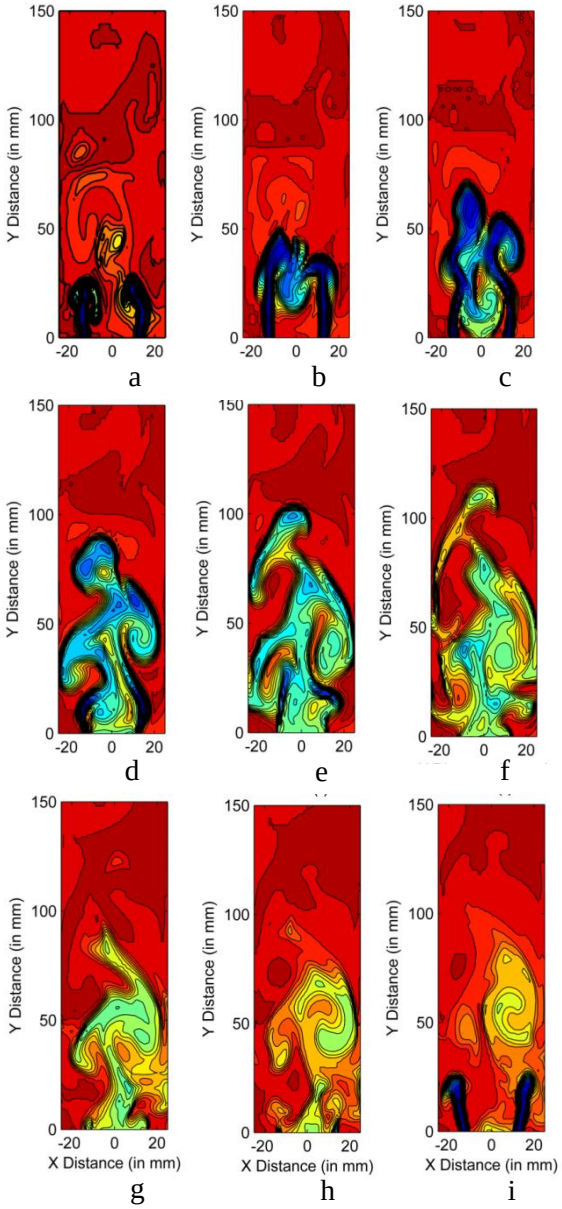

Figure 4-13 : Temperature contours (in K) for the combustor with adiabatic liner

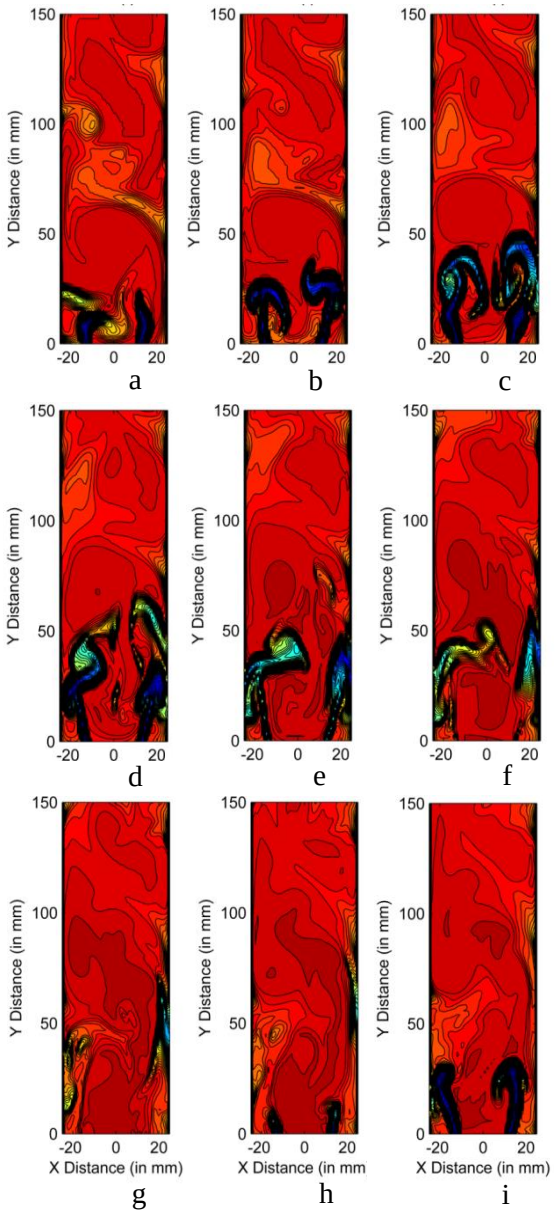

Figure 4-14: Temperature contours (in K) for the combustor with isothermal liner

Heat release

A flame heat release analysis can be used in the design phase to identify the critical frequency ranges for the arising of unstable thermoacoustic oscillations. The interest in these simulations is to model the oscillating heat release within the chamber as a function of imposed boundary conditions on the structure. The instantaneous rate of heat release term can be determined with knowledge of local species and temperature field via:

$$\dot{\omega}_T = -\sum_{k=1}^{N} \Delta h_{f,k}^0 \dot{\omega}_k \qquad 4\text{-}14$$

In which h_f^0 and $\dot{\omega}_k$ respectively stand for the formation enthalpy and the reaction rate of species k.

Since the maximum rate of heat release is localized near the flame zone and considering the fact that OH and CH species radicals are only produced in the flame front, therefore they can be taken as a qualitative indicator of the flame heat release. Figure 4-15 represents the average OH* emission. The heat release of the flame is measured using a Photo Multiplier Tube. It is a device that provides a voltage output proportional to the incident intensity of the light [23]; since it is not possible to predict the excited OH* radicals with CFD, therefore the evolution of the weighted reaction progress source is taken as a variable qualitatively representing the heat release as presented in Figure 4-16 for cases with the adiabatic and the non-adiabatic liner. Compared to Figure 4-15, these figures indicate that the flame is anchored on the bluff body while average intensity shows a flame lifted at the flame holder. The current predictions show a deviation of the CFD predictions from measurements. However not much difference between the adiabatic and isothermal simulations is observed in the heat release contours. Hence the higher pressure amplitude observed in the adiabatic case is not explained by a different flame shape but by the leakage of thermal energy in the isothermal case. The obtained results for RMS stream wise velocity component (V_y') shown in Figure 4-17 indicate higher velocity fluctuations in the adiabatic liner assumption pointing to the fact that the stability of the flame is decreased by increasing the turbulent intensity.

Figure 4-18 shows variations of pressure and reaction rate (heat release) in the combustor over a short time period. The pressure amplitude is amplified as long as

it is in phase with the reaction rate. This plot confirms that the unsteady reaction rate is controlled by acoustic oscillations (i.e. fluctuation of pressure field), which are the source of strong movement of the flame.

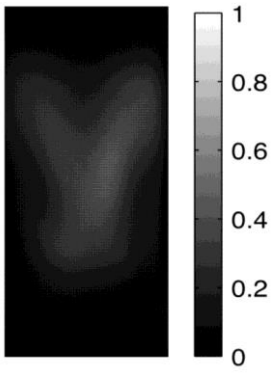

Figure 4-15: Averaged intensity plot from experiments for 40kw and λ = 1.40

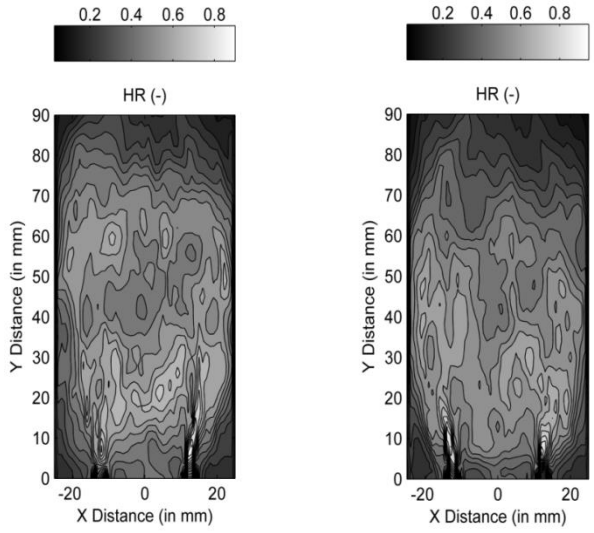

Figure 4-16: Heat release contour for the adiabatic (LHS) (b) isothermal liner case (RHS)

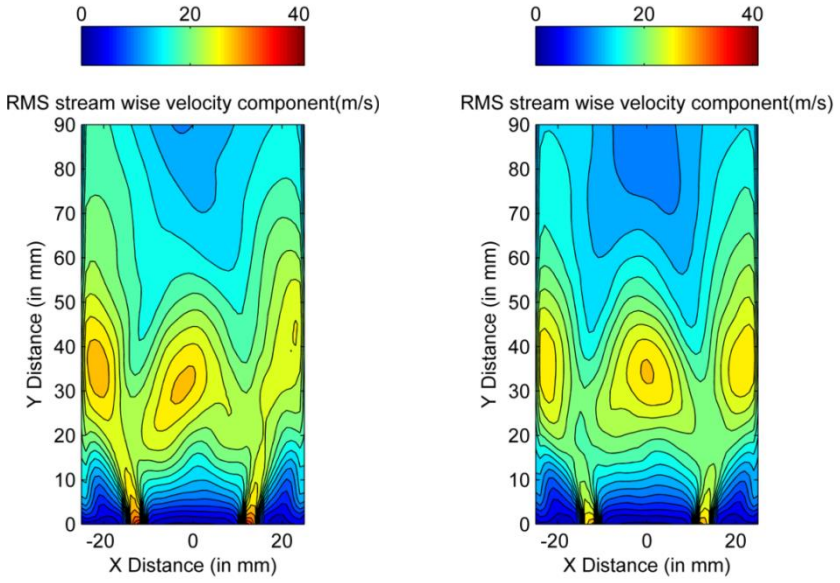

(a) (b)

Figure 4-17: CFD data representing the rms stream wise velocity component ($\mathbf{V_y'}$) for (a) adiabatic (b) isothermal liner

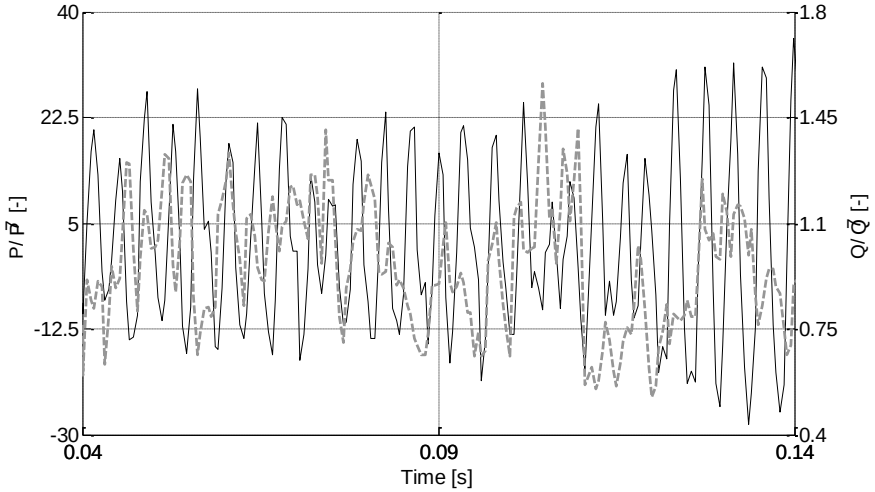

(a)

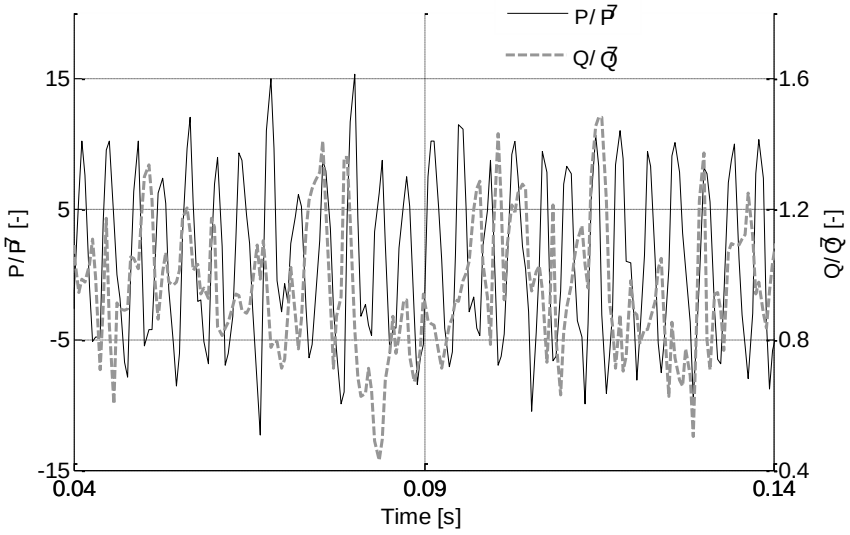

(b)

Figure 4-18: Pressure (solid line) and heat release (dash line) signals for the (a) adiabatic (b) isothermal liner case

4.5.5 Convective time delay

Time delays and characteristic times correspond to the elementary processes play a major role in the stability of the system. Since the convection process has usually the longest time scale, it is essential to be estimated for analyzing the combustion instability. Torres et al. [35] reported for their low NOx gas turbines (LNGT), combustion instabilities are function of the ratio of the acoustic period and the convective time from the fuel injector to the flame front, and instabilities occur for the specific values of this ratio. The mean convective time delay between heat release and the perturbation in the flow can also be determined by steady state computation of the considered configuration or by deriving the mean field of the transient calculations. In this case no forced response is calculated. Fresh reactants injected into the chamber in one instant are convected into products at a later time. This concept introduces some time lags in the system. A system with delay can be shown by a second-order vibration model as suggested by Candel [1]. The model features a linear damping and a restoring force with a delay according to:

$$\frac{d^2x}{dt^2} + 2\xi\omega_0\frac{dx}{dt} + \omega_0^2 x(t-\tau) = 0 \qquad 4\text{-}15$$

Where ξ is the damping ratio, ω_0 is the angular frequency and the τ represents the time lag of the system. By assuming a small value of delay, τ, and using a first order term in a Taylor series, above equation can be rewritten as:

$$\frac{d^2x}{dt^2} + \omega_0(2\xi - \omega_0\tau)\frac{dx}{dt} + \omega_0^2 x(t) = 0 \qquad 4\text{-}16$$

The system has a negative damping coefficient for $\omega_0\tau > 2\xi$ indicating that the amplitude grows up exponentially, for big time lags.

Prior studies performed by Lieuwen et al. [36] suggested that to predict instability conditions of the system, the ratio $\tau_{conv,eff}/T$ should be determined, since instability regions are primarily its function. This ratio is equal to the summation of the convective times $\tau_{convect}$ and τ_{eq}. The convective time, τ_{convect}, can be approximated as the distance from the fuel injector to the base of the flame. Since the reactants are not consumed instantly when they reach the base of the flame, another time delay, τ_{eq} is introduced, pointing to the fact that the mixture is not completely consumed until it reaches the end of the flame. According to that study, the instability regions are located at:

$$C_n - 1/4 < \tau_{conv,eff}/T < C_n + 1/4 \quad \text{4-17}$$

where C_n is a constant which depends on the combustor configuration. In the current configuration C_n can be taken as 1 [23].

Candel [1], distinguished also another time delay, τ_i, which appears in the system and corresponds to the phase shift between the pressure oscillation at the injector and the fuel mass flow rate. However, the dominant delay in the system is associated to the convection. To determine characteristic convection time delay ($\tau_{conv,eff}$) for a partially-premixed combustor, Alemela et al. [37] considered the mean convective time delay to be proportional to the ratio between the distance in which the highest reaction occurs (approximately the length of the flame) and the effective mean speed. This approach can give a rough estimation of the time delay as:

$$\tau_{conv,eff} \sim X_{OH^* max}/U_{eff} \quad \text{4-18}$$

In the numerical calculations, the position of the flame is extracted from the computed heat release field (i.e. by weighted reaction progress source) and the convective time delay, $\tau_{conv,eff}$ can be calculated based on the mean velocity in the downstream duct, as given by [37]:

$$U_{eff} = U_{inj,C}\left[1 + \frac{1}{2}\left(\frac{U_h}{U_{inj,C}} - 1\right)\right] \quad \text{4-19}$$

where U_h is the average velocity at the location where the maximum heat release occurs and $U_{inj,C}$ corresponds to the location of the fuel injection.

A time lag analysis of an unstable combustion was also carried out by Roman Casado [23] and Alemela et al. [38] for the same duct configuration. In both works, the length and the fuel injection location were varied based on the time delays of the system in order to design a combustor prone to thermoacoustic phenomenon. It was shown that the analysis of time lag offers accurate prediction of instability.

Table 4-7 represents the computed mean convective delay. As it is found, the combustion instability occurs when the acoustic (resonant) time scale of the combustor is in the same order as the characteristic convective time scale of the combustor. However this estimation of delay of the flame response can just give a rough idea about the stability of the combustor. The predicted stability condition of the system is in line with majority of the obtained experimental data; although, as

presented in the Figure 4-4, for the λ=1.6 case, the flame is in the transient region representing a stable or unstable behavior.

Table 4-7: mean convective time delay calculated for different operating conditions

Th. Power [kW]	Air factor λ [-]	$\tau_{conv,eff}/T$	Instability condition according to eq. 4-17
40	1.4	1.23	Unstable
40	1.6	1.62	Stable
40	1.8	1.79	Stable

4.6 Conclusions

In this paper the flame dynamics of the LIMOUSINE burner has been studied and compared with experimental data. The limit cycle oscillations (LCO) and combustion driven thermoacoustic instabilities have been characterized and predicted. The performance of the combustion model for the reacting configuration has been presented and the main issues of combustion modeling were addressed. Since the acoustic boundaries of the combustor have the important role to characterize the thermoacoustic instabilities, for their accurate representation, the CFD domain downstream the wedge was extended. In order to determine the uncertainty related to the imposed thermal boundary condition, an adiabatic and isothermal domain was investigated. Considering that the time delays and characteristic times play a major role in the stability of the system, the convective time, τ_{convect}, has been approximated.

The present study has revealed the following observations:

- Among the available combustion models in ANSYS CFX, the Burning Velocity Model (BVM) using a new model option for non-premixed flames (referred as Modified BVM in this paper), gives the best consistency with the experiments.
- Predicted results show the important effect of implementing correct thermal boundary condition for proper characterization of the LCO. The combustion

instabilities are highly influenced by the mean properties of the flow field which are determining different flame structures.

- Due to the importance of correct prediction of heat losses, this subject deserves further investigations to understand the mechanism regulating the coupling between heat release rate fluctuations and the acoustic field. For this reason, and to determine the heat penetration depth in the structure of the test rig, the thermal coupled fluid structure interaction modeling is recommended for present configuration.
- The ratio of $\tau_{conv,eff}/T$ predicted by RANS calculations is used to estimate the instability condition of the combustion system, showing good match with experimental data.

Acknowledgments

The authors would like to acknowledge the funding of this research by the EC in the Marie Curie Actions Networks for Initial Training, under call FP7-PEOPLE-2007-1-1-ITN, Project LIMOUSINE with project number 214905. Special thanks go to Dr. Phil Stopford for the support in the use of ANSYS-CFX.

References

[1] Candel, S., 2002, "Combustion dynamics and control: Progress and challenges," Proceedings of the Combustion Institute, 29(1), pp. 1-28.
[2] Lartigue, G., Meier, U., and Bérat, C., 2004, "Experimental and numerical investigation of self-excited combustion oscillations in a scaled gas turbine combustor," Applied Thermal Engineering, 24(11–12), pp. 1583-1592.
[3] Kelsall, G., and Troger, C., 2004, "Prediction and control of combustion instabilities in industrial gas turbines," Applied Thermal Engineering, 24(11–12), pp. 1571-1582.
[4] Juan Carlos Roman Casado, Reddy Alemela, and Kok, J. W. B., "Combustion dynamics coupled to structural vibrations," Proc. 17th International Congress on Sound & Vibration, ICSV 17.
[5] A. Can Altunlu, Peter van der Hoogt, and ., A. d. B., "Life assessment by fracture mechanics analysis and damage, monitoring technique on combustion liners," Proc. ASME Turbo Expo.
[6] Toffolo, A., Masi, M., and Lazzaretto, A., 2010, "Low computational cost CFD analysis of thermoacoustic oscillations," Applied Thermal Engineering, 30(6–7), pp. 544-552.
[7] Huls, R., 2006, "Acousto-Elastic Interaction in Combustion Chambers," PhD, University of Twente, Enschede.
[8] Ahn, K., and Yu, K. H., 2012, "Effects of Damköhler number on vortex–flame interaction," Combustion and Flame, 159(2), pp. 686-696.

[9] Foucher, F., Burnel, S., Mounaïm-Rousselle, C., Boukhalfa, M., Renou, B., and Trinité, M., 2003, "Flame wall interaction: effect of stretch," Experimental Thermal and Fluid Science, 27(4), pp. 431-437.
[10] Pozarlik, A. K., and Kok, J. B. W., 2014, "Fluid-Structure Interaction in Combustion System of a Gas Turbine—Effect of Liner Vibrations," Journal of Engineering for Gas Turbines and Power, 136(9), pp. 091502-091502.
[11] Vera, I. H., 2011, "Soot modeling in flames and Large-Eddy Simulations of thermo-acoustic instabilities," PhD, Universite de Toulouse.
[12] Lighthill, M. J., 1952, "On Sound Generated Aerodynamically, I. General Theory," Porceedings of the Royal Society of London, Series A, Mathematical and Physical Sciences, 211(564-587).
[13] Lighthill, M. J., 1954, "On Sound Generated Aerodynamically. II. Turbulence as a Source of Sound," Proceedings of the Royal Society of London, Series A. Mathematical and Physcal Sciences, 222, pp. 1-31.
[14] Klein, S., 2000, "On the acoustics of turbulent non-premixed flames," PhD, University of Twente, Enschede.
[15] Pozarlik, A. K., 2010, "Vibro-acoustical instabilities induced by combustion dynamics in gas turbine combustors," PhD, University of Twente, Enschede.
[16] Rayleigh, J., 1878, "The explanation of certain acoustic phenomena," Nature, 18, pp. 319-321.
[17] Nicoud, F., and Poinsot, T., 2005, "Thermoacoustic instabilities: Should the Rayleigh criterion be extended to include entropy changes?," Combustion and Flame, 142(1–2), pp. 153-159.
[18] Rijke, P. L., 1859, " On the vibration of the air in a tube open at both ends," Philosophical Magazine, 17, pp. 419-422
[19] Patankar, S. V., 1980, Numerical Heat Transfer and Fluid Flow, Hemisphere Publishing Corp.
[20] C.M.Rhie, and W.L.Chow, 1982, "a numerical study of Turbulent Flow Past an Isolated Airfoil with the Trailing Edge Separation," Aiaa Journal, pp. 82-0998.
[21] Majumdar, S., 1988, "Role of underrelaxation in momentum interpolation for calculation of flow with nonstaggered grids," Numerical Heat Transfer, 13(1), pp. 125-132.
[22] L.Y.M. Gicquel, G. Staffelbach, and Poinsot, T., 2012, "Large Eddy simulations of gaseous flames in gas turbine combustion chambers," Progress in Energy and Combustion Science, 38(6), pp. 782–817.
[23] Roman Casado, J. C., 2013, "Nonlinear behavior of the thermoacoustic instabilities in the limousine combustor," PhD, University of Twente, Enschede.
[24] Thierry J. Poinsot, Arnaud C. Trouve, Denis P. Veynante, Sebastien M. Candel , and Esposito, Emile J., 1987, "Vortex-driven acoustically coupled combustion instabilities," Journal of Fluid Mechanics, 177, pp. 265-292.
[25] Yu, K. H., Trouve, A., and Daily, J. W., 1991, "Low-frequency pressure oscillations in a model ramjet combustor," Journal of Fluid Mechanics, 232, pp. 47-72.
[26] Roman Casado, J. C., and Kok, J. B. W., "Non-linear effects in a lean partially premixed combustor during limit cycle operation," Proc. Proceeding of ASME Turbo Expo.
[27] A. Can Altunlu, Mina Shahi, Artur Pozarlik, P.J.M. van der Hoogt, J.B.W.Kok, and Boer, A. d., "Fluid-structure interaction on the combustion instability," Proc. ICSV19.

[28] Parente, A., Galletti, C., and Tognotti, L., 2008, "Effect of the combustion model and kinetic mechanism on the MILD combustion in an industrial burner fed with hydrogen enriched fuels," International Journal of Hydrogen Energy, 33(24), pp. 7553-7564.
[29] Kapucu, M., Kok, J. B. W., and Alemela, R., "Characterization of acoustic oscillations in fuel supply lines," Proc. ICSV18.
[30] Ozcan, E., 2012, "Tuning the self -excited thermo-acoustic oscilations of a gas turbine combustor to Limit Cycle Operations by means of numerical analysis " Master Thesis, University of Twente.
[31] Blackstock, D. T., 2000, Fundamentals of Physical Acoustics, Wiley.
[32] Peters, M. C. A. M., Hirschberg, A., Reijnen, A. J., and Wijnands, A. P. J., 1993, "Damping and reflection coefficient measurements for an open pipe at low Mach and low Helmholtz numbers," Journal of Fluid Mechanics, 256, pp. 499-534.
[33] Shahi, M., Kok, J. B. W., Sponfeldner, T., and Pozarlik, A., 2013, "Thermal and fluid dynamic analysis of partially premixed turbulent combustion driven by thermo acoustic effects," ICSV20Bangkok, Thailand.
[34] Filosa, A., Shahi, M., Tomasello, A., Noll, B., Aigner, M., and Kok, J., "numerical studies of unsteady heat transfer with thermoacustics oscillations," Proc. 20th International Congress on Sound & Vibration.
[35] Torres, H., Lieuwen, T.C., Johnson, C., Daniel B.R., and Zinn, B.T., 1999, "Experimental investigation of combustion instabilities in a gas turbine combustor simulator," Aiaa Journal, pp. 99-0712.
[36] Lieuwen, T., Torres, H., Johnson, C., and Zinn, B. T., 2000, "A Mechanism of Combustion Instability in Lean Premixed Gas Turbine Combustors," Journal of Engineering for Gas Turbines and Power, 123(1), pp. 182-189.
[37] Alemela, P., Fanaca, D., Hirsch, C., Sattelmayer, T., and Schuermans, B., 2010, "Determination and scaling of thermo acoustic characteristics of premixed flames," International Journal of Spray and Combustion Dynamics, 2(2), pp. 169-198.
[38] Alemela, P., Casado, J., Kumar, S., and Kok, J., 2013, "Thermoacoustic analysis of the dynamic pressure inside a model combustor during limit cycle oscillations," International Journal of Spray and Combustion Dynamics, 5(1), pp. 25-48.

5

Transient Heat Transfer between a Turbulent Lean Partially Premixed Flame in Limit Cycle Oscillation and the Walls of a Can type Combustor

Mina Shahi, Jim. B.W.Kok, J.C. Roman Casado, Artur Pozarlik

University of Twente, Faculty of Engineering Technology, Laboratory of Thermal Engineering, Enschede, the Netherlands

Submitted to Appl. Therm. Eng. (2014)

Abstract

In this paper transient fluid-structure thermal analyses of the Limousine test rig have been conducted while the combustor was exposed to saturated amplitude limit cycle combustion oscillations (LCO). The heat transfer between hot combustion gases and the liner wall cooled by convection will affect thermo-acoustic instabilities, and therefore the relevance of prediction of the transient heat transfer rate in gas turbine combustors is explored. The commercial CFD code ANSYS-CFX is used to analyze the problem. Fluid and solid regions are resolved simultaneously in a monolithical approach with application of a finite volume approach. Since the spatial scales of the solid temperature profiles are different in case of steady state and transient oscillatory heat transfer, special care has to be taken in the meshing strategy. It is shown that for the transient oscillatory heat transfer in to the solid in LCO operation, the mesh distribution and size of the grid in the solid part of the domain will play a very important role in determining the magnitude for the heat flow in the solid and the gas pressure fluctuations, and the grid resolution needs to be adapted to the thermal penetration depth. Moreover, compared to the calculations of only the fluid

domain with adiabatic/isothermal boundary wall conditions, the results demonstrated that application of the Conjugated Heat Transfer (CHT) model leads to significant accuracy improvements in the prediction of the characteristics of the combustion instability.

Keywords: *Combustion modeling, Conjugate heat transfer, RANS solver, Partially premixed combustion, Penetration depth*

5.1 Introduction

To improve the thermodynamic efficiency and decrease harmful emissions of gas turbine engine combustors, the amount of wall cooling air is reduced more and more, while the turbine inlet temperature is increased [1, 2]. This development requires an increasingly accurate prediction of the heat transfer to the walls of the combustion chamber. The interaction between the hot reactants and burned gases with the adjacent colder wall is a main constraint in the design of gas turbine combustion chambers in view of the life time and the reliability [3, 4]. As discussed by Carter [5] the temperature gradient in the hot component of a gas turbine increases with the turbine inlet temperature, causing high thermal stresses which may lead to creep failure of the system. To enhance the efficiency and performance of the gas turbine power plant especially in high temperature ambient conditions, different cooling schemes have been analyzed [6, 7] and influence of the water-air ratio on the blade heat transfer and hence the blade creep life of industrial gas turbine has been examined [8].

Considering that turbine nozzles and blades are exposed to the maximum and limiting temperature of a cycle, in recent years several researches have been conducted in order to investigate the heat transfer of gas turbine blades by conducting either steady state or transient Conjugate Heat Transfer calculations (CHT) [9, 10]. However, it will have to be recognized that the gas turbine combustor locally is exposed to the highest temperatures in the engine. But unfortunately no attempt has been made to evaluate the influence of transient heat transfer on characterization of Limit Cycle Oscillations (LCO) and creep life of the combustion system. Duchaine et al. [11-13] used separate solvers and codes to solve the transport equations in the fluid and solid domains, developing a strategy to couple the solvers in an accurate and stable fashion. In this method, the accuracy of results relies heavily on the coupling and interface data exchange between the flow solver and the solid heat conduction code. Kim et al. [14] used the CHT method to calculate the heat transfer and stresses in a gas turbine blade to design

the internal cooling passages. The focus of their work was on the prediction of deformation and stresses, whereas the transient thermal effects were excluded.

Since a small variation of the temperature of the blade and wall leads to considerable change of their life time, the numerical methods and tools must be optimized. The improvement in the prediction of heat loss and temperature of the system is of high importance for mechanical integrity assessments. In earlier work of Shahi et al. [15], the effect of cooling on the wall has been taken into account by specifying a wall heat flux correlation as a modified thermal wall boundary condition. A Heat Transfer Coefficient (HTC) model was used and a 1-D heat transfer model through the wall was applied, rather than implementing adiabatic or isothermal conditions. Since the largest temperature gradients are located across the liner, not along it, conventionally it is assumed that 1D heat transfer across the liner should be a good modeling approximation. However by applying the HTC model as the liner boundary condition in a fluid-domain-only calculation, the wall heat transfer is instantaneous, without any delay or heat accumulation due to the wall thermal inertia. In case of a limit cycle oscillation during the combustion process with accompanying gas temperature fluctuations, at frequencies around 300 – 500 Hz, neglecting the wall thermal inertia is not correct any more. The hot gas temperature fluctuations have a limited depth of penetration into the liner wall, and the time averaged wall temperature profile may be different from the profile predicted by the HTC model. Hence the time mean heat exchange and gas temperature can be changed due to the dynamics of the heat transfer and wall heat storage. Besides, in order to provide access to models for the life assessment of the structure, it is necessary to evaluate the temperature distribution and its oscillation amplitudes within and along the liner of the gas turbine. This is especially important in the case when the limit cycle combustion oscillations occur.

The main focus in the current work is on the transient heat transfer to the liner in the situation of limit cycle flow variations and the resulting effects on the acoustics of the system. In this work, the commercial CFD code ANSYS-CFX is used to solve the problem, in which fluid and solid regions are computed simultaneously in a monolithical finite volume approach. In the fluid region, the three dimensional compressible Favre Averaged Navier-Stokes equations are solved, while for the solid region only the enthalpy conservation equation is resolved. Simultaneous solution of the governing equations in a monolithic approach gives more accurate prediction of the transient heat transfer from/to the liner. This approach removes the uncertainties related to the coupling strategy as is necessary in partitioned

approaches [16]. Experimental data taken from Ref. [17] is used for validating the numerical results. This paper also reveals the correlation between the heat penetration depth and the solid mesh resolution which has a great effect on the predicted development of instability in the combustion system. Even though this work is performed on an atmospheric combustor, the obtained results can be relevant for the gas turbine community as it addresses the change in heat flux conditions as a key parameter controlling the speed of sound during realistic operation conditions.

5.2 Computational domain and grids

The LIMOUSINE burner configuration in limit cycle oscillatory operation is displayed in Figure 5-1. Clearly the high wall temperature zone can be observed where the flame is located. A sketch of the combustor lay out with sensor locations is shown in Figure 5-2; the detailed information about the measurement tools etc. is given in Ref. [17]. This combustor is different from the industrial gas turbine combustors, as it has an acoustically open instead of closed outlet condition, imposing atmospheric mean pressure in the combustor. But it does share with gas turbine burners a flame stabilized by a recirculation area, a narrow burner flow passage, an upstream cold flow area and an acoustically closed air inlet. Therefore it is expected that the combustion dynamics coupled to the acoustics that induce the limit cycle phenomenon are similar, and the generated data and methodology are relevant for the subsequent investigation of flame characteristics.

The computational domain employed in this work, including both solid and fluid regions is sketched in Figure 5-3. The simulation takes the advantage of the symmetry of the prismatic geometry, by considering only a thin slice of the combustor. Therefore the span wise size of the numerical domain is 4 mm wide with symmetry enforced on each side.

Figure 5-1:The LIMOUSINE combustor: thermal load on the structure in an unstable operating condition. Red dot on structure center is the laser vibrometer beam

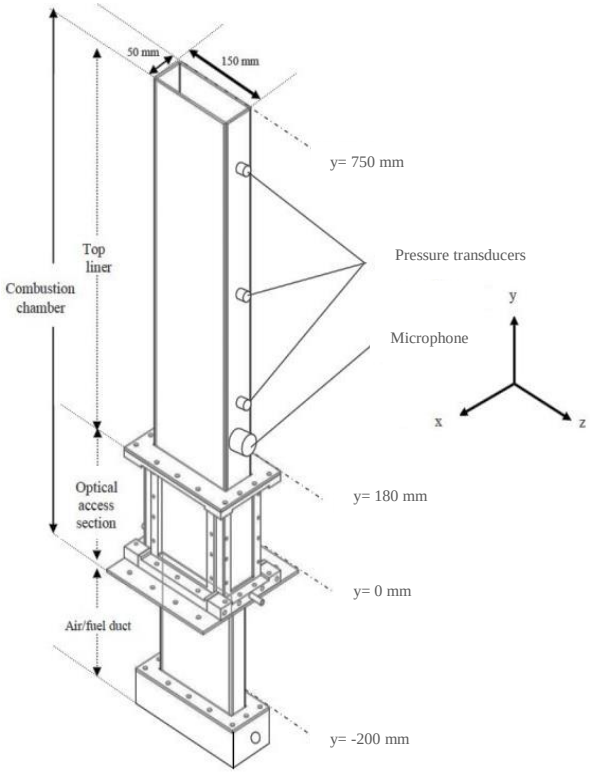

(a)

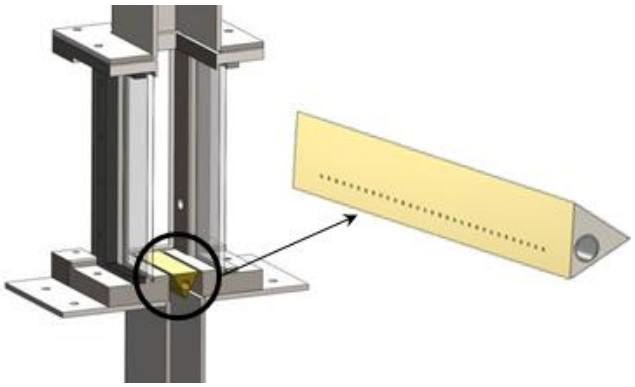

(b)

Figure 5-2: (a) General view of the set up (b) Close up view of the wedge and injection holes

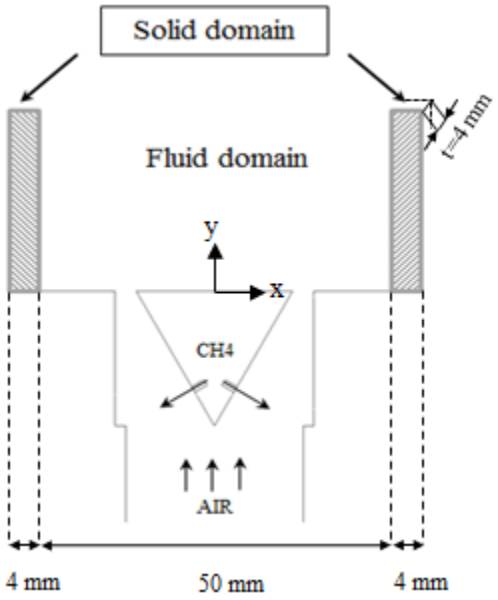

Figure 5-3: Sketch of the fluid and solid regions as one computational domain

The computational domain is composed of the fluid region and the solid region surrounding the fluid. A structured mesh system is employed for discretization of the governing equations. The impact of the meshing technology and sensitivity of the results on the grid have been studied by the authors in Ref. [18] focusing on the fluid-only simulation. All the meshes used in this study are generated using the meshing tool ANSYS Workbench 14.5. The fluid region consists of 644k structured elements. The flow and heat transport in the near wall fluid layer are fully resolved by using the SAS-SST turbulence model. This was achieved by using a mesh in the fluid domain with the cell closest to the wall at the coordinate Y^+ at a value less than 2 in 94% of the domain. For the sake of reducing the computational efforts, the solid domain has been simplified as compared to the actual combustor set up. Therefore it has been modeled without considering quartz glass windows or ports for thermocouples and pressure transducers. The solid mesh has been created in such a way that the fluid and solid grids are similar in the interface. The solid mesh requirements are less stringent, as the volume of the solid structure is very small as compared to the fluid zone (the solid wall thickness is

just 4 mm), allowing a fine mesh without large numbers of mesh points. In this work three different grids have been generated as presented in Table 5-1. In the third mesh (M3) the inflated layer option in the x- direction has been used, with a mesh spacing which is gradually growing towards the center of the liner. This spatial refinement from the initial coarse mesh (M1) to the final version (M3) has been done based on the temperature distribution in the thermal penetration depth to ensure the obtained results are grid independent (see Figure 5-4). The dependency of predicted results on the solid grid will be discussed in the result section. Here, it is assumed that the properties of the solid are constant and independent of temperature. Hence the solid region is modelled with the following properties: density of 7,854 kg/m3, thermal conductivity of 60 $W/m.K$ and heat capacity of 434 $J/kg.K$.

Table 5-1: Properties of three meshes used for the solid region

	M1	M2	M3
Nodes	7,452	13,550	27,642
Elements	3,304	8,640	17,280
First cell height [m]	2e-03	1e-03	1e-06

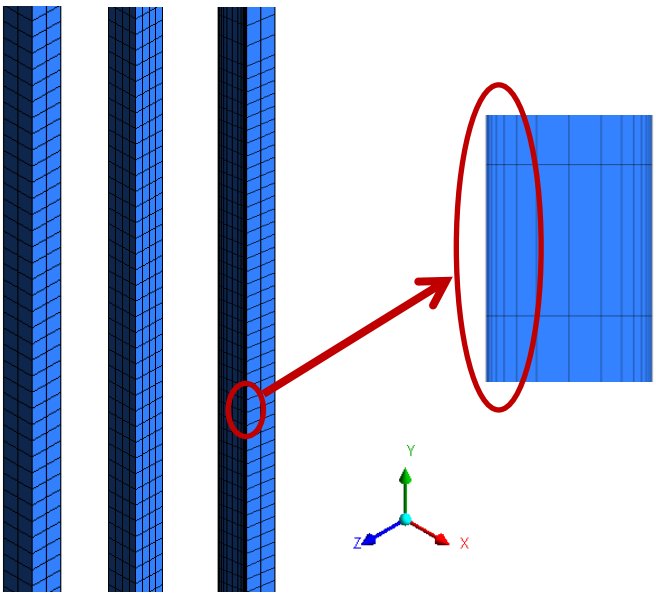

(a) (b) (c)

Figure 5-4: Close up view of the solid domain (left liner) for three different grid resolutions: (a) M1, (b) M2 and (c) M3

5.3 Numerical method

The CFD code employed here is ANSYS-CFX 14.5. It uses an implicit finite volume formulation to construct the discretized equations representing the Reynolds Averaged Navier-Stokes equations for the fluid flow. The model consists of a compressible solver with a co-located (non-staggered) finite volume method, such that the control volumes are identical for all transport equations [19]. The basic set of balance equations solved by ANSYS-CFX comprises the continuity, momentum, species and energy transport equations. The Favre averaged mass, momentum and energy conservation equations can be written as following:

- Conservation of mass

$$\frac{\partial \bar{\rho}}{\partial t} + \frac{\partial (\bar{\rho}\tilde{u}_i)}{\partial x_i} = 0 \qquad 5\text{-}1$$

- Momentum

$$\frac{\partial(\bar{\rho}\tilde{u}_i)}{\partial t}+\frac{\partial(\bar{\rho}\tilde{u}_i\tilde{u}_j)}{\partial x_i}=-\frac{\partial \bar{p}}{\partial x_i}+\frac{\partial}{\partial x_i}\left(\overline{\tau_{ij}}-\overline{\rho u_i^{"} u_j^{"}}\right) \quad 5\text{-}2$$

τ is the stress tensor which is related to the strain rate by:

$$\overline{\tau_{ij}}=\widetilde{\tau_{ij}}+\overline{\tau_{ij}^{"}} \quad 5\text{-}3$$

- Chemical species

$$\frac{\partial(\bar{\rho}\tilde{Y}_k)}{\partial t}+\frac{\partial\,(\bar{\rho}\tilde{Y}_k\tilde{u}_i)}{\partial x_i}=-\frac{\partial\left(\bar{\rho}\widetilde{u_i^{"}Y_k^{"}}\right)}{\partial x_i}-\frac{\partial(\overline{V_{k,i}Y_k})}{\partial x_i}+\bar{\dot{\omega}}_k \quad 5\text{-}4$$

- Energy equation

$$\frac{\partial(\bar{\rho}\widetilde{e_0})}{\partial t}+\frac{\partial}{\partial x_j}\left(\bar{\rho}\tilde{u}_i\widetilde{e_0}+\tilde{u}_j\bar{p}+\overline{u_j^{"}p}+\overline{\rho u_j^{"}e_0^{"}}+\overline{q_j}-\overline{u_i\tau_{ij}}\right)=\bar{\dot{\omega}}_T \quad 5\text{-}5$$

Which $\widetilde{e_0}$is given by:

$$\widetilde{e_0}\equiv\tilde{e}+\tilde{u}_k\,\tilde{u}_k\,/2+k \quad 5\text{-}6$$

Where the turbulent energy, k, is defined by:

$$k=\frac{\widetilde{u_k^{"}u_k^{"}}}{2} \quad 5\text{-}7$$

q_j in Equation 5-5 is the heat flux which represents the heat conduction and transport through species gradients given by ($q_j=-\lambda\frac{\partial T}{\partial x_j}+\rho\sum_{k=1}^{N}V_{k,j}Y_k\,h_{s,k}$).

The unclosed terms contain products of fluctuating values (e. g. $\overline{\rho u_i^{"}u_j^{"}}$ and $\bar{\rho}\widetilde{u_i^{"}Y_k^{"}}$) which need to be closed by modeled terms. The choice of turbulence model greatly influences the prediction of turbulent mixing rate and hence limit cycle oscillations. A comparison between the standard k-omega and Scale-Adaptive Simulation model (SAS) model for the combustor under study here, has been reported by Kumar et al. [20], showing that the SAS model is able to give the best prediction. Therefore in this work, the effects of turbulence are simulated by using the SAS turbulence model. The reacting flow simulations are carried out on the model combustor by using the Burning Velocity Model (BVM) for the combustion processes, applying a new model option for improving accuracy for non-premixed flames [21]. BVM uses a RIF flamelet library for the 'burnt' mixture; this mechanism involves a 16 species and 46 reversible reactions scheme for methane-air gas mixtures [22].

Considering the radiation across the duct, while assuming the liner to be adiabatic, does not change the temperature pattern inside the system. Also in non-adiabatic situations the effect of radiation is expected to be small, as the flue gas residence time is very short, and convective heat loss is much higher than radiative heat loss. In addition, adding the radiation model into the CHT approach and into the BVM combustion model brings an additional uncertainty into the modeling and makes it difficult to compare with the adiabatic cases. The effect of radiative heat transfer is therefore neglected. The choice to neglect radiation is supported by[23], which states that typically the effect of radiative heat loss is in the range of a few percent.

The energy equation employed for the solid is a simplified form of the energy equation for the fluid, which can account for heat transport due to solid motion, conduction and volumetric heat sources:

$$\frac{\partial(\rho_s h_{s)}}{\partial t} + \nabla.(\rho_s u_s h_s) = \nabla.(\lambda_s \nabla T) + s_e \qquad 5\text{-}8$$

In which h_s, ρ_s and λ_s are the enthalpy, density, and thermal conductivity of the solid, respectively. Here the source term s_e accounts for the interphase energy flow which is the result of convective heat transfer between the solid and the adjacent flue gas flow. The effect of the solid deformation induced by the mechanical loads is neglected (i.e. $u_s = 0$) and hence no change in the shape of the solid and fluid domain is taken into account; this assumption is well supported with the reported very small deformation amplitudes of the solid body in the work done by Shahi et al. [24], on the same combustor configuration.

5.3.1 Boundary condition

Definition of the boundary conditions in the gaseous domain is performed on basis of the known properties and behavior of the laboratory combustor. The CFD domain at the outlet end of the combustor has some additional computational length as compared to the test rig, to represent the complex boundary condition in the form of an end correction. Therefore in the exhaust of the combustor, a zero relative pressure could be imposed as a boundary condition. The mass flow rate of fuel and the velocity of the injected air are defined corresponding to Table 5-2. Except for the interface surfaces, all solid boundaries are specified as a wall with assigned no-slip condition, in which no mass and momentum are allowed in the direction perpendicular to them. The continuity of the energy flux is enforced at the fluid-solid interfaces. Since the outer surface of the solid parts is exposed to the ambient air and it is cooled by means of natural convection, the heat transfer

coefficient and the external temperature are defined there. All boundaries are set to be stationary in space and time, so the vibration of the liner is neglected.

Table 5-2: Operating condition

Power (kW)	Air factor	Methane mass flow rate [g/s]	Air mass flow rate [g/s]
40	1.4	0.8	19.152

5.4 Results and discussions

In this section numerical results are presented and validated with available experimental data.

5.4.1 Grid effect in the solid region

This section presents results obtained for a CHT approach using different grid sizes in the solid region, and compares them to the experimental data. The combustor exhibits a self-excited oscillation of high amplitude in pressure and rate of combustion, which are linked to the phase relationship between the acoustic pressure field and unsteady heat release. The Rayleigh criterion which recognizes the difference between damped or amplified interaction between pressure and heat release, as a function of phase between these phenomena, is often used to investigate and predict combustion instabilities. It states that if pressure and heat release fluctuations are in phase, the instabilities are enhanced, whereas the instabilities are damped when the pressure oscillations and heat release are out of phase. The stability of the combustor is determined by the net mechanical energy added to the combustor domain. Indeed when the acoustic energy losses match the energy gain, a stationary oscillatory behaviour is obtained which is referred to as the limit cycle oscillation. The measured frequencies of the instability in the current configuration are related to the acoustic eigenmodes of the combustion chamber [18]. The acoustic driving at these frequencies is a consequence of the pressure profile discontinuity after and before the burner. According to Heckl [25] due to the area blockage of the burner, only the downstream duct determines the combustor acoustics. The upstream and the downstream part of the combustor are acoustically decoupled and the combustion chamber acts as a single duct, with

closed-open boundary conditions. The pressure profile shape points to an active region around the flame and the rest of the combustor behaves as a resonator as it has been presented in Ref. [26]. This means that both ducts (combustion chamber and plenum) can vibrate in their own eigenfrequencies. This is well presented and discussed in Ref. [18,25-26].

Experimental results from the gas pressure measurements are obtained from the installed pressure transducers which are shown in Figure 5-2 for a location at 200 mm downstream the burner wedge. This data was seen as a good validation tool for the investigation of the conjugated heat transfer calculation and the sensitivity of results to the used grid for the solid region. Since the solid has been modeled explicitly then it is required to start the transient simulation from a steady state calculation in which the solid temperature has reached equilibrium with the hot combustion gases and the outside temperature. In the transient simulation the same time step for fluid and solid domain has been set, with a maximum value dictated by the acoustic CFL number. The residuals are small enough at the end of each time step to resolve the small changes in temperature at the surface of the solid. The convergences of residuals for all variables except for energy were resolved to a level of 1e-5. For the energy equation it is in the order of 1e-7.

The important point that should be noticed is that due to the existence of high temperatures in the chamber and also because of strong temperature fluctuations during the limit cycle oscillation, it is very difficult to measure the mean temperature and its variance. That is why the temperature data is not presented here. However, according to previous studies [18, 20] on the same configuration, and by keeping all affecting parameters constant, the only effective parameter which may control the frequency of pressure oscillations (i.e. speed of sound and acoustic) is the imposed thermal boundary condition. As a matter of fact the pressure oscillations govern the speed of sound which is dependent on the temperature. Hence the value of the observed frequency of the limit cycle is a good measure for the effective temperature in the duct. This principle is used also for example by the sonic thermometer. Therefore with the observed limited measurement accuracy, transient pressure data can be considered as a validating tool, and the improvement of the pressure prediction can be interpreted as a consequence of the more accurate prediction of the heat loss.

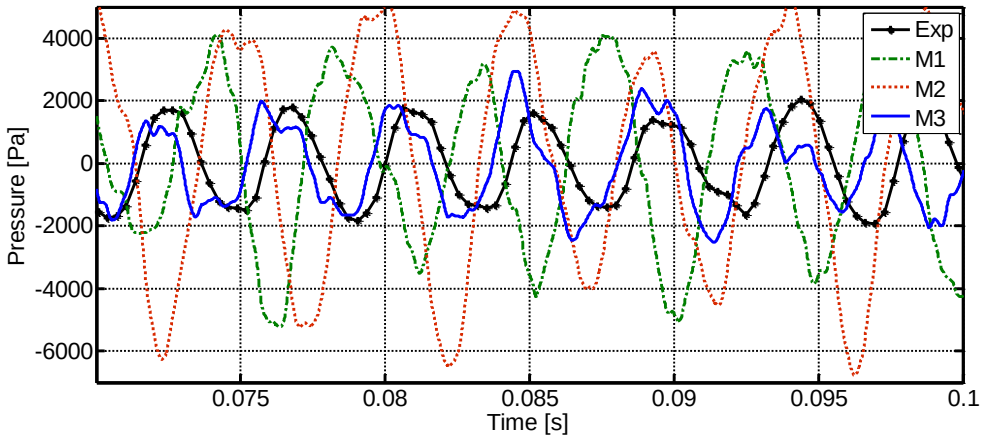

Figure 5-5: Measured and predicted pressure signal

Figure 5-5 shows how the grid size in the solid region changes the results of the simulation. Although it seems that the predicted value when using the mesh (M1) is not as far from the experiment as of the grid (M2) is, running the simulation for longer period of time shows that there is just a bigger time delay in this case to reach a saturated limit cycle oscillation at a higher pressure level than the predicted value when using the grid (M2), meaning that after a certain time the pressure level in this case also reaches to 6 kPa. This might be due to the large thermal inertia of the wall which requires much greater timescales to find the equilibrium state than required for the fluid flow. It can be concluded that the prediction of the amplitude of pressure oscillations is highly dependent on the grid size, and can be over predicted by a factor of 2 or even 3 (in the case that the first layer of grid in the solid is as far as 1 mm away from the fluid-solid interface).

Considering that the spatial scales of the solid temperature profiles are different in case of steady state or transient oscillatory heat transfer, care has to be taken into account for the different requirements of the meshing in these two situations. Here, the knowledge of analytical solutions for transient solid thermal behavior can be used for interpretation, as available from the semi-infinite solid approach. When meshing for a transient oscillatory heat transfer case, the solid mesh resolution needs to be adapted to the thermal penetration depth of the surface temperature oscillations. Hence for the transient heat transfer in limit cycle combustion oscillations, the meshing strategy and size of the grid in the solid part of the domain will play a very important role in determining the magnitude for the

pressure fluctuations. This can be used to determine and interpret the transient response of the solid. Because the solid region in this simulation is a finite body, the approximation would be valid for the behavior of the transient, neglecting the mean temperature gradient and effect of the proximity of the outer surface. For instance for the time scale of dt=1e-5 s, heat can penetrate into the solid only a distance of $dx \propto \sqrt{\alpha dt}$, where α is the thermal diffusivity, $\alpha = k/(\rho c_p)$. For the current parameter settings, in the beginning of the simulation this gives the penetration depth in order of magnitude of microns! Then by creating coarser grids, the heat penetration depth will be discarded by the calculation and the surface temperature of the solid will not be predicted to change on short time scales and the heat transfer to (and from) the solid will be either over or under estimated, resulting in a low/high magnitude of the pressure fluctuations. More details are available in Ref. [27]. Therefore by adding an inflation layer on the solid side of the fluid-solid interface with a first cell height of 1e-6 m, the resolution is increased, giving predicted results closer to the experimental results. That explains why the predicted results by grid (M3) are closer to the experimental results, and hence more accurate.

In order to predict the penetration depth of heat into the liner after about 0.32 s, the temperature changes over the time are plotted in Figure 5-6. As it can be seen in the coarse mesh results, after the depth of 1.6 mm the temperature remains constant, while calculations done by using the fine mesh show a penetration depth of about 3 mm, which is closer to the analytical value of 2.9 mm [27].

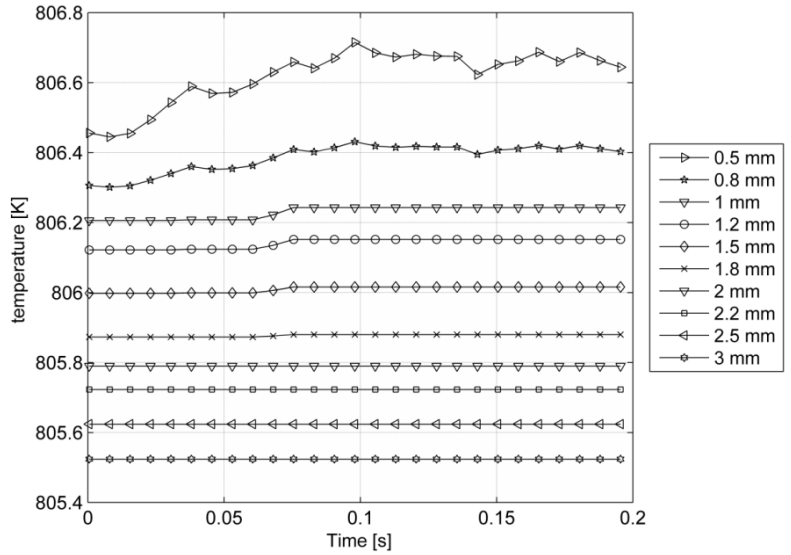

(a)

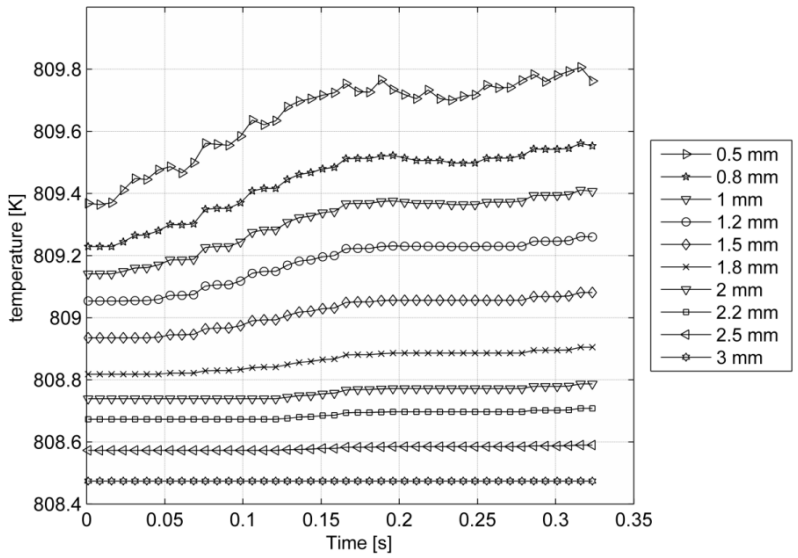

(b)

Figure 5-6: Time history of temperature at different locations for (a) coarse mesh M1, (b) fine mesh M3

The pressure signal obtained from the CHT calculation and also from the fluid-only simulation with the isothermal liner as well as the measured data are presented in Figure 5-7. In the isothermal case the temperature of the liner is assumed to be 1,000 K. Obviously the simulation with isothermal liner settings over-predicts the amplitude of the pressure oscillations, while the CHT approach gives a much better prediction. This can be clearly observed in Figure 5-8.

The first observed peak frequency of the LCO, which is associated with the first harmonic of the downstream part of the combustor [26] is presented in Table 5-3 for both CFD and experiments. According to this table, the first excited mode of the considered case is well predicted by the CHT model, and the error in the CFD calculation is 0.6 %. This is much more accurate than in the case of the fluid-only simulation, assuming a constant liner temperature, where results have about 10% error. Apparently the time dependent accumulation of heat, and the heat transferred from the hot gases to the liner and then to the surroundings, is under-predicted in the fluid-only calculation, resulting in a higher speed of sound and hence higher frequency of instability. Since the prediction of the unstable frequency is of great importance, CHT modeling is necessary for highest accuracy.

Figure 5-9 represents the post processed pressure spectrum of the time signal measured in the test rig. As it can be seen, the periodic oscillation of the pressure signal in the time domain appears as a peak frequency of about 232 Hz surrounded by many secondary peaks, the source of these peaks is discussed in Refs. [17, 18]. The mode at about 600 Hz which is missing in the CFD prediction corresponds to the structural mode of the combustor. Overall good comparison between the measured data and the CHT results is achieved.

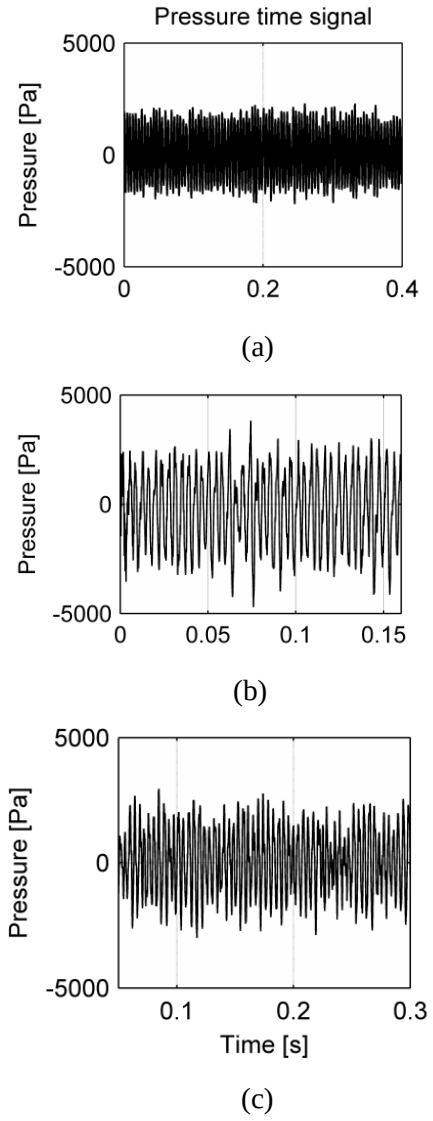

Figure 5-7: Pressure signal captured from (a)Experiment (b) fluid-only calculation with isothermal liner (c) CHT approach (used mesh is M3)

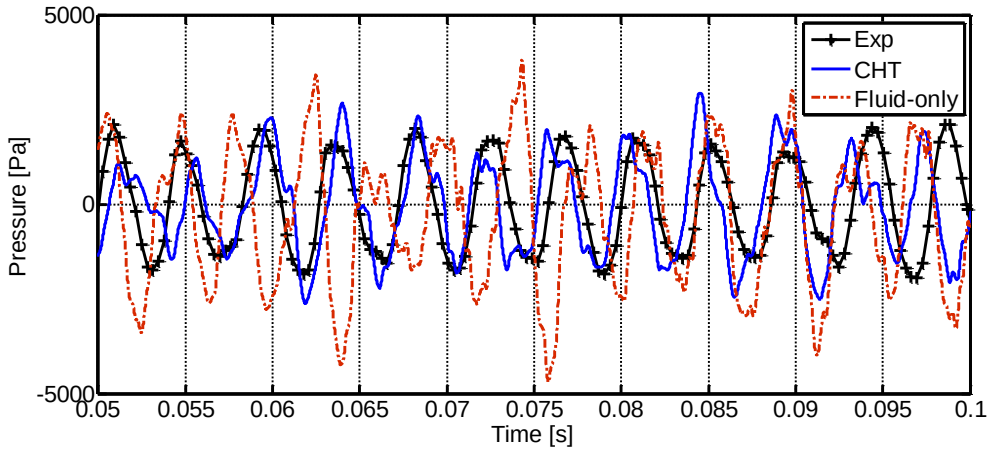

Figure 5-8: Pressure evolution over 0.05 s calculated with different approaches

Table 5-3: Calculated and measured the first self-excited modes

	CFD		Experiment
	Isothermal liner	CHT	
f_1 (Hz)	256	232	234

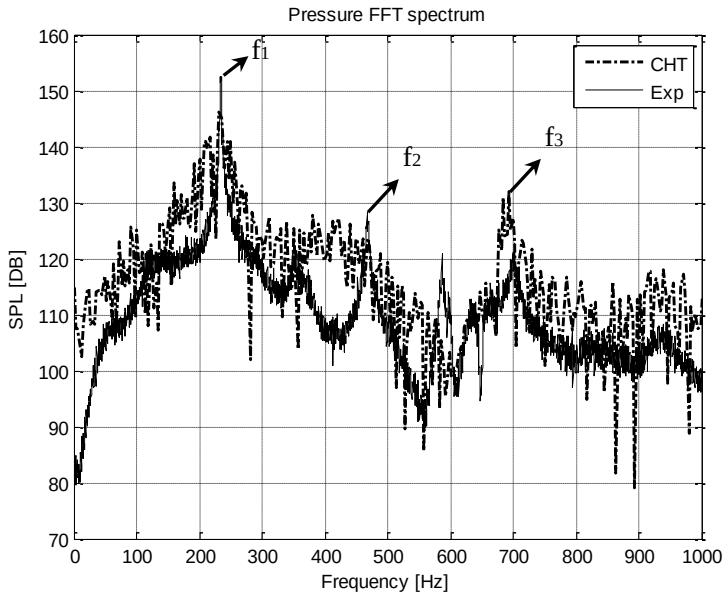

Figure 5-9: Pressure spectrum for 40kW and λ=1.4: experiment (solid line), CHT (dash-dot)

5.4.2 Heat transfer

The heat flux at the wall of the combustor represents the transfer of energy from the operating gas to the solid walls in contact. Capturing the near-wall behavior of the hot gases in contact with the solid is a step towards better understanding of the heat transfer process. In the previous section, the effect of the solid domain grid size, especially the first cell height, on the accuracy of the results was discussed. Therefore all the results from now on correspond to the most accurate grid (i.e. M3).

Figure 5-10 shows the transient time averaged temperature field in both the solid and fluid regions. The simulation has been done for the total physical time of 0.32 s; hence data is averaged over approximately 75 cycles. It should be noticed that the temperature contour presented here corresponds to just 200 mm of the full height of the combustion chamber. According to Figure 5-10 burned gases reach to a temperature of 2,000 K, while the wall temperature remains between 500 and 900 K. Therefore the temperature should decrease from the hot gases level to the wall level; this change occurs in a near-wall layer and creates large temperature

gradients. That is the reason for using a high density of very small grid cells in the near wall region in both domains of interest.

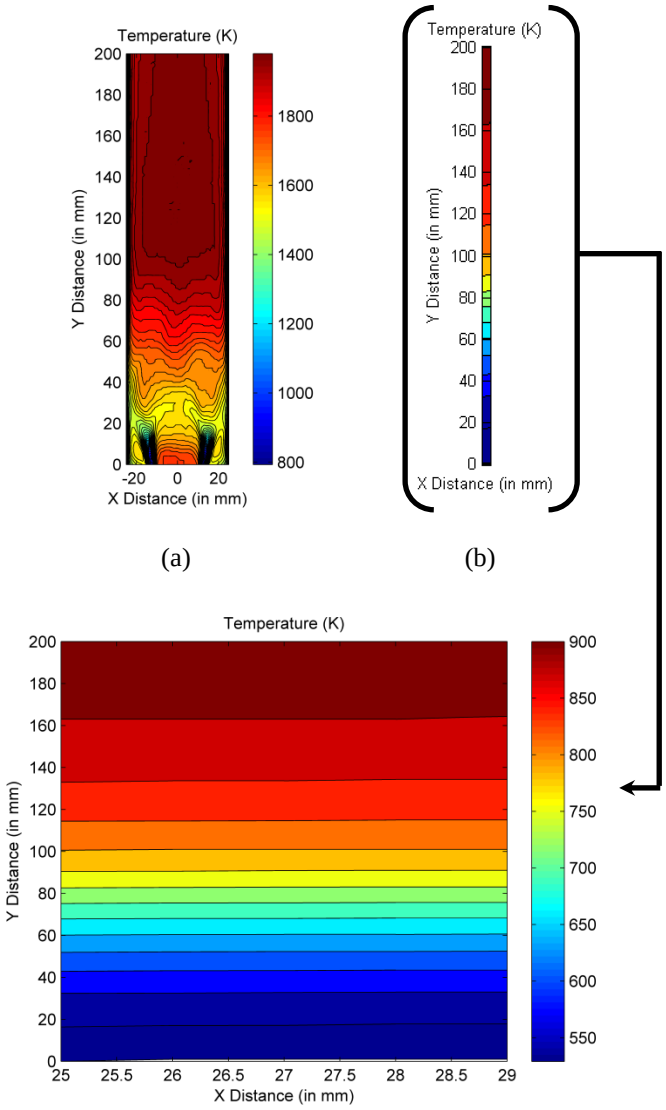

Figure 5-10: Transient time averaged temperature in the plane Z=0 for (a) fluid domain, (b) solid domain

The achieved solution is far from the assumed isothermal wall at 1,000 K or other calculations done for the same combustor imposing the adiabatic boundary condition on the wall [28, 29]. It seems that the underestimations of the convective heat transfer in the first case leads to under prediction of the heat flux at the liner. This can be observed in Figure 5-11 along the line of Z=0 over the Y-Z plane. The heat loss through the wall, predicted by the CHT approach is more than that of predicted by the fluid-only calculations with the isothermal liner. The difference in the predicted heat loss by these two mentioned approaches is significant especially within the 200 mm distance from the burner wedge, while above that height using the CHT approach does not change the prediction much. The modelling of the heat transfer in this first 200 mm height of the liner, where the main dynamic combustion reactions occur, is very critical to estimate the correct frequency and amplitude of instabilities.

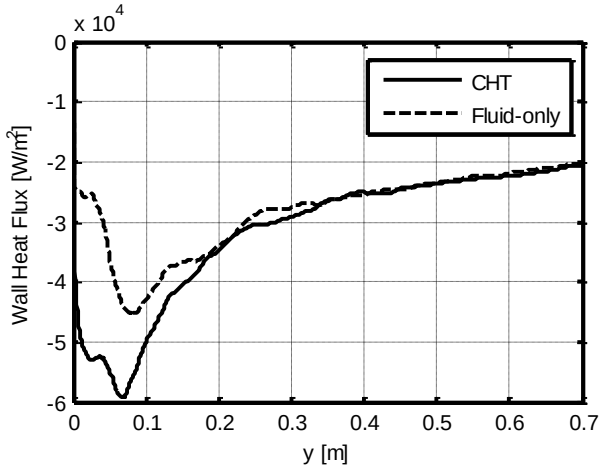

Figure 5-11: Predicted heat flux through the inner surface of the liner (over Z-Y plane, along the line of Z=0) with different approaches

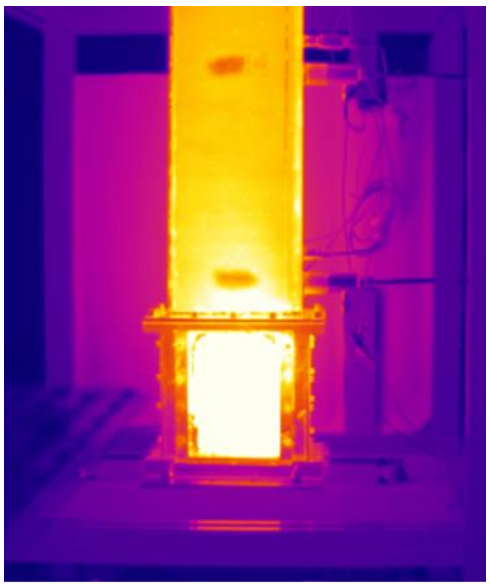

Figure 5-12: The IR camera measurement (taken from [30])

Figure 5-12 shows the temperature contour obtained from the thermal image during the combustion. The IR camera data is limited to some height of the combustor, and it does not include the full length data [30]. The maximum temperature which can be measured with this camera is 500°C; the bright region with high temperature (above the camera limit) corresponds to the gas temperature and not the liner (there is a window serving for the flame observation at this location). The important information which can be derived from this image is that the liner temperature stays almost uniform after the height of the flame box (i.e. after 150 mm) which confirms the numerical predictions. However this constant value deviates by 150 K from the measured value. This can be due to neglecting the heat loss from the quartz glass windows in the simulation which leads to the over prediction of the wall temperature in the model or due to the omitting the radiation effect from the model. The other explanation is the uncertainty in the measurements due to the radiation between hot surfaces and the surrounding ambient, pointing to the fact that the measured value is less than the actual surface temperature. Regardless of how this simplification has effect on the mean wall temperature, since the gas temperature is much higher than the wall temperature, this deviation does not change the transient heat transfer effect.

Contour plots showing the heat flux calculated based on the CHT model and fluid-only simulation are given in Figure 5-13. Unfortunately there is no measurement for the temperature of the liner; however according to the pressure time history which was previously presented in Figure 5-8, it is clear that the underestimation of heat flux by fluid-only calculation at this critical location (i.e. the distance of 200 mm) leads to the amplification of the pressure amplitude by adding to the acoustic energy of the system. Besides that, the heat flux distribution over the interface looks very inhomogeneous in the fluid-only case.

The time averaged transient solution of the wall adjacent gas temperature, which is the average temperature of hot gases in the cell adjacent to the wall is shown in Figure 5-14 for the different approaches. The maximum achieved temperature in the CHT model and fluid-only model with the isothermal liner occurs in the location of the maximum heat flux (as presented in Figure 5-11), where the maximum heat transfer from the hot gases to the colder liner is taking place. While in the case with the adiabatic liner after 100 mm above the flame holder the temperature reaches 2,030 K and it remains constant which is very far from what was predicted by other approaches.

Figure 5-15 shows the predicted heat transfer coefficient (h_c) over the interface surface. The observation is that in the first 50 mm of the liner the heat transfer coefficient is increasing and then afterwards it starts to decrease; however it increases again after y=100 mm and reaches the maximum value of 98 $\left(\frac{\mathrm{W}}{\mathrm{m}^2.K}\right)$ between 150 and 250 mm; while going further downstream it remains almost constant. It is worthwhile to pay more attention to the wall heat flux plotted in Figure 5-11. This plot shows that the maximum heat loss occurs at the location of y=71 mm which is not the place of maximum h_c. Since the wall heat transfer coefficient, h_c, is defined based on T_{wall} and the wall adjacent temperature, this may be ascribed to the higher temperature gradient, which renders heat transfer on this location higher (see Figure 5-14). The flame indeed sits in the area between (0-200) mm, but over time it is not evenly distributed over the height causing the local peaks on the heat flux. Initially the flame contacts with the wall but due to the vortex effects it separates later and then farther from the burner it touches the wall again.

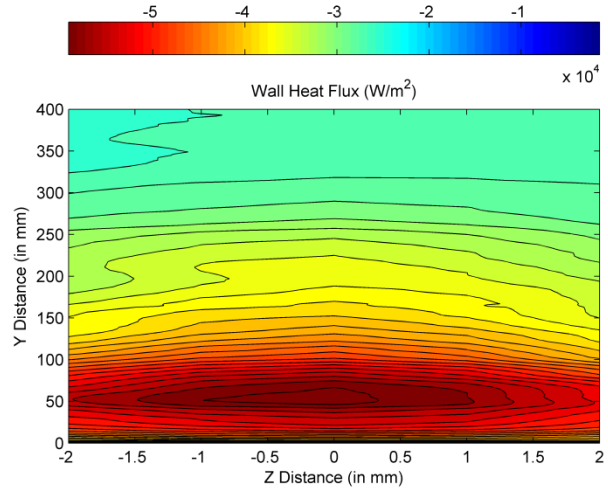

(a)

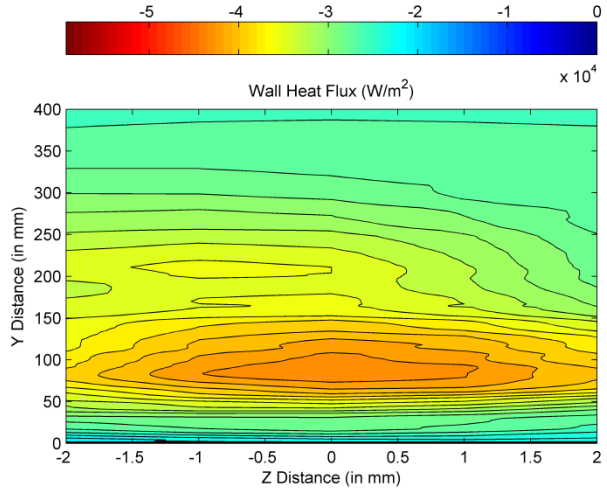

(b)

Figure 5-13: Contour plot of heat flux leaving the inner surface of the liner (a) CHT (b) fluid-only Simulation

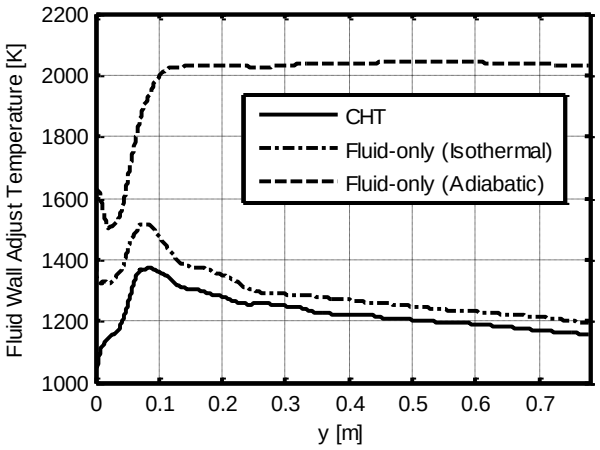

Figure 5-14: Wall adjacent temperature along the height of the combustor

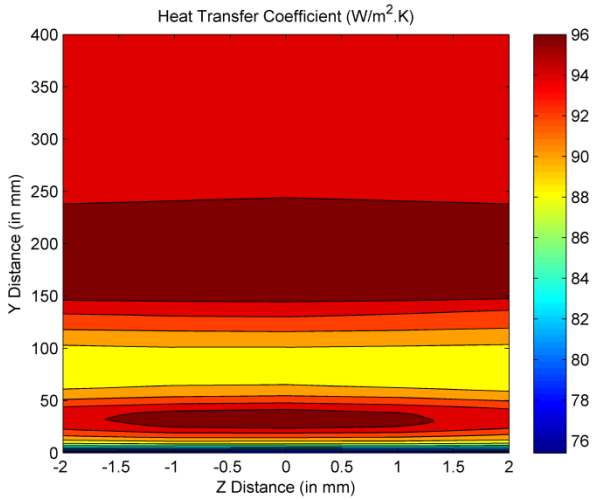

Figure 5-15: Wall heat transfer coefficient predicted using CHT model

Contour plots from CHT and fluid-only simulations showing the temperature distribution over time are given in Figure 5-16 and Figure 5-17. The temperature evolution in the CHT case obviously takes longer time meaning that the acoustic limit cycle oscillation has a lower frequency/longer period. The incoming mixture of air and the fuel travels further beyond the flame holder before it is getting ignited, and still after 100 mm above the wedge, some cold spots of fresh mixture penetrating to the hot products can be observed cooling down the hot gases. This leads to a lengthening of the reattachment region and makes the central recirculation zone more stretched. Earlier it was already observed that assuming the liner to be isothermal, predicts oscillations with shorter wavelength and therefore higher frequency. In this case, there is no remaining fuel far downstream; everything is consumed 50 mm downstream the burner. As it is expected due to modeling the heat loss through and within the liner, the temperature in the CHT case is generally lower than in the isothermal liner case.

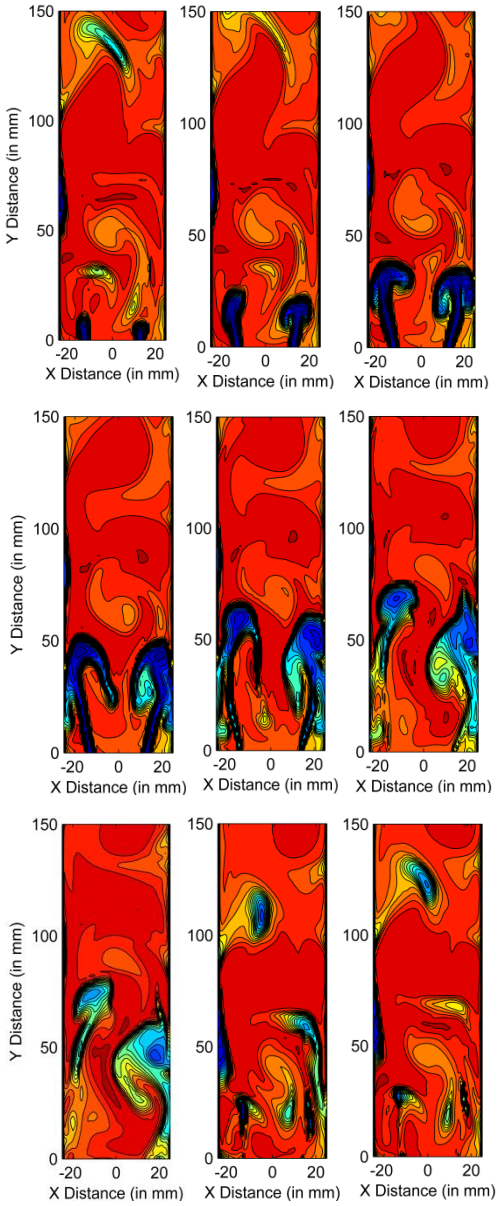

Figure 5-16: Instantaneous gas temperature contours (over one cycle of oscillation) taken form Z=0 mm plane, for the combustor including the solid (CHT)

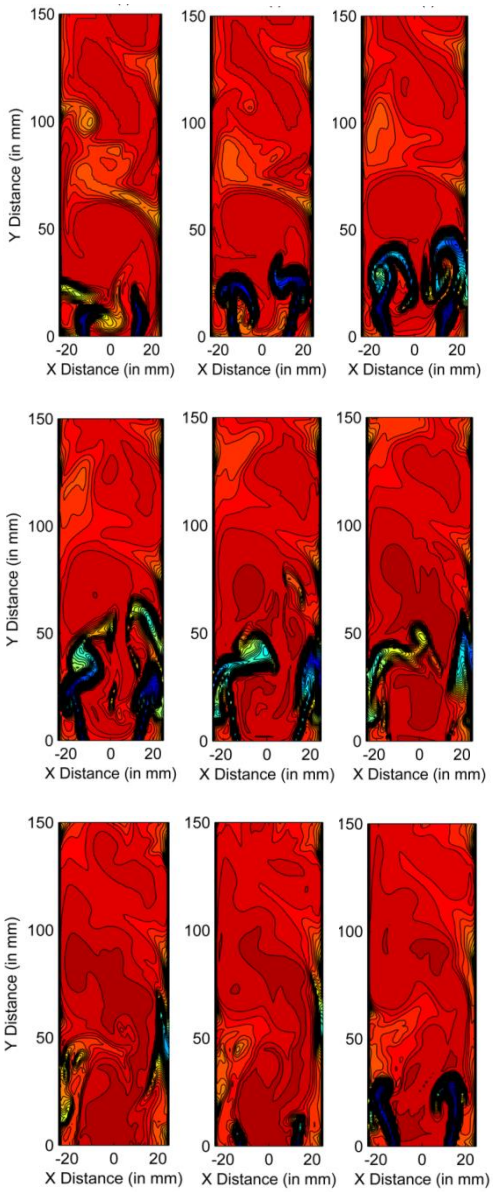

Figure 5-17: Instantaneous gas temperature contours (over one cycle of oscillation) taken form Z=0 mm plane, for the fluid-only simulation with the isothermal liner

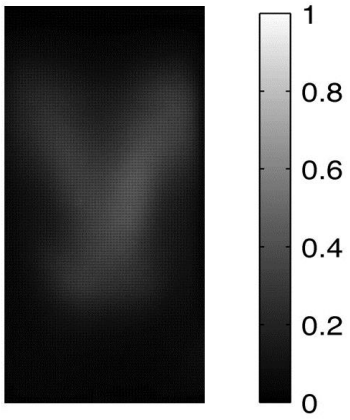

Figure 5-18: Averaged intensity plot from experiments for 40kW and λ = 1.40.

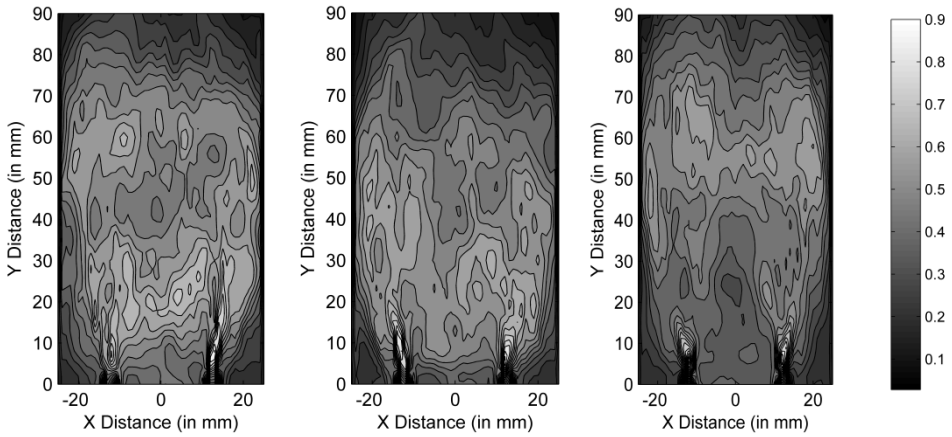

(a) (b) (c)

Figure 5-19: Heat release contour for the (a) adiabatic (b) isothermal liner cases and (c) conjugated approach.

Since the maximum heat release is localized in the flame zone and considering the fact that OH and CH species radicals are only produced and consumed in the flame front, therefore they can be taken as a qualitative indicator of the flame rate of heat release. Figure 5-18 represents the measured time averaged OH* emission. The

heat release of the flame is measured using a Photo Multiplier Tube (PMT). It is a device that provides a voltage output proportional to the incident intensity of the light. More details can be found in Ref. [17]; Since it is not possible to predict the excited OH* radicals with the employed CFD combustion model, the weighted reaction progress source as a variable qualitatively representing the heat release has been calculated and presented in Figure 5-19 for three cases of fluid-only simulation with the imposed adiabatic (Figure 5-19-a) and isothermal condition on liner (Figure 5-19-b) and also the CHT approach (Figure 5-19-c). Compared to Figure 5-18, the predicted flame with the fluid-only approach is rather anchored on the bluff body while the measured average intensity shows a flame lifted off the flame holder. In the CHT approach, higher reaction rates take place at some downstream distance from the flame holder, which is closer to the experimental observation.

5.5 Conclusions

In this paper, transient fluid-structure thermal analyses of the Limousine combustor have been conducted for more accurate prediction of the frequencies of unstable modes of the combustor as well as estimating the temperature distribution of the liner during the LCO. In this approach a monolithic solution procedure has been used, meaning that the coupled equations for both solid and fluid domain are solved together. Calculations have been done using the ANSYS-CFX code. The same time scales for both fluid and solid regions were defined.

The present study has revealed the following observations:

- The presented results demonstrate the relevance and effect of high accuracy, high spatial and temporal resolution of transient heat flow, and the correlation between the solid grid size and the heat penetration depth. The calculations showed that the evaluation of the pressure oscillation amplitude highly depends on the height of the first layer of the grid in the solid, close to the solid interface. This layer should be in order of heat penetration depth (i.e.$\mathrm{sqrt}(\alpha dt)$).
- Compared to the fluid-only simulations, the results proved that utilization of a transient CHT model in calculations, more accurately predicts the frequency of the unstable mode of the combustor (just 0.6% error). This is very promising and shows the ability of current schemes to calculate the instability of combustion system. Indeed, the appearance of the thermo-acoustic instabilities,

as presented in this work, is very sensitive to the temperature distribution in the combustion chamber. That is why the CHT model predicted the instabilities matching with experimental data, whereas other models revealed significant errors. Any errors in the temperature distribution have direct influence on the speed of sound within the combustor and in consequence may enhance/damp the fluctuations. The heat transfer could actually affect the development of instabilities through removal or addition of energy to the fluid flow. This has been demonstrated by the investigated models where the main frequency of the instability shifts between 256 and 232 Hz depends on the wall boundary conditions.

In this current study, the dependence of the physical input parameters on the temperature distribution has not been taken into account. However it is advised to check the uncertainty regarding the material properties (for instance the thermal conductivity), and this deserves further investigation.

Acknowledgments

The authors would like to acknowledge the funding of this research by the EC in the Marie Curie Actions Networks for Initial Training, under call FP7-PEOPLE-2007-1-1-ITN, Project LIMOUSINE with project number 214905. Special thanks go to Dr. Phil Stopford for the support in the use of ANSYS-CFX.

Appendix A:
One-Dimensional Transient Heat Conduction in Semi-Infinite Body

A semi-infinite solid is an idealized body that has a single plane surface and extends to infinity in all directions. For short periods of time, most bodies can be modeled as semi-infinite solids since heat does not have sufficient time to penetrate deep into the body, and the thickness of the body does not enter into the heat transfer analysis. The heat equation for transient conduction in a semi-infinite solid is given by:

$$\frac{\partial T}{\partial x^2} = \frac{1}{\alpha}\frac{\partial T}{\partial t} \qquad 5\text{-}9$$

To solve this equation, an initial condition and two boundary conditions should be specified, which in this case can be expressed as:

$$T(x,0) = T_i \tag{5-10}$$

$$T(0,t) = T_s \tag{5-11}$$

$$T\left(x \to \infty, t\right) = T_i \tag{5-12}$$

The temperature near the surface of the semi-infinite body will increase because of the surface temperature change, while the temperature far from the surface of the semi-infinite body is not affected and remains at the initial temperature T_i.

The analytical solution of the problem can be found in [27]. The temperature distribution and the heat transfer can be expressed as:

$$\frac{T(x,t) - T_s}{T_i - T_s} = \text{erf}\left(\frac{x}{2\sqrt{\alpha t}}\right) \tag{5-13}$$

$$q_s''(t) = \frac{k(T_s - T_i)}{\sqrt{\alpha t}} \tag{5-14}$$

Where $\text{erf}(w)$ is the Gaussian error function and is defined as:

$$\text{erf(w)} = \frac{2}{\sqrt{\pi}} \int_0^w e^{-v^2} dv \tag{5-15}$$

According to the definition of the thermal penetration depth, the temperature, at the thermal penetration depth should satisfy the following conditions:

$$\frac{\partial T(x,t)}{\partial x} = 0 \qquad at \quad x = \delta(t) \tag{5-16}$$

$$T(x,t) = T_i \qquad at \quad x = \delta(t) \tag{5-17}$$

By integrating Equation 5-16 in the interval $(0, \delta)$, it can be written as :

$$\frac{\partial T}{\partial x}\Big]_{x=\delta(t)} - \frac{\partial T}{\partial x}\Big]_{x=0} = \frac{1}{\alpha} \int_0^{\delta(t)} \frac{\partial T(x,t)}{\partial t} dx \tag{5-18}$$

The right hand side of Equation 5-18 can be rewritten as:

$$\frac{\partial T}{\partial x}\Big]_{x=\delta(t)} - \frac{\partial T}{\partial x}\Big]_{x=0} = \frac{1}{\alpha}\left[\frac{d}{dt}\left(\int_0^{\delta} T\, dx\right) - T\right]_{x=\delta\frac{d\delta}{dt}}\Bigg] \tag{5-19}$$

which represents the energy balance within the thermal penetration depth. Substituting Equations 5-16 and 5-17 into Equation 5-19 yields:

$$-\alpha \frac{\partial T}{\partial x}\Big]_{x=0} = \frac{d}{dt}(\theta - T_i\delta) \quad 5\text{-}20$$

Where

$$\theta(t) = \int_0^{\delta(t)} T(x,t)\,dx \quad 5\text{-}21$$

By assuming that the temperature distribution in the thermal penetration depth is a third-order polynomial function of x, and considering that the surface temperature of the semi-infinite body, T_s, is not a function of time, the temperature distribution in the thermal penetration depth becomes:

$$\frac{T(x,t) - T_i}{T_s - T_i} = 1 - \frac{3}{2}\left(\frac{x}{\delta}\right) + \frac{1}{2}\left(\frac{x}{\delta}\right)^3 \quad 5\text{-}22$$

where the thermal penetration depth, δ, is still unknown. Substituting Equation 5-22 into Equation 5-20, an ordinary differential equation for δ is obtained:

$$4\alpha = \delta \frac{d\delta}{dt} \qquad t > 0 \quad 5\text{-}23$$

Since the thermal penetration depth equals zero at the beginning of the heat conduction, the thermal penetration depth for a semi-infinite body can be written as:

$$\delta = \sqrt{8\alpha t} \quad 5\text{-}24$$

The surface may also exposed to a constant heat flux $q_0^{"}$ or to a fluid characterized by $T_\infty$and the convection coefficient of h. The temperature distribution in the first case can be expressed as:

$$T(x,t) - T_i = \frac{2q_0^{"}\sqrt{\alpha t/\pi}}{k}\exp\left(\frac{-x^2}{4\alpha t}\right) - \frac{q_0^{"}x}{k}erfc\left(\frac{x}{2\sqrt{\alpha t}}\right) \quad 5\text{-}25$$

while in the second case when the surface is exposed to the convection heat transfer, the temperature distribution can be written as:

$$\frac{T(x,t) - T_s}{T_i - T_s} = \mathrm{erf}\left(\frac{x}{2\sqrt{\alpha t}}\right) - \left[\exp\left(\frac{hx}{k} + \frac{h^2\alpha t}{k^2}\right)\right]\left[erfc\left(\frac{x}{2\sqrt{\alpha t}} + \frac{h\sqrt{\alpha t}}{k}\right)\right] \quad 5\text{-}26$$

The complementary error function $erfc(w)$is defined as $(1 - \mathrm{erf(w)})$.

References

[1] De Sa, A., and Al Zubaidy, S., 2011, "Gas turbine performance at varying ambient temperature," Applied Thermal Engineering, 31(14–15), pp. 2735-2739.
[2] Canière, H., Willockx, A., Dick, E., and De Paepe, M., 2006, "Raising cycle efficiency by intercooling in air-cooled gas turbines," Applied Thermal Engineering, 26(16), pp. 1780-1787.
[3] Park, J. S., Park, S., Kim, K. M., Choi, B. S., and Cho, H. H., 2013, "Effect of the thermal insulation on generator and micro gas turbine system," Energy, 59(0), pp. 581-589.
[4] Boudier, G., Gicquel, L. Y. M., Poinsot, T., Bissières, D., and Bérat, C., 2007, "Comparison of LES, RANS and experiments in an aeronautical gas turbine combustion chamber," Proceedings of the Combustion Institute, 31(2), pp. 3075-3082.
[5] Carter, T. J., 2005, "Common failures in gas turbine blades," Engineering Failure Analysis, 12(2), pp. 237-247.
[6] Albeirutty, M. H., Alghamdi, A. S., and Najjar, Y. S., 2004, "Heat transfer analysis for a multistage gas turbine using different blade-cooling schemes," Applied Thermal Engineering, 24(4), pp. 563-577.
[7] Alhazmy, M. M., and Najjar, Y. S. H., 2004, "Augmentation of gas turbine performance using air coolers," Applied Thermal Engineering, 24(2–3), pp. 415-429.
[8] Eshati, S., Abu, A., Laskaridis, P., and Khan, F., 2013, "Influence of water–air ratio on the heat transfer and creep life of a high pressure gas turbine blade," Applied Thermal Engineering, 60(1–2), pp. 335-347.
[9] Mazur, Z., Hernández-Rossette, A., García-Illescas, R., and Luna-Ramírez, A., 2006, "Analysis of conjugate heat transfer of a gas turbine first stage nozzle," Applied Thermal Engineering, 26(16), pp. 1796-1806.
[10] Alizadeh, M., Izadi, A., and Fathi, A., 2013, "Sensitivity Analysis on Turbine Blade Temperature Distribution Using Conjugate Heat Transfer Simulation," Journal of Turbomachinery, 136(1), pp. 011001-011001.
[11] Duchaine, F., Corpron, A., Pons, L., Moureau, V., Nicoud, F., and Poinsot, T., 2009, "Development and assessment of a coupled strategy for conjugate heat transfer with Large Eddy Simulation: Application to a cooled turbine blade," International Journal of Heat and Fluid Flow, 30(6), pp. 1129-1141.
[12] Duchaine, F., Mendez, S., Nicoud, F., Corpron, A., Moureau, V., and Poinsot, T., 2009, "Conjugate heat transfer with Large Eddy Simulation for gas turbine components," Comptes Rendus Mécanique, 337(6–7), pp. 550-561.
[13] Duchaine, F., Maheu, N., Moureau, V., Balarac, G., and Moreau, S., 2013, "Large-Eddy Simulation and Conjugate Heat Transfer Around a Low-Mach Turbine Blade," Journal of Turbomachinery, 136(5), pp. 051015-051015.
[14] Kim, K. M., Park, J. S., Lee, D. H., Lee, T. W., and Cho, H. H., 2011, "Analysis of conjugated heat transfer, stress and failure in a gas turbine blade with circular cooling passages," Engineering Failure Analysis, 18(4), pp. 1212-1222.
[15] Shahi, M., Kok, J. B. W., Sponfeldner, T., and Pozarlik, A., 2013, "Thermal and fluid dynamic analysis of partially premixed turbulent combustion driven by thermo acoustic

effects," 20th International Congress on Sound & Vibration, Bangkok, Thailand, pp. 2994 - 3002.
[16] Meynen, S., and Schäfer, M., 2003, "Efficient solution procedures for the simulation of fluid-structure interaction problems," Computational Fluid and Solid Mechanics 2003, K. J. Bathe, ed., Elsevier Science Ltd, Oxford, pp. 1462-1466.
[17] Roman Casado, J. C., 2013, "Nonlinear behavior of the thermoacoustic instabilities in the limousine combustor," PhD, University of Twente, Enschede, The Netherlands.
[18] Shahi, M., Kok, J. B. W., Pozarlik, A. K., Roman Casado, J. C., and Sponfeldner, T., 2014, "Sensitivity of the Numerical Prediction of Turbulent Combustion Dynamics in the LIMOUSINE Combustor," Journal of Engineering for Gas Turbines and Power, 136(2), pp. 021504-021504.
[19] Patankar, S. V., 1980, Numerical Heat Transfer and Fluid Flow, Hemisphere, New York.
[20] Santosh Kumar, T. V., Alemela, P. R., and Kok, J. B. W., 2011, "Dynamics of flame stabilized by triangular bluff body in partially premixed methane-air combustion," Proceeding of ASME Turbo Expo, Vancouver, Canada, pp. 1017-1026.
[21] Forkel, H., 2012, "CFX 14.5 Burning Velocity Model discretization for non-premixed combustion," ANSYS Germany GmbH.
[22] Smooke, M. D., Puri, I. K., and Seshadri, K., 1988, "A comparison between numerical calculations and experimental measurements of the structure of a counterflow diffusion flame burning diluted methane in diluted air," Symposium (International) on Combustion, 21(1), pp. 1783-1792.
[23] Sallevelt, J. L. H. P., Pozarlik, A. K., Beran, M., Axelsson, L., and Brem, G., 2014, "Bioethanol combustion in an industrial gas turbine combustor: simulations and experiments," Journal of engineering for gas turbines and power, 136(7), p. 071501.
[24] Shahi, M., Kok, J. B. W., and Alemela, P. R., "Simulation of 2-way fluid structure interaction in a 3D model combustor," Proceeding of ASME Turbo Expo 2012, pp. 1571-1580.
[25] Heckl, M., 2010, "the Rijke tube: A green's function approach in the frequency domain," Acta Acustica united with Acustica, 96(4), pp. 743-752.
[26] Roman Casado, J. C., and Kok, J. B. W., 2012, "Non-linear effects in a lean partially premixed combustor during limit cycle operation," Proceeding of ASME Turbo Expo 2012, Copenhagen, Denamrk, pp. 837-846.
[27] Incropera, F. P., and DeWitt, D. P., 2002, Fundamentals of heat and mass transfer, John Wiley & Sons Australia, Limited.
[28] Hernández, I., Staffelbach, G., Poinsot, T., Román Casado, J. C., and Kok, J. B. W., 2013, "LES and acoustic analysis of thermo-acoustic instabilities in a partially premixed model combustor," Comptes Rendus Mécanique, 341(1–2), pp. 121-130.
[29] Filosa, A., Shahi, M., Tomasello, A., Noll, B., Aigner, M., and Kok, J., 2013, "numerical studies of unsteady heat transfer with thermoacustics oscillations," 20th International Congress on Sound & Vibration, Bangkok, Thailand, pp. 3018 - 3026.
[30] Altunlu, A. C., 2013, "The analysis of mechanical integrity in gas turbine engines subjected to combustion instabilities," PhD Thesis, University of Twente, Enschede.

6

Strongly Coupled Fluid-Structure Interaction in a 3D Model Combustor during Limit Cycle Oscillations

Mina Shahi, Jim. B.W.Kok, J.C. Roman Casado, Artur Pozarlik

University of Twente, Faculty of Engineering Technology, Laboratory of Thermal Engineering, Enschede, the Netherlands

Submitted to J. Sound Vib. (2014)

Abstract

Wall cooling is extremely important for the liner of a gas turbine engine combustor, due to the high temperature of the flue gas flowing at high velocity and pressure. The liner material is heat resistant steel with relatively low heat conductivity. To accommodate outside wall forced air cooling, the liner is designed to be thin, which unfortunately facilitates the possibility of high amplitude wall vibration (and failure due to fatigue) in case of pressure fluctuations in the combustor. The latter may occur due to a possible occurrence of a feedback loop between the aerodynamics, the combustion, the acoustics and the structure. The structural vibrations act as a source of acoustic emitting the acoustic waves to the confined fluid. This leads to amplification in the acoustic filed and hence the magnitude of instability in the system. The aim of this paper is to explore the mechanism of fluid-structure interaction on the LIMOUSINE setup which leads to the LCO. Computational fluid dynamics analysis using a RANS approach is performed to obtain the thermal and mechanical loading of the combustor liner and finite element analysis renders the temperature, stress distribution, and deformation in the liner. Obtained results are also compared to other numerical approaches like zero-way interaction and CHT. To recognize the advantage/disadvantage of each method a comparison is made with the available

measured data for the pressure and vibration signals, showing that the zero-way interaction model results give the largest discrepancy from experimental results, while the frequencies of the thermoacoustic instabilities are well predicted using the CHT and two-way coupled approaches. However in the latter case the magnitude is slightly overpredicted.

Keywords: *Fluid structure interaction, pressure oscillation, 3D combustor, thermo-acoustic instability*

6.1 Introduction

A well-known problem of lean premixed combustion of natural gas in gas turbine combustors is the sensitivity to thermoacoustic instability. These combustors can spontaneously exhibit significant flow and pressure oscillations. These oscillations may reach such high amplitudes that they cause flame extinction, structural vibration, flame flashback and ultimately failure of the system [1, 2]. Several coupled mechanisms are known to promote such interactions, for example, flame-acoustic wave interactions, flame vortex interactions, thermal-structure interactions, fluid-structure interactions, all of them may be present in a system individually or simultaneously [3-6].

The liner of a gas turbine combustor is a flexible structure that is exposed to the pressure oscillations occurring inside the combustor. These pressure oscillations can be of very high amplitude due to the thermoacoustic instability, when the fluctuations of the rate of heat release and the acoustic pressure waves amplify each other. The liner structure is a dynamic mechanical system that vibrates at its own eigenfrequencies and at the frequencies by which it is forced by the exposed pressure oscillations. On the other hand the liner vibrations force a displacement of the flue gas near the wall in the combustor. The displacement is very small but this acts like a distributed acoustic source which is proportional to the liner wall acceleration. Hence the liner and combustor are a coupled elasto-acoustic system. When this is exposed to a limit cycle oscillation, the liner may ultimately fail due to fatigue. Modeling the interaction between the fluid and structure in a combustion system allows us to predict the effect of vibrating walls on the flame dynamics and also recognize the hazard frequencies at which thermoacoustic instabilities may occur. The main phenomena involved in the above described feedback mechanism process are depicted in Figure 6-1. The feedback mechanism of thermoacoustic instabilities has attracted much attention in the past decade and

has been extensively reviewed [7-9]; however research on the issues related to interaction between the combustion processes and the structure during the LCO is very limited. Developing efficient and accurate solvers to model complex fluid–structure interaction problems for this application is still a challenging task. This is due to the fact that in comparison with for example airplane wing structural vibration, the vibrations of a gas turbine combustor liner are high in frequency and small in amplitude. This combination of characteristics is however very dangerous with a view to high cycle fatigue.

Huls et al. [10] reported measurements and calculations carried out on a 500kW test rig. They calculated the excitation pressure on the structure by using large eddy simulation (LES), and used the calculated pressure field as a load in a finite element model to measure the wall vibrations. In their approach only one-way coupling was considered with the structure, and indeed no information from the structural domain was fed back into the LES. Later Pozarlik [11] performed FSI numerical simulations with application on the same test rig with both one and two-way approaches using a weak coupling method. However his work was limited to a stable combustion condition, as the combustor could not be operated in the LCO regime. A similar analysis was done by Alemela et al. [12, 13] on a bluff body flame stabilized combustor (the same test rig as is under study in this paper), considering a 2D slice instead of the full geometry; nevertheless, this study was done using the two-way coupling and during the LCO condition, the work did not explore the effect of the combustion model and modelling approach. Unfortunately at the time validation data for the predicted displacement were not available yet. Altunlu et al. [14] performed the coupled FSI simulation on the same combustor. They extended the model to full 3D, modeling half of the combustor instead of a 2D slice to include the 3D flow patterns and to take into account the structural system stiffness due to the rectangularly connected geometry of the 4 walls. However, it is shown here that their model fails in the prediction of the unstable combustion due to the assumed symmetry condition in the middle plane (Appendix A). The study presented in this paper shows that this mentioned assumption pushes the flame to the stable regime and avoids the uneven distribution of the flame and hence the rate of heat release in time which is the root cause of the instability.

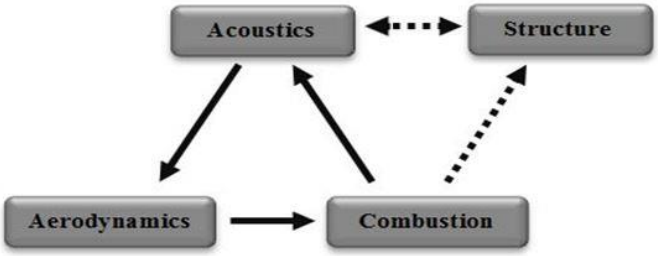

Figure 6-1: The feedback mechanism of thermoacoustic instabilities

In this paper two-way fluid structure interaction is studied for turbulent partially premixed methane air combustion. The method employed is the partitioned simulation of the coupled system composed of the liner and the flue gas domain, and both the method and the results will be presented. Despite the one-way interaction method which allows sending information only from the Computational Fluid Dynamics code to the Computational Structural Dynamics code, the two-way coupling method gives the possibility for the full exchange of data between fluid and solid solvers. This work is done in the framework of the LIMOUSINE project. The model combustor is different from the industrial gas turbine combustors, but it does have some similarities with gas turbine burners like: a flame stabilized by a recirculation area, a narrow burner flow passage, an upstream cold flow area and an acoustically closed air inlet. Therefore it is expected that the limit cycle phenomenon under study is relevant for the situation of a gas turbine combustor; moreover the methodology and generated data are of interest for the subsequent investigation of flame characteristics.

6.2 Thermo-acoustic instability

Thermo-acoustic instability is a phenomenon in which pressure and heat release interact with each other in a confined domain. The relation between a flame and the acoustic field was studied by Lord Rayleigh. The Rayleigh criterion characterizes the thermoacoustic system to be damped or to have amplified interaction between pressure and heat release. It states that if pressure and heat release fluctuations are in phase, the instabilities are enhanced, whereas the instabilities are damped when the pressure oscillations and heat release are out of phase. This criterion is expressed in the following Equation:

$$\iiint_V p'q'\, dV > 0 \qquad 6\text{-}1$$

Where p' and q' are pressure and heat release fluctuations, respectively, integrated over one cycle of the oscillation and V is the flow domain. Note that the integrals are also spatial, which means that both effects, destabilizing and stabilizing, can occur in different locations of the combustor and at different times, so the stability of the combustor will be decided by the net mechanical energy added to the combustor domain. Indeed when the acoustic energy losses match the energy gain a stationary oscillatory behavior is obtained which is referred to as the limit cycle oscillation.

However Rayleigh's criterion is a necessary but not a sufficient condition for the instabilities to occur [15]. Therefore Equation 6-1 has been extended to Equation 6-2 to include the losses of acoustic energy at the boundaries and entropy effects. According to Equation 6-2 the acoustic energy growth rate depends on the Rayleigh term but also on the acoustic fluxes, therefore the Rayleigh criterion is only a necessary condition for instability to occur.

$$\int_V \int_T p'(x,t)\, Q'(x,t)\, dt\, dV - \frac{\gamma \bar{p}}{\gamma - 1} \int_A \int_T p'(x,t)\, u'(x,t)\, dt\, dA > 0 \qquad 6\text{-}2$$

6.3 Combustor setup description

The test case, which is modeled in the work presented here, is based on a test rig developed within the framework of the European LIMOUSINE project, and it is shown in Figure 6-2. The setup is designed specifically to study limit cycles due to thermoacoustic instability. The combustion chamber consists of two rectangular ducts with different widths. The upstream duct has a 25x150 mm^2 cross section and is 275 mm long, whereas the downstream duct has a 50x150 mm^2 cross sectional area to compensate the volume expansion due to the combustion. In the transition between the ducts a wedge is mounted that stabilizes the flame. In this configuration, the total length of the combustor is 1,050 mm. This configuration behaves like a variation of a Rijke tube [16]. It deviates from the standard Rijke tube because it is acoustically closed at the bottom end and opens to the atmosphere at the downstream end. Air as the oxidizer is injected by means of 2 choked nozzles at the upstream end. The flow recirculation that stabilizes the flame

is in this case created by a wedge, which is placed at the point where the small duct is attached to the large duct. From the 2 upstream facing sides of the wedge, gaseous fuel is injected through 62 holes fed by choked nozzles at either end of the wedge (see Figure 6-2-c). The fuel used here is methane at room temperature. All pieces, except the brass wedge shaped bluff body, are made from heat resistant stainless steel S310. The only cooling of the combustor is by natural convection and radiation at the outside surfaces. The burner can operate at a range of power of 20-80 kW and air factor 0.8-2.

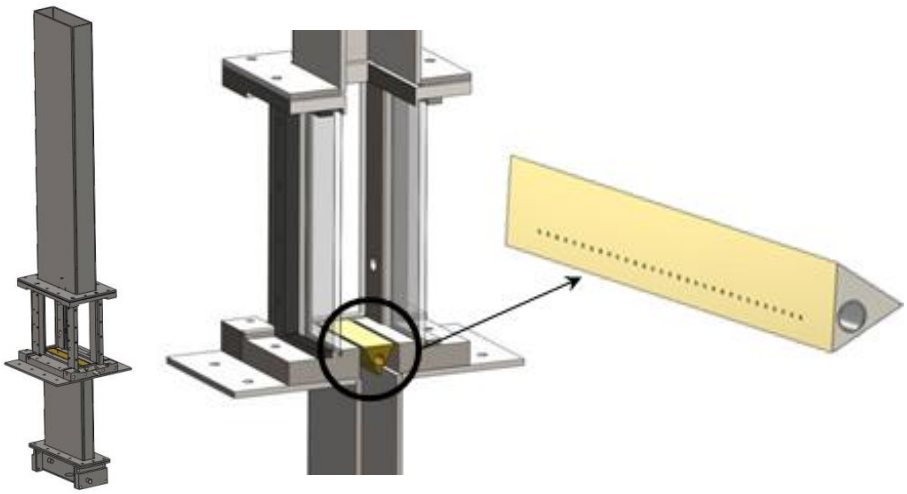

(a) (b) (c)

Figure 6-2: (a) LIMOUSINE test rig (b) optical access section (c) triangular bluff body with injection holes

6.4 Fluid structure interaction approach

Coupled fluid-solid interaction phenomena, which are characterized by the interaction of the fluid forces and structural deformations, appear in many applications on different fields of science and engineering. In order to reduce development time and cost in such multi physics problems, the methods used for numerical simulation of coupled systems becomes more and more important. In general, the approaches to the field of coupled problems can be subdivided into

two classes: one being called monolithic [17, 18] and the other partitioned [19-21]. Monolithic or so called simultaneous procedure solves the coupled system in a single iteration loop with consistent time integration schemes for all physical fields using one single computer code; this leads to time accurate coupled solutions, and larger time steps can be used as compared to partitioned schemes for the same level of accuracy [22]. However, it is still computationally more expensive per time step compared to the partitioned approach. In this work the latter approach for the fluid-structure interaction has been used. The partitioned method is an approach in which the two separate solvers with the appropriate interface boundary conditions for the flow domain and the structural domain operate in a coupled way. In this method there is always a time lag in the integration of the fluid and structure, which is the main drawback of this approach. However the principal advantage of the partitioned approach is that it allows applying the existing appropriate and sophisticated solvers for each subsystem, which can be replaced with less effort. This approach strives to solve each physical field separately with communication of interface data in between to connect the components. Interface conditions are enforced asynchronously meaning that the flow of the fluid does not change while the structural equations is being solved and vice versa. The total mesh displacement is transferred across the interface by preserving the profile between the two fields, while the total force will be transferred using a conservative formulation (see more details in [11]). Thus at the interface between fluid and solid regions the matching conditions should satisfy the Euler equation and Cauchy stress, as:

$$\rho_f . \vec{n} . \ddot{\vec{U}} = -\nabla p . \vec{n} \qquad 6\text{-}3$$
$$\vec{T} = -p . \vec{n}$$

Where p is the pressure, ρ_f the fluid density, $\vec{n}$ is the normal direction vector, $\vec{T}$ is the Chauchy stress vector in the solid, and $\vec{U}$ is the displacement.

In view of the strength of preserving the overall system stability, the partitioned method can be categorized into weak and strong coupling schemes [23, 24], which are also named respectively as explicit and implicit [24]. The weak scheme with staggered solution procedure is shown in Figure 6-3. The dashed lines indicate the time axis for each solver. The solution procedure starts with the solver B at time t_n , and it sends its initial interface values a_n to the solver A. Then, Solver A computes its next time step t_{n+1} and sends the updated interface values b_{n+1} to the solver B, letting it to move on to the next time step.

Figure 6-4 represents the strong coupling method with the interface iterations. Here, again dashed lines indicate the time axis. The solution procedure starts with the solver A at time t_n. Solver A computes b_{n+1}^1 as a first prediction to be used for solver B's interface values of the next time step. Solver B uses then the obtained prediction (b_{n+1}^1) to compute a prediction a_{n+1}^1 for solver A's interface values and returns it to solver A. This procedure repeats with both solvers until the solution convergences to the target value. Then solver A and solver B can both advance to the next time step (i.e.t_{n+1}).

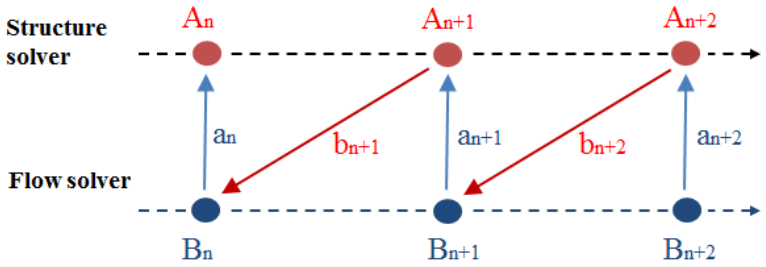

Figure 6-3: Weak coupling scheme with staggered solution procedure.

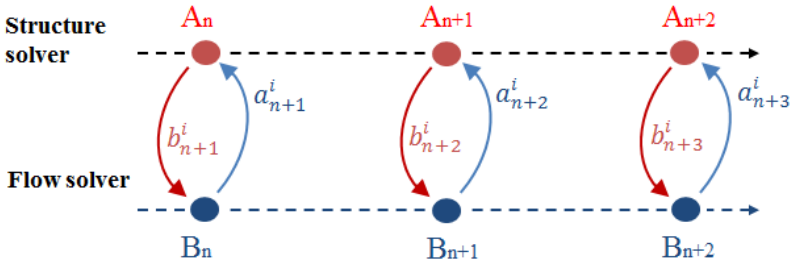

Figure 6-4: Strong coupling scheme with interface iterations.

The interface iterations of the strong coupling scheme can be computationally very expensive, especially for the fluid part of the FSI simulation which has many unknowns. However, in case of a highly flexible structure, weak coupling introduces a major error and might even lead to failure of the entire simulation[25].

Here due to the complexity of the problem under study, the partitioned approach is being used. Since the liner of the combustor has a small thickness, and therefore might be very flexible, the weak coupling scheme might not be an appropriate approach. Therefore the strong coupling is being selected. The schematic view of two-way fluid structure interaction (FSI) numerical simulation, conducted in this paper is shown in Figure 6-5. During the two way interaction analysis the ANSYS-CFX and ANSYS Mechanical softwares exchange information dynamically every time step. The data from a steady state solution is fed into the static structural analysis and then to the transient structural and fluid flow. A two-way coupling between the fluid and structure is obtained by linking the transient modules and then transferring surface loads/displacements across the interface. In this way the quantities from the fluid computations are applied directly on the liner and then the new deformed structure is updated in the fluid simulation, this allows to observe the impact of the wall vibration on the pressure distribution inside the combustion chamber as well as the effect of the modified pressure on the wall vibration. This procedure will be repeated until a converged solution is obtained, then the calculation will continue in the next time step. This procedure has three levels of iterations which are shown in Figure 6-6.

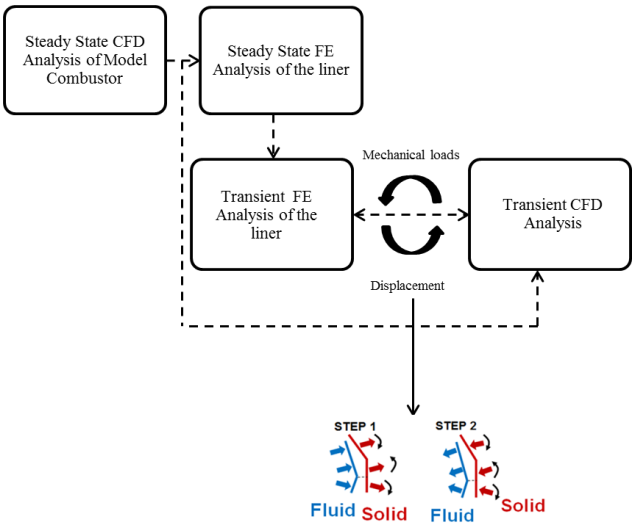

Figure 6-5: Schematic representation of FSI approach

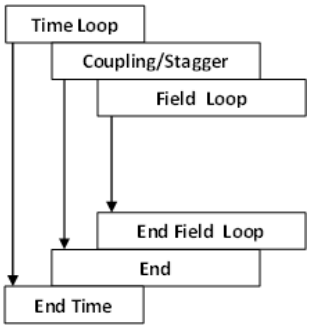

Figure 6-6: Process scheme of 2-way FSI simulation

6.4.1 CFD numerical simulation

In order to reduce the computational effort, numerical calculations of the reacting flow inside the chamber are done only for a thin slice of the combustor. Therefore the span wise size of the numerical domain is 4 mm wide with symmetry conditions enforced on each side (see Figure 6-7). The importance and effect of the chosen CFD domain on the accuracy of predicted combustion instability is explained in Appendix A. The choice of the CFD domain and hence the boundary conditions is important for estimating the magnitude of the instability, as it can add an artificial damping to the system by restricting the three dimensional turbulent motion of the reacting flow.

Since the resolution of the grid has significant effects on the accuracy of results, several different meshes with various element sizes and distributions were tested for steady case and finally a total number of 644,050 elements are used for the mesh. All the meshes used in this study are generated using the meshing tool ANSYS Workbench 14.5. The impact of the meshing technology and sensitivity of the results on the grid have been studied by the authors in [26] focusing on the fluid-only simulation. The mesh is refined in the combustion zone and around the fuel inlets. The CFD code employed here is ANSYS-CFX 14.5 (within the workbench code). It uses an implicit finite volume formulation to construct the discretized equations representing the Reynolds Averaged Navier-Stokes equations for the fluid flow. The model consists of a compressible solver with a co-located (non-staggered) finite volume method, such that the control volumes are identical for all transport equations [27]. The basic set of balance equations solved by ANSYS-CFX comprises the continuity, momentum, species and energy transport

equations. The instantaneous balance equations with the application of Favre averaging for the fluid domain can be written in Cartesian coordinates as:

- Conservation of mass

$$\frac{\partial \bar{\rho}}{\partial t} + \frac{\partial (\bar{\rho}\tilde{u}_i)}{\partial x_i} = 0 \qquad 6\text{-}4$$

- Momentum

$$\frac{\partial (\bar{\rho}\tilde{u}_i)}{\partial t} + \frac{\partial (\bar{\rho}\tilde{u}_i\tilde{u}_j)}{\partial x_i} = -\frac{\partial \bar{p}}{\partial x_i} + \frac{\partial}{\partial x_i}\left(\overline{\tau_{ij}} - \overline{\rho u_i^{"} u_j^{"}}\right) \qquad 6\text{-}5$$

τ is the stress tensor which is related to the strain rate by:

$$\overline{\tau_{ij}} = \widetilde{\tau_{ij}} + \overline{\tau_{ij}^{"}} \qquad 6\text{-}6$$

- Chemical species

$$\frac{\partial (\bar{\rho}\tilde{Y}_k)}{\partial t} + \frac{\partial (\bar{\rho}\tilde{Y}_k\tilde{u}_i)}{\partial x_i} = -\frac{\partial \left(\bar{\rho}\widetilde{u_i^{"} Y_k^{"}}\right)}{\partial x_i} - \frac{\partial (\overline{V_{k,i} Y_k})}{\partial x_i} + \bar{\dot{\omega}}_k \qquad 6\text{-}7$$

The source term in the species transport equations is shown by $\dot{\omega}_k$; V_k is the diffusive velocity of the *k*th species.

- Energy equation

$$\frac{\partial (\bar{\rho}\widetilde{e_0})}{\partial t} + \frac{\partial}{\partial x_j}\left(\bar{\rho}\tilde{u}_i\widetilde{e_0} + \tilde{u}_j\bar{p} + \overline{u_j^{"} p} + \overline{\rho u_j^{"} e_0^{"}} + \overline{q_j} - \overline{u_i\tau_{ij}}\right) = \bar{\dot{\omega}}_T \qquad 6\text{-}8$$

q_j is the heat flux which represents heat conduction and transport through species gradients given by ($q_j = -\lambda \frac{\partial T}{\partial x_j} + \rho \sum_{k=1}^{N} V_{k,j} Y_k h_{s,k}$).

$\bar{\dot{\omega}}_T$ is a chemical source term, and $\widetilde{e_0}$ is given by:

$$\widetilde{e_0} \equiv \widetilde{e} + \tilde{u}_k \tilde{u}_k /2 + k \qquad 6\text{-}9$$

Where the turbulent energy, k, is defined by:

$$k = \frac{\widetilde{u_k^{"} u_k^{"}}}{2} \qquad 6\text{-}10$$

For the discretization of the governing equations a high resolution advection scheme spatial method and a second order backward Euler discretization for time accuracy is used to solve the unsteady RANS equations. The unclosed terms

contain products of fluctuating values which need to be closed by modeled terms. In this work the effects of turbulence are described by using the Shear Stress Transport Turbulence Model (SST) in the steady state calculations, while for the transient calculations the Scale-Adaptive Simulation model (SAS) is used. The choice of turbulence model greatly influences the prediction of turbulent mixing rate and hence limit cycle oscillations. A comparison between the standard k-ω and SAS-SST model for the similar combustor has been reported earlier by Kumar et al. [28]. Reacting flow simulations are carried out on the model combustor by using the Burning Velocity Model (BVM) using a new model option for improving accuracy for non-premixed flames [26, 29]. BVM uses a RIF flamelet library for the 'burnt' mixture; This mechanism involves 16 species 46 reversible reactions scheme for methane-air gas chemistry [30].

The flow parameters are set consistent with the experimental conditions depicted in Table 6-1. URANS simulations are carried out with a time step of 1e-5. The convergence criterion of the RMS normalized residual values is set to 1e-5. Pressure fluctuations and the walls displacement are monitored at locations shown in Figure 6-8. At the monitor points the data is stored at every time step giving a sampling frequency of 100 kHz.

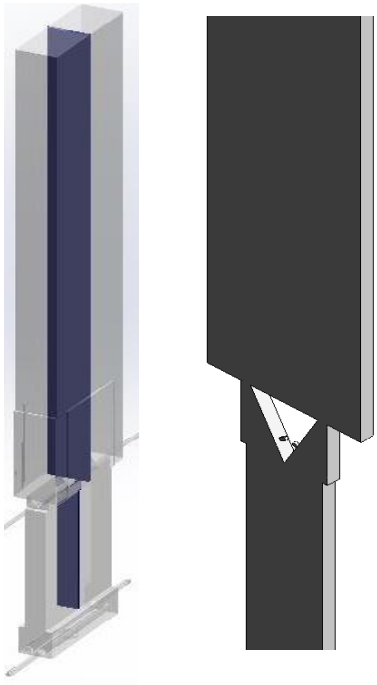

(a) (b)

Figure 6-7: (a) CFD domain: 4mm slice of the total geometry (b) enlarged view around the burner

Table 6-1: Operating condition

Power (kW)	Air factor	Methane mass flow rate [g/s]	Air mass flow rate [g/s]
40	1.4	0.8	19.152

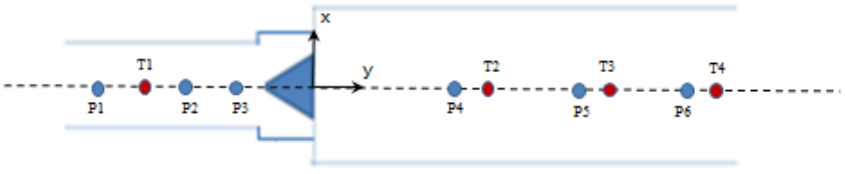

Figure 6-8: Pressure and temperature monitoring points in the CFD domain

Mesh deformation

In order to account for the mesh movement, it is necessary to modify the governing equations to include the mesh deformation. The transient convection term must change as the control volumes deform in time. These modifications follow from the application of the Leibnitz Rule:

$$\frac{d}{dt}\int_{V(t)} \varphi \, dV = \int_V \frac{\partial \varphi}{\partial t} \, dV + \int_s \varphi W_j \, dn_j \qquad 6\text{-}11$$

where W_j is the velocity of the control volume boundary.

The differential conservation equations are integrated over a given control volume. At this juncture, the Leibnitz Rule is applied, and the integral conservation equations become:

$$\frac{d}{dt}\int_{V(t)} \rho \, dV + \int_s \rho(u_j - W_j) \, dn_j = 0 \qquad 6\text{-}12$$

$$\frac{d}{dt}\int_{V(t)} \rho u_j \, dV + \int_s \rho(u_j - W_j)u_j \, dn_j = -\int_s P \, dn_j + \int_s \mu_{eff}\left(\frac{\partial u_i}{\partial x_j} + \frac{\partial u_j}{\partial x_i}\right) dn_j + \int_V S_{u_i} \, dV \qquad 6\text{-}13$$

V is the volume, S is the surface, and μ_{eff} is the effective viscosity including the dynamic viscosity and the turbulent viscosity.

$$\frac{d}{dt}\int_{V(t)} \rho\varphi \, dV + \int_s \rho(u_j - W_j)\varphi \, dn_j = \int_s \Gamma_{eff}\left(\frac{\partial \varphi}{\partial x_j}\right) dn_j + \int_V S_\varphi \, dV \qquad 6\text{-}14$$

The transient term accounts for the rate of change of storage in the deforming control volume, and the advection term accounts for the net advective transport across the control volume's moving boundaries.

The mesh deformation given by Equation 6-14 is only attributed to the motion of nodes on the boundary. The motion of all remaining nodes (i.e. the regions of nodes with the same degrees of freedom) is determined with the Displacement Diffusion Model. With this model the displacement of domain boundaries are diffused to other mesh points by solving the following equation:

$$\nabla.(\Gamma_{dis}\nabla\delta) = 0 \qquad 6\text{-}15$$

In this equation, δ is the displacement relative to previous mesh locations and $\Gamma_{dis}$is the mesh stiffness, which determines the degree to which regions of nodes move together. It is worth noting that the displacement diffusion model for mesh

motion is designed to preserve the relative mesh distribution of the initial mesh. (more details are given in [31])

6.4.2 CSD numerical computation

The finite element solver available in the ANSYS suite of software is used for the calculation of the structural domain. Because most of the dynamic coupling between the fluid and structure occurs in the region downstream of the wedge where the reaction takes place, in this simulation only the structure downstream of the wedge is considered. For the sake of reducing the necessary computational efforts, the solid domain has been simplified; therefore quartz glass windows or holes for thermocouples and pressure transducers have been removed. In order to determine the structural eigenfrequencies and mode shapes, modal analysis is first performed using the element type solid 186. Since the liner is clamped at the burner inlet plane, the air/fuel duct (i.e. plenum) is removed from the structural domain. The mode shape and eigenfrequencies of the first seven modes of the structure are presented respectively in Figure 6-9 and Table 6-2. Compared to the measurements performed by Altunlu [32], the predicted eigenfrequencies are acceptable except for the first torsional and the second bending mode in which 18% deviation can be observed. The deviation between the measurements and predictions can be caused by the effect of welds in the structure which is neglected in the FEM [33]. It can be also attributed to other simplifications made in the model such as neglecting the effect of thermocouples, and pressure transducers. Besides, in the FEM the plenum is removed and only the top liner is considered. Overall, frequencies predicted by the model are close to the experimental data. However, considering that the plate modes of the structure are the only modes influencing the acoustic response of the combustor due to the associated change in the acoustic volume, the chosen FE model is claimed to be in line with the physical model. It is important to mention that both the measurements and calculations have been performed for the room temperature condition, as it is not possible to do such measurements in high temperature with the available tools in the laboratory. Therefore a reduction in the represented eigenfrequencies is expected, as the Young's modulus is decreased for higher values of temperature (see Figure 6-10). The structural eigenfrequency is indeed proportional to the square root of the Young modules [34]. As the Young modules (E) reduces from 198GPa to 176 GPa, an approximate reduction of 7% in the predicted eigenfrequencies is expected in the assumed hot condition (i.e. 400 °C). Further increase in the structure temperature leads to the further reduction in the predicted eigenfrequencies.

Despite all simplifications of the studied geometry made in the FE model, the domain (according to the Figure 6-9) for the coupled simulation is still computationally very expensive when used for FSI. Therefore only a slice of the structure, with symmetry surfaces (i.e. frictionless supports), is used for the further calculations. The chosen solid domain is sketched in Figure 6-11. The structural mesh consists of 3,304 elements of type solid 185 [35]. The linear elements have eight nodes with three degrees of freedom at each node. For simplification, a uniform temperature of 400 °C is assumed along the liner wall and the material properties are determined as presented in Table 6-3. The clamped boundary condition is implemented at the burner inlet plane, while the rest of the surface is allowed to deform freely depending on the dynamic pressure loads.

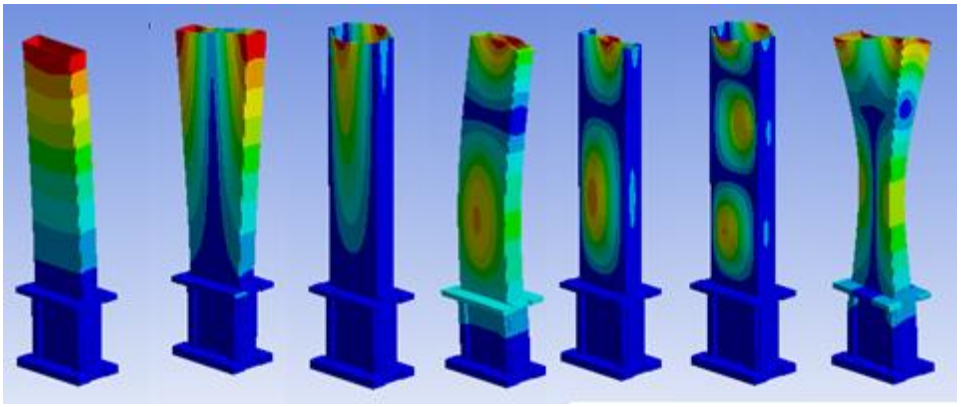

Figure 6-9: Mode shape of the combustor (without the plenum) predicted by FEM

Table 6-2: Structural eigenfrequencies of the LIMOUSINE combustor at room temperature

	Structure Eigen frequencies	
Mode	Hammer test [32]	FEM Solid elements
Bending (1st)	125	126
Torsional (1st)	534	437
Plate (1st)	639	633
Bending (2nd)	645	532
Plate (2nd)	673	671
Plate (3rd)	744	750
Torsional (2nd)	764	761

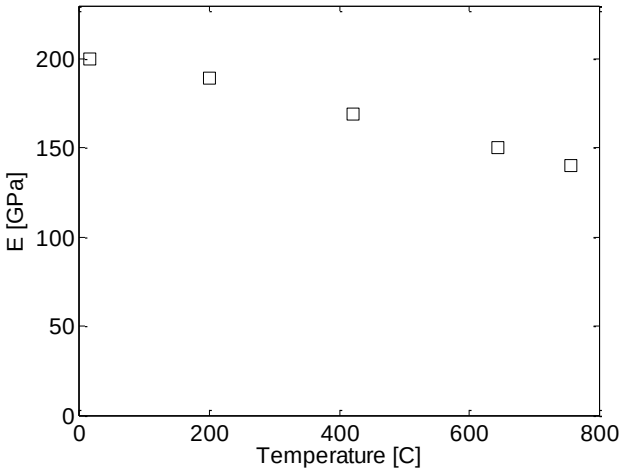

Figure 6-10: Evolution of the Young's modulus of the SS310 with temperature [6]

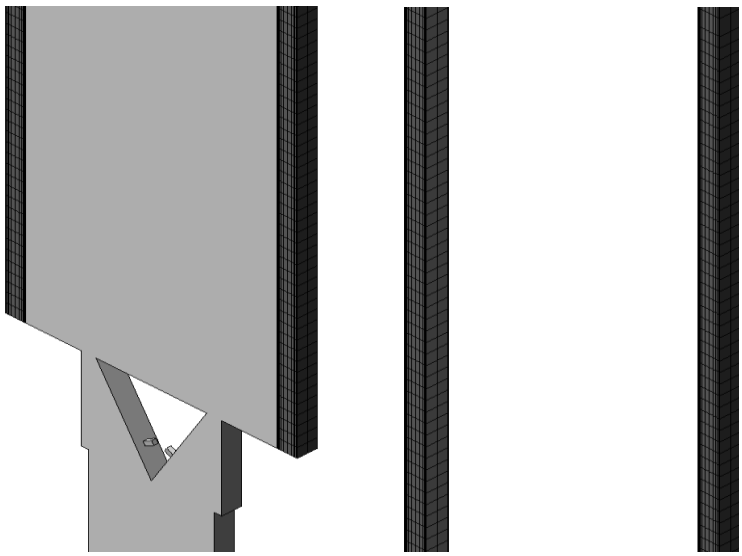

(a) (b)

Figure 6-11: (a) reduced structure domain attached to the fluid (b) sketch of the solid mesh in the FE solver

Table 6-3: Material Properties of SS310 at 400 ˚C

Young's modulus (Gpa)	Poisson's ratio	Density [kg/m^3]
1.76	0.3	7,715

6.5 Results

The outcome of the coupled FSI modeling is divided to into the results representing the physics of the fluid influenced by the structure, and results showing the deformation of the structure. The obtained results are compared with the other approaches like zero-way interaction so-called fluid-only model and also the thermal coupling approach of fluid and structure (CHT). Details about these models can be found in previous work done by the authors [36]. In this section numerical results are presented and validated with available experimental data. However, prior to the discussion on the predicted multi-physics data, it is

necessary to make sure that the strong coupling is achieved by having the converged loads passing between two solvers. Here, minimum values of 1 and maximum values of 10 were selected for the staggered iteration; however during the calculations always less than 10 loops were required, proving that the convergences occur before reaching to the upper limit. The convergence level of the force (F_x, F_y) and displacement (U_x, U_y) which are presented in Figure 6-12 show that each quantity is converged as the residual drops below zero [31].

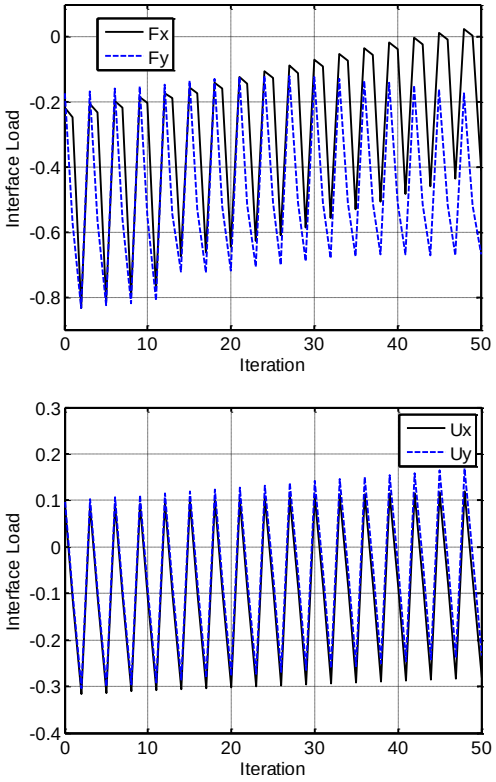

Figure 6-12: Convergence of the interface loads: Mechanical load (LHS) and Wall displacement (RHS)

6.5.1 Acoustic behavior

The geometric enclosure of the combustor may act as a resonator. Pressure waves which are reflected at the boundaries of the burner may interact with the heat

release process; If the dissipation of acoustic energy within the chamber and also at the boundaries is smaller than the energy gained by the acoustic disturbances, pressure waves are excited and pressure amplitudes will soon grow up to a saturation limit. Figure 6-13 shows the calculated evolution of pressure over time within the burner recorded by the first control point above the wedge, which corresponds to the physical location of the first pressure transducer in the experiment. Due to the rapid growth of the oscillation amplitude characterizing the phase of oscillation, the system will soon reach to saturated constant amplitude.

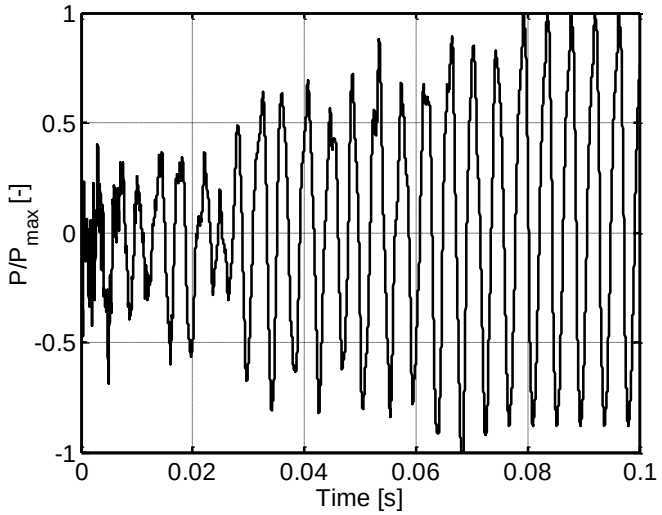

Figure 6-13: Calculated self-exited pressure oscillation as a function of time

The frequency spectrum of the pressure signal corresponding to the thermal power of 40KW and λ=1.4 using three different numerical approaches (Fluid-only, CHT and two-way) together with the experimental measurements are plotted in Figure 6-14. Both CHT approach and two-way coupled model predict the primary instability at 232 Hz giving the error of 0.6%; however the numerical results based on the two-way approach show an overprediction of the instability magnitude inside the combustion chamber, giving 5% discrepancy from experimental results. This is mainly due to the overprediction of the temperature in the CFD domain in the two-way coupled approach compared to the CHT model, as a constant temperature has been set at the structure. It results in the underprediction of the

heat losses through the combustion chamber, which is shown in the Figure 6-15. The area integral of the heat flux over the liner of the combustor in each case shows the clear difference between the two-way FSI approach and the CHT model. Considering that the observed difference in the predicted heat loss is just attributed to a 4mm slice of the total depth of the combustor, the importance of this diversity will be even more significant. Among the used models, the zero-way interaction model shows the largest discrepancy from experimental results (an error about 10%) in the prediction of instability frequencies. However, the pressure spectrum presented in Figure 6-14, show the fundamental quarter wave mode frequency for each approach. According to the calculation the first and third amplitude peaks are observed at frequencies presenting the first and the third quarter wave modes, with the part downstream the bluff body driving the instability process, meaning that the instabilities are originating from the combustion chamber and not the whole combustor; this is discussed in more details in Appendix B. Another observed peak is exactly double of the first eigenfrequency of the combustor; according to Roman Casado [37] this second peak is not an acoustic harmonic, and it is identified to be due to the frequency doubling of the first eigenfrequency, which is mainly due to the presence of high non-linearities in the combustion process when a system reaches high amplitude limit cycle oscillations. The measured pressure field shows a strong harmonic component near 600 Hz (period 1.67 ms), which is related to the structural dynamics of the combustion chamber. While in the two-way approach the presence of structural dynamics is rather in the frequency range of 700-800 Hz. This can be due to the higher stiffness compared to the experiments caused by the assumed uniform temperature and therefore constant Young modules in the simulations.

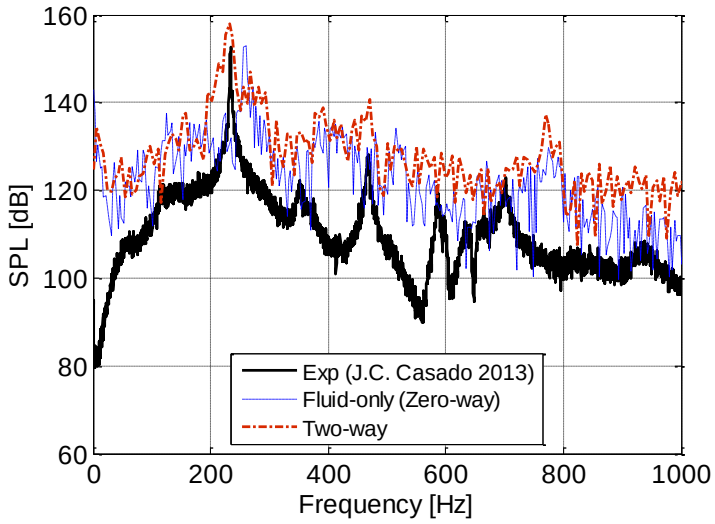

(a)

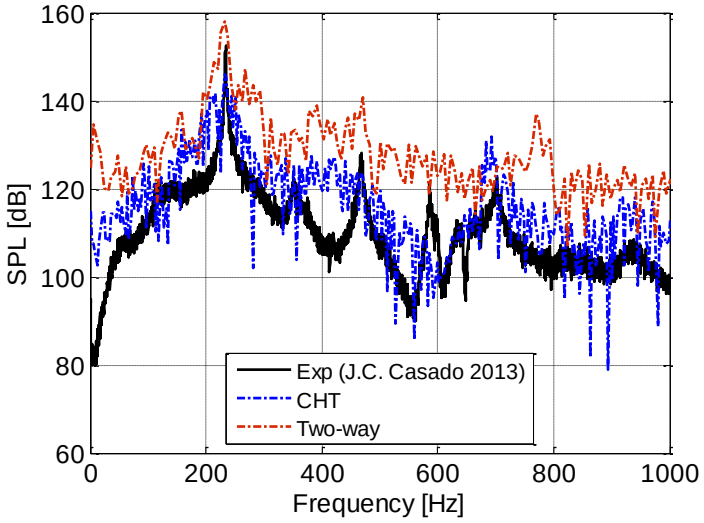

(b)

Figure 6-14: Pressure spectrum for 40kW and λ=1.4: (a) experiment, zero-way and two-way interactions (b) experiment, CHT and two way interaction

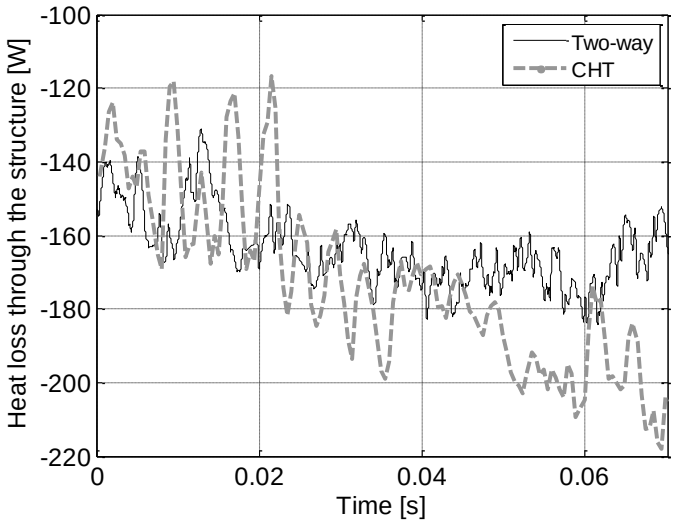

Figure 6-15: Total calculated heat loss through the structured (i.e. 4mm slice)

Table 6-4 reports CFD, FEM and experimental resonant frequencies, showing a good level of agreement. Furthermore, the FEM results show that the main frequency of instability is related to acoustics of combustion chamber and not the full geometry. Details of FE modeling of the acoustic eigenfrequencies are given in Appendix B.

Table 6-4: experimental, CFD and analytical frequencies of first predicted peak frequency

Power [kW]	λ [-]	Resonance frequency [Hz]				
		Experiment ref. [37]	CFD Fluid-only (zero-way)	CFD (CHT)	CFD (FSI)	FEM Combustion chamber No mean flow
40	1.4	234	256	232	232	249

To explore the origin of instability observed in the Figure 6-14, further analyze is conducted. As reported by Sivakumar et al. [38] for a bluff body combustor, variation of dimensionless quantities such as the Helmholtz and Strouhal numbers

with the Reynolds number can determine the origin of the LCO. The Helmholtz and Strouhal numbers are respectively defined as:

$$He = f\frac{L}{c} \qquad 6\text{-}16$$

In which c is the average speed of sound in the plenum and the combustion chamber weighted by their relative length. *f* is the dominant frequency and L is the total length of the combustor.

$$St = f\frac{h}{u} \qquad 6\text{-}17$$

In which *f* is the dominant frequency, *u* is the characteristic speed of the upstream cold flow, and *h* is the characteristics length of the bluff body.

If the dominant frequency is driven by the acoustics of the system, the Helmholtz number remains constant, while the Strouhal number varies hyperbolically as the Reynolds number of the incoming flow changes. The recorded Helmholtz and Strouhal numbers at the observed dominant frequencies, shown in Figure 6-16 for different Reynolds numbers confirm that the LCO is driven by the acoustics of the LIMOUSINE combustor as the Helmholtz number stays almost constant at an approximate value of 0.4.

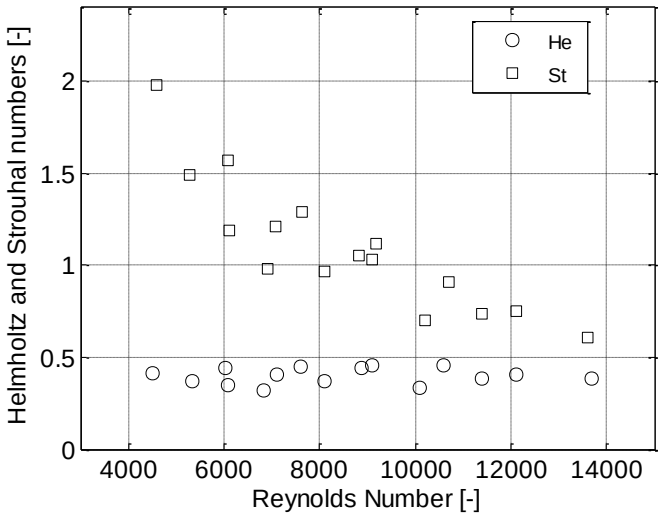

Figure 6-16: Variation of the measured Helmholtz number (He), and Strouhal number (St) with the Reynolds

6.5.2 Structural behavior

Figure 6-17 shows the calculated and measured wall displacement at a location 200 mm downstream the burner. The time domain indicates a wall displacement in order of 100 micrometer from the not loaded position. Figure 6-18 shows the measured and calculated liner displacement frequency spectra; one can see that the peaks present in the pressure spectrum are approximately reproduced in the wall displacement results. This indicates a strong fluid-structure interaction around the natural modes of the combustor. In the experiment frequencies of 237 Hz and 474 originate from the gas phase flame dynamics. In the numerical data, the main instability peak is observed approximately at 250 Hz which is close to the first experimental value of 237 Hz. However because the physical time for the computation of the two-way numerical calculations is limited, the pressure plots have low frequency resolution. The peaks observed at 550 Hz and 650 Hz are coming from the structural dynamics. These oscillations are fed by energy derived from the acoustic fluid oscillation but vibrate at the structural eigenfrequencies. As it was mentioned before, due to the existence of the temperature gradient along the chamber and therefore variable material properties as a function of temperature, the structural frequencies observed in the pressure and displacement spectra deviate from the presented values in Table 6-2. In the experiment, the instability peak at 650 is as strong as the one observed at 237 Hz, which is not the case in the simulation.

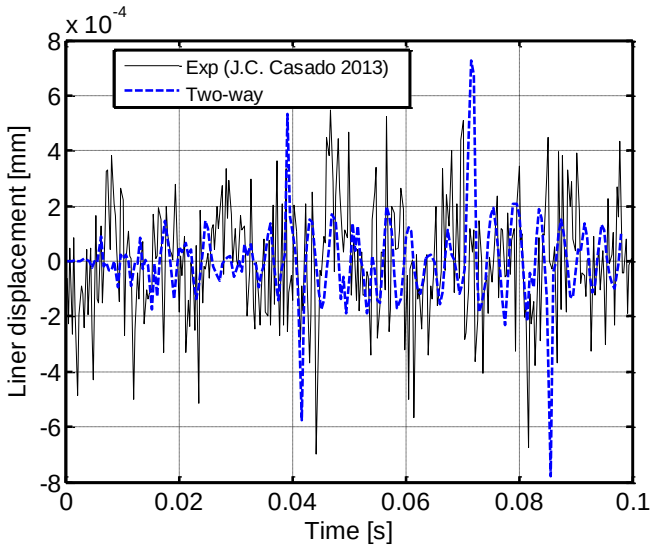

Figure 6-17: Two-way FSI (dash line) and Experimental (solid line) results for the wall displacement of the case 40kW and λ=1.4

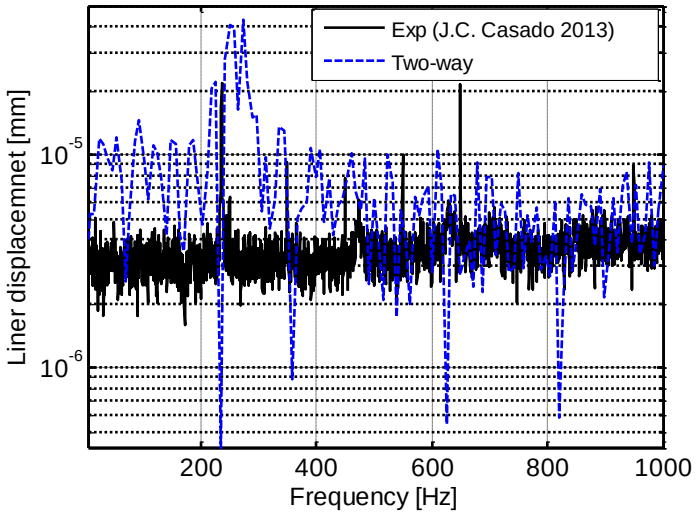

Figure 6-18: Wall displacement results obtained from the two-way FSI approach (dash line) and Experimental data (solid line) versus the frequency for the case 40kW and λ=1.4

6.6 Conclusion

Thermoacoustic instability can be caused by the feedback mechanism between unsteady heat release, acoustic oscillations and flow perturbations. In a gas turbine combustor, limit cycles of pressure oscillations at elevated temperatures generated by the unstable combustion process enhance the structural vibration levels of the combustor. Depending on the operating conditions, the flame may show a stable or an unstable behavior. In order to predict the frequency and magnitude of the thermoacoustic instabilities, and also to capture the reacting flow physics coupled to the structure, calculations were performed for an unstable flame condition. In this work transient CFD and CSD analysis using ANSYS workbench V14.5, was carried out. The transient information (pressure and displacement) was exchanged between the fluid and structural domain by means of 2-way coupling. The obtained results using this approach were compared with zero-way interaction model as well as the CHT approach. The main outcome of this research is summarized as:

- Among the used models, the zero-way interaction model results show the largest discrepancy from experimental results in the prediction of instability frequencies.
- The frequencies of the thermoacoustic instabilities are well predicted using the CHT and two-way coupled approaches, while in the latter case the magnitude is slightly overpredicted; this can be explained by overprediction of the temperature in the CFD domain due to the assumed constant temperature at the structure. While in the CHT modeling results, due to the modeling of the transient heat transfer and therefore considering the correct heat losses from the system, the predicted pressure field is closer to the experiments.
- In general, all used numerical approaches show the occurrence of the main instability at a frequency close to the first quarter wave acoustic mode of the combustion chamber, pointing to the fact that the LCO is driven by the chamber's acoustics. It shows the ability of URANS model to explore the influence of limit cycle behavior.
- Although the CHT approach gives very accurate information of the characteristics frequencies and amplitude, to determine the influence of the LCO behavior on the structure and/or the effect of structural vibrations on the confined fluid in the unstable regime a coupled FSI model is required.
- The preliminary results of solid deformation show that the maximal displacement exhibited by the structure is very small, a fraction of a

millimeter. Such displacements are extremely small but can act like a strong acoustic source due to the high acceleration rate of the structure.

Acknowledgments

The authors would like to acknowledge the funding of this research by the EC in the Marie Curie Actions Networks for Initial Training, under call FP7-PEOPLE-2007-1-1-ITN, Project LIMOUSINE with project number 214905.

Appendix A:
Proper choice of the CFD domain

Here, to investigate the effect of the chosen domain on the accuracy of the results, the coupled FSI analyses are done for the half part of the geometry as reported by [14] and [39]; the domain comprises half of the wedge and is 25 mm wide (Figure 6-19). For this coupled problem, all numerical methods and boundary conditions are set as previously mentioned in section 6.4.1 and 6.4.2 (CFD/CSD numerical simulations); while the symmetry condition is prescribed to the side surface which is the mid-plane of the combustor (x=0). Simulations are performed for one specified operating condition in which the strongest instability and high level of pressure loads occur.

Predicted and measured pressure spectra shown in Figure 6-20, represent the distinct characteristic frequencies with peak pressure levels; however the predicted main frequency by the numerical model is very high compared to the experimental value of 272 Hz resulting in a prediction error of 17%. Besides, in the calculations the pressure amplitudes at the characteristics frequencies are underpredicted by one order of magnitude, meaning that the combustor is in the stable regime which is inconsistent with the experimental observation. Overall, it can be concluded that the simplification in the CFD domain and assuming the symmetry condition in the X-direction (symmetry plane of Y-Z at x=0), brings the deviation between the experimental and numerical observations, leading to the failure of the numerical model in the prediction of instability.

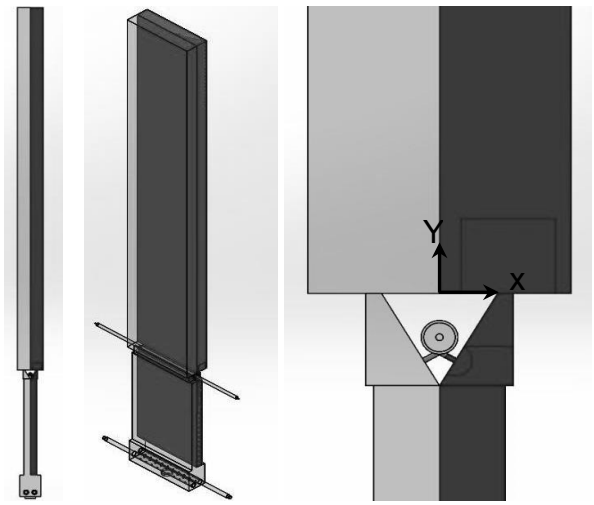

Figure 6-19: Chosen CFD domain (Black part) with symmetry plane X=0

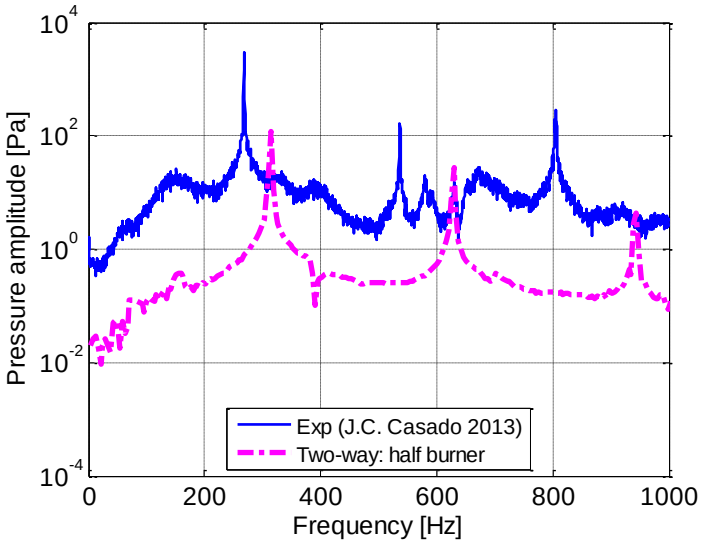

Figure 6-20: Pressure spectrum for 60kW and λ=1.2: comparison of the experiment and the two-way coupled model with the imposed symmetry condition in the middle plane

Appendix B:
FEM approach to calculate the acoustic modes of the combustion system

The interpretation of the predicted resonances as acoustic modes for the present configuration is also supported by the commercial finite element method (FEM) software ANSYS: one for the full geometry, and one for the combustion chamber (CC). Here, the linear wave equation by assuming the fluid to be compressible and inviscid is solved. It is also assumed that the mean density and pressure are uniform throughout the fluid and also there is no mean flow of the fluid.

$$\nabla^2 P = \frac{1}{c^2}\frac{\partial^2 P}{\partial t^2} \qquad 6\text{-}18$$

The acoustic element type Fluid 30 is used to model the acoustic domain, which is a 8-node brick element. For this model a fully tetrahedral mesh is generated. It is important to make sure that the mesh is fine enough for acoustic analyses. It is recommended to use 15-20 elements per wavelength as a minimum. The working fluid is air. First the whole combustor is modeled which is presented in Figure 6-21. Every boundary is acoustically closed, while the outlet is open. Thereafter, the geometry which corresponds to the combustion chamber has modeled (see Figure 6-22). The combustion chamber has only one cross section, and one temperature. In this case, the outlet boundary condition will remain as an open end, but the inlet which is the burner exit is assumed to be closed. The first and second modes predicted by using the full combustor approach and the combustion chamber approach are reported in Table 6-5. For the full combustor, the frequency of the first mode is low as compared to the measured value of 234 Hz. In fact the blockage in the burner makes a deviation from the Rijke tube.

Table 6-5: Predicted acoustic eigenmodes using FEM code

	FEM	
	Full combustor	Only combustion chamber
First mode [Hz]	195.91	249.043
Second mode [Hz]	564.39	747.229

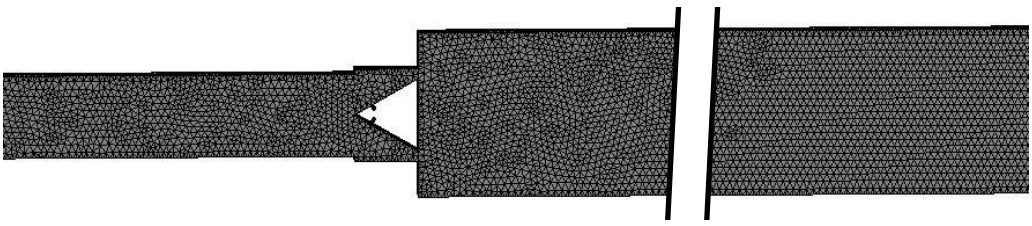

Figure 6-21: Full combustor grid used in FE code

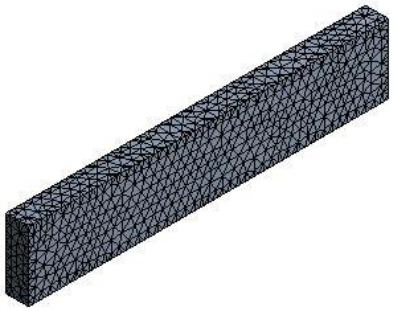

Figure 6-22: Combustion chamber used in FE code

References

[1] A. Can Altunlu, Peter van der Hoogt, and ., A. d. B., 2011, "Life assessment by fracture mechanics analysis and damage, monitoring technique on combustion liners," Proceeding of ASME Turbo Expo 2011,Vancouver, Canada, pp. 133-143.
[2] Roman Casado, J. C., Alemela, P., and Kok, J. B. W., 2010, "Combustion dynamics coupled to structural vibrations," 17th International Congress on Sound & Vibration, Egypt, Cairo.
[3] Petchenko, A., Bychkov, V., Akkerman, V. y., and Eriksson, L.-E., 2007, "Flame–sound interaction in tubes with nonslip walls," Combustion and Flame, 149(4), pp. 418-434.
[4] Foucher, F., Burnel, S., Mounaïm-Rousselle, C., Boukhalfa, M., Renou, B., and Trinité, M., 2003, "Flame wall interaction: effect of stretch," Experimental Thermal and Fluid Science, 27(4), pp. 431-437.
[5] Ahn, K., and Yu, K. H., 2012, "Effects of Damköhler number on vortex–flame interaction," Combustion and Flame, 159(2), pp. 686-696.
[6] Huls, R., 2006, "Acousto-Elastic Interaction in Combustion Chambers," PhD, University of Twente, Enschede, The Netherlands.

[7] Lefebvre, A. H., and Ballal, D. R., 2010, "Gas Turbine Combustion: Alternative Fuels and Emissions," Taylor & Francis.
[8] Candel, S., 2002, "Combustion dynamics and control: Progress and challenges," Proceedings of the Combustion Institute, 29(1), pp. 1-28.
[9] Lieuwen, T., Torres, H., Johnson, C., and Zinn, B. T., 2000, "A Mechanism of Combustion Instability in Lean Premixed Gas Turbine Combustors," Journal of Engineering for Gas Turbines and Power, 123(1), pp. 182-189.
[10] Huls, R. A., Sengissen, A. X., Hoogt, P. J. M. v. d., Kok, J. B. W., Poinsot, T., and Boer, A. d., 2007, "Vibration prediction in combustion chambers by coupling finite elements and large eddy simulations," Journal of Sound and Vibration, 304(1-2), pp. 224-229.
[11] Pozarlik, A. K., 2010, "Vibro-acoustical instabilities induced by combustion dynamics in gas turbine combustors," PhD Thesis, University of Twente, Enschede, The Netherlands.
[12] Alemela, P., Casado, J., Kumar, S., and Kok, J., 2013, "Thermoacoustic analysis of the dynamic pressure inside a model combustor during limit cycle oscillations," International Journal of Spray and Combustion Dynamics, 5(1), pp. 25-48.
[13] Alemela, R., Casado, J. C. R., Santosh Kumar, T. V., and J.B.W.Kok, 2011, "Simulation of limit cycle pressure oscillations with coupled fluid-structure interactions in a model combustor," 18th International Congress on Sound & Vibratiom, Rio de Janeiro, Brazil.
[14] A. Can Altunlu, Mina Shahi, Artur Pozarlik, P.J.M. van der Hoogt, J.B.W.Kok, and Boer, A. d., 2012, "Fluid-structure interaction on the combustion instability," 19th International Congress on Sound and Vibration, Vilnius, Lithuania, pp. 291-298.
[15] Nicoud, F., and Poinsot, T., 2005, "Thermoacoustic instabilities: Should the Rayleigh criterion be extended to include entropy changes?," Combustion and Flame, 142(1–2), pp. 153-159.
[16] Rijke, P. L., 1859, " On the vibration of the air in a tube open at both ends," Philosophical Magazine, 17, pp. 419-422
[17] Michler, C., Hulshoff, S. J., van Brummelen, E. H., and de Borst, R., 2004, "A monolithic approach to fluid–structure interaction," Computers & Fluids, 33(5–6), pp. 839-848.
[18] J.Blom, F., 1998, "A monolithical fluid -structure interaction algorithm applied to the piston problem," Computer Methods in Applied Mechanics and Engineering, 167, pp. 369-391.
[19] Carlos, A., Park, K. C., and Farhat, C., 2001, "Partitioned analysis of coupled mechanical systems," Computer Methods in Applied Mechanics and Engineering, 190(24–25), pp. 3247-3270.
[20] Piperno, S., Farhat, C., and Larrouturou, B., 1995, "Partitioned procedures for the transient solution of coupled aroelastic problems Part I: Model problem, theory and two-dimensional application," Computer Methods in Applied Mechanics and Engineering, 124(1–2), pp. 79-112.
[21] Piperno, S., and Farhat, C., 2001, "Partitioned procedures for the transient solution of coupled aeroelastic problems – Part II: energy transfer analysis and three-dimensional applications," Computer Methods in Applied Mechanics and Engineering, 190(24–25), pp. 3147-3170.

[22] Hübner, B., Walhorn, E., and Dinkler, D., 2004, "A monolithic approach to fluid–structure interaction using space–time finite elements," Computer Methods in Applied Mechanics and Engineering, 193(23–26), pp. 2087-2104.
[23] Schäfer, M., Heck, M., and Yigit, S., 2006, "An Implicit Partitioned Method for the Numerical Simulation of Fluid-Structure Interaction," Fluid-Structure Interaction, H.-J. Bungartz, and M. Schäfer, eds., Springer Berlin Heidelberg, pp. 171-194.
[24] Gatzhammer, B., 2008, "A partitioned approach for Fluid-Structure Interaction on cartesian grids," Master's Dessertation, Technische Universitat Munchen.
[25] Gövert, S., and Kok, J. B. W., 2013, "Fluid-Structure coupling for numerical simulation of a gas turbine combustor " , 20th International Congress on Sound and Vibration , Bangkok, Thailand, pp. 2986 - 2994.
[26] Filosa, A., Shahi, M., Tomasello, A., Noll, B., Aigner, M., and Kok, J., 2013, "numerical studies of unsteady heat transfer with thermoacustics oscillations," 20th International Congress on Sound & Vibration, Bangkok, Thailand, pp. 3018 - 3026.
[27] Patankar, S. V., 1980, Numerical Heat Transfer and Fluid Flow, Hemisphere, New York.
[28] Santosh Kumar, T. V., Alemela, P. R., and Kok, J. B. W., 2011, "Dynamics of flame stabilized by triangular bluff body in partially premixed methane-air combustion," Proceeding of ASME Turbo Expo, Vancouver, Canada, pp. 1017-1026.
[29] Forkel, H., 2012, "CFX 14.5 Burning Velocity Model discretization for non-premixed combustion," ANSYS Germany GmbH.
[30] Smooke, M. D., Puri, I. K., and Seshadri, K., 1988, "A comparison between numerical calculations and experimental measurements of the structure of a counterflow diffusion flame burning diluted methane in diluted air," Symposium (International) on Combustion, 21(1), pp. 1783-1792.
[31] 2011, ANSYS CFX solver manager user's guide. Release 14.0. .
[32] Altunlu, A. C., 2013, "The analysis of mechanical integrity in gas turbine engines subjected to combustion instabilities," PhD Thesis, University of Twente, Enschede.
[33] Altunlu, A. C., Hoogt, P. J. M. v. d., and Boer, A. d., 2013, "Sensitivity of combustion driven structural dynamics and damage to thermo-acoustic instability: Combustion-acoustics-vibration," Journal of engineering for gas turbines and power, 136(5).
[34] Blevins, R. D., 1984, Formulas for Natural Frequency and Mode Shape, Krieger Publishing Company.
[35] 2011, ANSYS Mechanical APDL element reference. Release 14.0.
[36] Shahi, M., J.B.W.Kok, Roman Casado, J. C., and Pozarlik, A., "Study of unsteady heat transfer as a key parameter to characterize limit cycle of high amplitude pressure oscillations," Proceeding of ASME Turbo Expo 2014, Dusseldorf, Germany.
[37] Roman Casado, J. C., 2013, "Nonlinear behavior of the thermoacoustic instabilities in the limousine combustor," PhD Thesis, University of Twente, Enschede, The Netherlands.
[38] Sivakumar, Sivakumar, R., Chakravarthy, and Chakravarthy, S. R., 2008, "Experimental investigation of the acoustic field in a bluff-body combustor," International Journal of Aeroacoustics, 7(3), pp. 267-299.
[39] Shahi, M., Kok, J. B. W., and Alemela, P. R., "Simulation of 2-way fluid structure interaction in a 3D model combustor," Proceeding of ASME Turbo Expo 2012, pp. 1571-1580.

7

Conclusions & Recommendations

In this chapter the main conclusions based on the research questions, defined in the chapter 1 "Introduction" will be summarized and followed with the recommendation for the further research.

7.1 Conclusions

- **What are the requirements for an accurate prediction of an unstable regime of a combustor using URANS?**

  To answer to this question, it is essential to consider the three important elements characterizing the feedback mechanisms of thermoacoustic instability including acoustic oscillations, flow/mixture perturbations and heat release fluctuations. In order to predict the key parameters regulating the coupling between heat release fluctuations and acoustic, the ANSYS-CFX code was used. Since the role of the combustion model and the approach used to resolve the flame front dynamics are of major importance to catch the most important physical processes, it is essential: 1- to verify the ability of the used method to predict the onset of the instability, 2- to achieve a description of the phenomenon and 3- to predict the frequency at which the instabilities occur. This was done in Chapter 2, 3 and 4 to find the models giving the best prediction compared to the experiments. However the limit cycle behavior of pressure oscillations in the combustion system is a multi-physics problem; the unsteady combustion process induces a strong acoustic field, increasing the vibration of the liner which itself can act as an external fluctuating force (i.e. source of sound) amplifying the pressure oscillations and hence enhancing heat release fluctuations. Apart from the mechanical vibration, the enhanced heat

transfer during the limit cycle adds to the damage to the hot section of the combustor, which shows the importance of considering the thermal-structure coupling effects. Therefore, it is required to take into account the mutual interaction between various phenomena which occur in the combustion system. In general, it can be concluded that the accuracy of the prediction of an unstable regime of the combustor is not only sensitive to the characteristics of the CFD domain (like: type of grids, the turbulence and combustion models, boundary conditions etc.), but it is also concluded that the results are more relevant only when the coupling with the liner is taken into account. Considering the multiple interactions between acoustics, aerodynamics, combustion and structural elements of a combustor, the limit cycle pressure of the LIMOUSINE combustor was successfully predicted in this work.

- **What is the sensitivity of models to the input parameters? What are effective parameters in the structure liner which are playing role in determining the magnitude of the pressure fluctuations?**

  Results revealed that numerical predictions are sensitive to chosen parameters in both CFD and CSD Domains as described below:

  - **CFD domain *(fully detailed geometry or half geometry)*:** Study done in Chapter 6 proves how important it is to consider the whole bluff body (burner) in the calculation rather than assuming the symmetry condition in mid-plane, because the latest can push the unstable flame to the stable regime, and damps the acoustic oscillations in the system arising due to the 3D effects.

  - **Grid Type:** From the studies done for the fluid-only calculation (Chapter 3) it is concluded that the structured grid has lower numerical dissipation and it shows better agreement with experimental data than the unstructured grid.

  - **Turbulence model:** Different turbulence models were used for different working conditions including reacting and non-reacting mixture, showing the fact that the SAS-SST model gives the best prediction compared to the experiment available in the literature (Chapter 2).

  - **Chemical models:** Depending on the operating conditions such as thermal power and air/fuel ratio, during the experiments the flame shows a stable or an

unstable behavior. According to the calculations (Chapter 3 and 4), among the available combustion models in ANSYS-CFX, the Burning Velocity Model (BVM), using a new model option for non-premixed flames, gives the best consistency with the experiments. Using other combustion models either fails in prediction of limit cycle oscillations or fails in prediction of the correct self-excited modes.

- **Acoustic boundary condition:** Results presented in Chapter 4 show that the acoustic boundaries of the combustor have the important role to characterize the thermoacoustic instabilities. For the accurate representation, the CFD domain downstream the wedge should be extended.

- **Wall temperature:** The prescribed liner boundary condition (temperature and/or emissivity of the walls) has a major impact on the predictions (Chapter 4 and 5). This influence is larger compared to the conventional stable combustion processes, which changes the frequency and magnitude of the instability. For this reason, and to determine the heat penetration depth in the structure of the test rig, it is required to perform the thermal coupled fluid structure interaction modeling.

- **Solid Grid:** a study done in the CSD domain (in Chapter 5), showed that the solid grid size highly influences the accuracy of the results. The evaluation of the pressure oscillation amplitude highly depends on the height of the first layer of the grid close to the solid interface, which should be in order of sqrt(αdt). As a matter of fact, by creating coarser grids the surface temperature of the solid will not change on the short time scale and the heat transfer to (and from) the solid will be either over or under estimated, resulting in a low/high magnitude of the pressure fluctuations.

- **What are the origin and the driving mechanisms of the Limit cycle pressure oscillation?**

  In Chapter 6, the evolution of the dimensionless numbers (He and St) taken from the experimental data with regard to the Reynolds number in the inlet, suggests that the instability is originated from the burner acoustic. Furthermore, the FEM results show that the main frequency of instability is related to acoustics of combustion chamber (not the full geometry). All used

numerical approaches (i.e. fluid-only, CHT and FSI) regardless of how much deviation they have from the experiments show the occurrence of the main instability at a frequency close to the first quarter acoustic mode of the combustion chamber. This proves the ability of the URANS model to explore the mechanisms of thermoacoustic instability.

- **How important is the role of heat transfer on the development of instabilities?**

  Due to the existence of high temperature in the combustion chamber and also strong temperature fluctuations during the limit cycle oscillation, it is very difficult to measure the temperature with thermocouples. Using the conjugated heat transfer approach (CHT) (Chapter 5) gives the possibility to predict temperature fluctuations within the liner. Presented results, (in Chapter 5) showed that without the CHT approach the level of heat losses and therefore the magnitude of the instability cannot be determined correctly. This proves that the combustion instabilities are very sensitive to heat losses. The main conclusion is that the conjugate approach allows us to obtain a more accurate prediction of the magnitude of thermoacoustic instabilities and also by providing the temperature profile over the solid gives the possibility to assess the thermal stresses. This is difficult to be done by measurements.

- **What are the consequences of the high pressure oscillations on the liner vibration and vice versa?**

  Lifetime of a liner can be threatened either due to the elevated oscillatory mechanical loads inducing the fatigue, or enhanced heat transfer which increases creep damages. This is the main constraint in the design of gas turbine combustion chambers. For this reason, it is important to consider the effect of structure in the chain of events controlling the limit cycle behavior. In the calculation performed in the Chapter 5, the thermal coupling between the solid and flow was taken into consideration, in which the mechanical loads on the liner could be also predicted. The predicted results from this approach could be used as an input for the further investigation on the possible creep damages. However, in this approach and also in the fluid-only model the effect of the solid deformation induced by the mechanical loads is neglected and hence no change in the shape of the solid and fluid domain is taken into

account. Contrary to the previous methods, in the FSI (or two-way) model (presented in Chapter 6), the quantities from the fluid computations are applied on the liner and then the new deformed structure is updated in the fluid simulation; the obtained pressure spectrum shows a peak which is originated from the structural dynamics corresponding to the plate mode of the structure. However, it is important to notice that in order to reduce the calculation time, many simplifications made on the structure which would change the frequency of the structure. Although, this change can cause the diversion from the experimental observation, existence of the structural frequency even though with different value compared to the experiments proves the fact that the vibration of the liner does have influence on the acoustic field.

7.2 Recommendations

In this section, some recommendations for the future research are proposed:

- Although use of the reduced computational domain in a form of 4mm slice burner with the assumed symmetry planes showed good consistency with the experiments, it neglects the interaction between adjacent fuel injection holes, as well as 3D turbulence on the flow. Those effects can be taken into account by using the full 3D domain. Furthermore, by considering two extra liner surfaces in the full 3D domain, more precise prediction of heat losses through the CHT approach is expected. Besides, as it has been already mentioned in the previous section “conclusions”, considering a slice of the liner as well as the simplifications made on the liner structure in the FSI modeling will change the stiffness of the structure, changing the eigenfrequencies and vibration level. Therefore, further investigating can be done with mechanical loads transferred from the CFD domain to the full 3D structure. Both however, will increase the time of calculation significantly.

- Radiation heat losses are neglected in the present work. However it may influence the temperature of the gases, which deserves further investigation. Moreover, to assess the energy transfer from the combustor to the ambient besides considering the convection from the liner, heat transfer due to the radiation (emission) from the quartz glass windows should be also taken into account. This can be also costly but offers more accurate results.

- Calculation of the coupled problem in which the thermal and the mechanical loads exchange between fluid and structure can give more precise prediction of magnitude and frequency of instability; in this thesis, these two tasks have been conducted individually with the use of CHT and FSI models, however by exchanging the temperature profile in the interface of two domains, it is possible to assess the heat losses in the FSI model as well. This can be done only when the solid elements are used. However keeping in mind that to capture the correct heat losses, the first layer of grid in the solid should be in order of penetration depth, and also considering the need for use of double precision in the FSI calculation, combining these two tasks will increase the computational cost dramatically.

Research Publications

Conference papers

1- Shahi, M., Kok, J. B. W., Pozarlik, A. K., Roman Casado, J. C., Sponfeldner, T., "*Sensitivity of the numerical prediction of flow in the limousine combustor on the chosen mesh and turbulent combustion model*", in Proceedings ASME Turbo Expo 2013, San Antonio, Texas, USA, June 2013.

2- Shahi, M., Kok, J. B. W., Sponfeldner, T., Pozarlik, A. K., "*Thermal and fluid dynamic analysis of partially premixed turbulent combustion driven by thermo acoustic effects*" in Proc.ICSV20, Bangkok, Thailand, July 2013.

3- Santosh Kumar, T.V., Kapucu, M., Shahi, M., Alemela, P. R., Kok, J. B. W., "*Combustion Stability of Dry Low NOx combustion system – Flame transfer function approach*", 6th European Combustion Meeting (ECM 2013), Lund, Sweden, June 2013.

4- Filosa, A., Tomasello, A., Shahi, M., Berthold, N., Kok, J. B. W., Manfred, A. "*Numerical studies of unsteady heat transfer with thermoacoustic oscillations*". In Proc.ICSV20, Bangkok, Thailand, July 2013.

5- Shahi, M., Kok, J. B. W., and Alemela, P. R., "*Simulation of 2-way fluid structure interaction in a 3D model combustor*", in Proceedings of ASME Turbo Expo 2012, Copenhagen, Denmark, June 2012.

6- Altunlu, A. Can. , Shahi, M., Pozarlik, A. K, van der Hoogt, P. J. M., Kok, J. B. W., de Boer, A., "Fluid-structure interaction on the combustion instability," in Proc. ICSV19, Vilnius, Lithuania, July 2012.

Journal papers

1- Shahi, M., Kok, J. B. W., Pozarlik, A. K., Roman Casado, J. C., and Sponfeldner, T., 2014, "*Sensitivity of the Numerical Prediction of Turbulent Combustion Dynamics in the LIMOUSINE Combustor*," Journal of Engineering for Gas Turbines and Power, 136(2), pp. 021504-021504. **[Chapter 3]**

2- Shahi, M., Kok, J. B. W., Roman Casado, J. C., Pozarlik, A. K., 2014, "Assessment of Thermoacoustic Instabilities in a Partially Premixed Model Combustor Using URANS Approach", Applied Thermal Engineering, 71(2), pp. 276-290. **[Chapter 4]**

3- Shahi, M., Kok, J. B. W., Roman Casado, J. C., Pozarlik, A. K., "*Transient Heat Transfer between a Turbulent Lean Partially Premixed Flame in Limit Cycle Oscillation and the Walls of a Can type Combustor*" (Submitted). **[Chapter 5]**

4- Shahi, M., Kok, J. B. W., Roman Casado, J. C., Pozarlik, A. K., "*Strongly Coupled Fluid-Structure Interaction in a 3D Model Combustor during Limit Cycle Oscillations*" (Submitted). **[Chapter 6]**

5- Shahi, M., Kok, J. B. W., Pozarlik, A. K. "*On Characteristics of a Non-Reacting and a Reacting Turbulent Flow over a Backward Facing Step (BFS)* " (in progress). **[Chapter 2]**

6- Altunlu, A. Can. , Shahi, M., Pozarlik, A. K, van der Hoogt, P. J. M., Kok, J. B. W., de Boer, A., "*Fluid-structure interaction of the combustion instabilities and fatigue/creep lifetime assessment*" (in progress).

Acknowledgement

This thesis has been carried out with support and contribution of many people. Here, I would like to express my gratitude to all people who had significant role during the past three and half years, working as a PhD fellow at University of Twente.

First of all, I would like to thank Prof. Theo van der Meer, my promoter and head of ThW group for his continuous support and supervision throughout the whole period of my PhD study.

I would like to thank Dr. Jim Kok, for giving me the opportunity to do research in the LIMOUSINE project. He accompanied me step by step in this project, giving me interesting ideas and remarks which always helped me deal with problems and find my way. His commitment and firm management approach have strongly contributed to my qualifications as a PhD graduate.

I am also grateful to Dr. Artur Pozarlik for fruitful discussion and comments. Artur's kind and patient attitude makes him quite special character. His support, guidance, and advice throughout the research project, and writing papers, are greatly appreciated.

The LIMOUSINE project involved several partners. I would like to thank all LIMOUSINE fellows, for interesting and fruitful meetings we had during my PhD research: Reddy, Antonio, Salvo, Thomas, Ignacio, Oliver, Bela, Sebastian, Harmen, Patrick, Basti, Can, Roel, Lukas, and Simone.

I would like to thank Dr.Phil Stopford from ANSYS, for his helpful comments and support during this project.

My sincere thanks go to Sally and Ceciel, who are just kind, friendly, supportive and helpful persons. Whenever I had any problems in the administrative issues, the first person I would turn to was either Sally or Ceciel. I just cannot thank them enough!

I would like to acknowledge all the ThW Group members: Prof. Gerrit Brem, Dr. Genie Stoffels, and also my Postdoc, PhD fellows: Miladin, Joost, Simon Govert, Simon Buhler, Virginia, Joris, Shang Long, Nikola, Anton Verbeek, Marc, Lixian, Alex, Citra. We had great time in and out of the group, during the coffee breaks

and social events. Thanks also to my great officemates: Anton Bijl, Jerry, Rafael. I extend my sincere thanks to all my Iranian friends specially Fatemeh, Somayeh, Mahdiyeh, Amir Ghaffari, Faraz, Kazem, Mahmoud, Majid (s), Morteza, Behnam, Mitra and Siavash for their support and friendship. I had great experience and good time in all events organized by Irnut (Iranian Network of University of Twente). Special thanks go to Mohammadreza, Mojtaba, Niloofar and Hamed for organizing such events.

I would like to thanks my great friends Mehmet, Juan, Santosh for all time we shared at UT and after working hours, conferences, workshops and dinners. I enjoyed working with them. I appreciate Juan's efforts to do experiments for me to validate this work, although I was always blaming his experimental data as it was sometimes deviating from numeric! Thanks to Mehmet and his nice wife, Damla, for being such good friends who always supported me whenever I needed. I am also offering my thanks to Taha for his endless discussion during coffee breaks which could easily piss me off! Thanks to Riza for modulating the atmosphere! I wish them success in their career.

I am grateful to my parents for giving me their deep love, sacrifice, encouragement and unconditional support during my whole life. I want to thank also my sisters and their families, for their constant support on this journey.

I would like to thank my beloved husband, Amir, for his support, advice and encourage. He is my best friend and my forever love, who has always encouraged me through my many times of stress, excitement and frustration.

Mina Shahi

September 2014

UNIVERSITY OF TWENTE.

ISBN: 978-90-365-3712-4